UNIVERSITY OF CALIFORNIA, SAN DIEGO

The Expanding Folding/Functional Landscape of the Interleukin-1 Family

A Dissertation submitted in partial satisfaction of the
Requirements for the degree of Doctor of Philosophy

in

Chemistry

by

Kendra Lynn Hailey

Committee in Charge:

Professor Patricia A. Jennings, Chair
Professor Alexander Hoffmann
Professor Susan S. Taylor
Professor Wei Wang
Professor Peter Wolynes
Professor Virgil L. Woods, Jr.

2010

The Dissertation of Kendra Lynn Hailey is approved, and it is acceptable in quality and form for publication on microfilm and electronically:

_____

_____

_____

_____

_____

_____
Chair

University of California, San Diego

2010

DEDICATION

This thesis is dedicated to my parents, Mark and Jackie Hailey, who have always supported my interest in science. They gave me every imaginable opportunity to pursue my passion, from buying dinosaur books for me in kindergarten, to taking me to science summer camp, to letting me observe a laparoscopic cholecystectomy in high school. This thesis is also dedicated to my grandparents, John and Shirley Steineck and Ray and Jackie Hailey. Between them, they bought me the best birthday present ever (a microscope!) and put up with my bug/shell/small-animal collecting during our visits. Finally, this thesis is dedicated to my husband, Kevin Dougherty, who has made me the luckiest person on earth. His love and support keep me going every day, and he is the reason behind my smile. I love you all.

EPIGRAPH

I’m sciencing as fast as I can!

-Professor Hubert J. Farnsworth

TABLE OF CONTENTS

LIST OF ABBREVIATIONS

$AmSO_4$	Ammonium sulfate
Bis-Tris	Bis(2-hydroxyethyl)-amino-tris(hydroxymethyl)-methane
CD	Circular dichroism
D_2O	Deuterium oxide
DMEM	Dulbecco's modified eagle medium
DSS	2,2-dimethyl-2-silapentane-5-sulfonate
DTT	Dithiothreitol
DXMS	Deuterium-exchange mass spectrometry
EDTA	Ethylenediaminetetraacetic acid
EMSA	Electrophoretic mobility shift assay
FGF	Fibroblast growth factor
FPLC	Fast protein liquid chromatography
IL-1α	Interleukin-1α
IL-1β	Interleukin-1β
IL-1Ra	Interleukin-1 receptor antagonist
IL-1RI	Interleukin-1 receptor type 1
IL-1RAcP	Interleukin-1 receptor accessory protein
IL-33	Interleukin-33
Gdn-HCl	Guanidine hydrochloride
HSQC	Heteronuclear single quantum coherence
IPTG	Isopropyl β-D-1-thiogalactopyranoside
LB	Luria broth
MES	2-(N-morpholino)ethanesulfonic acid

MW	Molecular weight
Nf-κB	nuclear factor kappa-light-chain-enhancer of activated B cells
NaOAc	Sodium acetate
NH_4OAc	Ammonium acetate
$NaPO_4$	Sodium phosphate buffer
PFG-NMR	Pulsed-field gradient nuclear magnetic resonance spectroscopy
PMSF	Phenylmethylsulphonylfluoride
SAXS	Small-angle x-ray scattering
SDS-PAGE	Sodium-dodecyl sulfate polyacrylamide gel electrophoresis
SEC	Size-exclustion chromatography
Tris-HCl	Tris(hydroxymethyl)aminomethane-hydrogen chloride

LIST OF FIGURES

LIST OF TABLES

ACKNOWLEDGEMENTS

First and most importantly, I would like to acknowledge my thesis advisor, Patricia Jennings. She truly inspires me with her scientific creativity, her vast knowledge of all things having to do with chemistry, biochemistry, medicine, and science in general, and her amazing amount of motivation to uncover new information about the natural world. Not only is she one of the best, or the best scientist I know, but is also one of the most unselfish and generous people I have met in life. I feel very lucky and grateful to have had the honor of working for her for my graduate studies. I also have her to thank for all my newly-acquired knowledge of all things in New Jersey and Philadelphia. I would also like to thank my committee members, Professor Alex Hoffmann, Professor Susan Taylor, Professor Wei Wang, Professor Peter Wolynes and Professor Virgil Woods. I admire all of your outstanding contributions to scientific knowledge, and your dedication to your respective fields.

Also, I would like to thank my lab mates for their generous amount of support, laughs, discussions and debates over the years. Melinda Roy provided excellent scientific discussion, often playing the role of devil's advocate to my more "optimistic" ideas and interpretations of data. She is also a very patient and insightful teacher, and I will always appreciate her help that she has given to me. I would also like to thank my senior lab mates, Dr. Will Anderson and Dr. Nicole Kruse, for all their help with "getting me started" in the lab. Will especially helped with the vesicle leakage work, and Nicole generously helped with the PFG-NMR work. I will always be grateful for their time. I would also like to thank Dr. Lilly Wong for her help with starting the DXMS work in collaboration with the Woods lab, as well as running a tight ship during her time as the senior graduate student. Ryan Bertsch was also always willing to answer my novice protein purification questions, and I could always count on him to make me laugh. Also on this list are my junior lab mates, Michael Jamros, John Zuris,

Elizabeth Baxter, Sulyman Barkho, and Kaitlin Fisher. They have always graciously put up with my "mega-bench" and "mega-desk" tendencies, and make great lab mates. I am confident you all will maintain our lab's reputation of being a great place to work, in terms of science and fun! I would also like to thank all the undergraduates/post-baccalaureates I have worked with over my time here, especially Nick Calta, Bob Wong, Christina Clark, Precious Cagungun, Eric Hsu, and Xioban Kuang. You all helped keep me on my toes and I am very grateful for all the help you have given me.

There are four of my lab mates in particular that have helped me the most over my time here, and they are Dr. Dominique Capraro, Dr. Jamie Mills, Dr. (can't believe I just typed that) Ben Andrews and "soon-to-be Dr." Andrea Conlan. These people were my "mitopeeps", the ones I would turn to first when I needed help. Jamie was always willing to help process my data, and tell me about her exciting life outside the lab. Besides being a great NMR spectroscopist, her attention to detail is really remarkable, and I aspire to be that detailed oriented some day. Andrea is always willing to help trouble-shoot a purification, taught me all the great molecular biology tricks she knows, and motivates me with her tireless work ethic. I don't think she fully understands how much she's achieved in her time here, and how much the scientific world would miss her if she leaves it. Ben was always willing to answer my protein folding questions, show me how to use his "middle-management" spreadsheets and Matlab scripts, and put up with my "practical jokes" with almost perfect patience. He was the most influential person involved with teaching me how to "keep it real" in and outside of lab. Finally, the person who has helped me the most is Dominique. She has always inspired me with her super-human work ethic, her generous spirit, passion for science, positive attitude, and she also happens to have the longest coattails around for a certain junior

graduate student to jump on. Her only downfall is her poor choices regarding which professional sports teams to support.

There were many people in other labs that have helped me in my time here as well. Dr. Shannon Werner in the Hoffmann lab taught me everything I know about cell culture and EMSAs. She was an amazingly generous person with her time and help, and an excellent teacher. I would also like to thank Dr. Ellen O'Dea, Dr. Jeff Kearns and Kim Ngo for their help as well. Dr. Sheng Li in the Woods lab was instrumental in getting the data for the DXMS studies, running the samples for us. I am very grateful for all the time he has spent on our project. I would also like to thank Sarah White and Chris Gessner for helping me with the data analysis. Dr. Xuemei Huang has been a huge help with the NMR work over the years, helping me trouble shoot the spectrometers or with setting up experiments. I would also like to thank Dr. Anthony Mrse for his advice over the years as well. Dr. Shachi Gosavi from the Onuchic lab has provided us with valuable insight into the folding pathways of IL-1β and IL-1Ra with her Go-model simulations, as well as many delightful discussions of IL-1 folding. Finally, I would like to thank Dr. Gabe Cook of the Opella lab, for always being there to help us out with a down instrument, leaky valve, broken gasket, or to lend us a hand. I will always appreciate the time he has given to our lab over the years.

I would like to thank my family and friends for their support they have given me over the years and during my time here. My friends Dr. Doug Fowler, Megan Westcott, Dr. Kiyomi Komori-Occhione, Mike Occhione, Dr. Anne Bunner, Dr. Rena Astronomo, Dr. Steve Johnson, Dr. Will Placzek, Becky Placzek, Lisa Jabbour-Kluch, Art Kluch, Bill Brown, Allison Gang, Jeff Martin, Ginger Martin, Jeff Kody and Dr. Lisa Coray have all helped me keep my sanity over these last 7 years. My parents, Mark and Jackie Hailey, have given everything to me, every opportunity and more support than I could ever ask for in life. They

believed in me even when I didn't believe in myself. My brothers Clint and Michael "toughened me up" and kept me laughing through the years. Both have become impressive young men, and I am really proud of them. Finally, I would like to thank my husband, Kevin Dougherty. Without you, my life would be much less brighter and much less happier. Your love, support and sacrifices over the years have made this possible, and there are no words to describe how much I appreciate you. I love you.

Chapter 4, in part, is a reprint of the material as it appears in the Journal of Biological Chemistry 2009. Hailey, Kendra L., Li, Sheng, Andersen, Mette D., Roy, Melinda, Woods, Jr., Virgil L., Jennings, Patricia A. The dissertation author was the primary investigator and author of this paper.

VITA

2000	Bachelor of Arts, Chemistry, University of Colorado, Boulder
2005	Master of Science, Chemistry, University of California, San Diego
2010	Doctor of Philosophy, Chemistry, University of California, San Diego

PUBLICATIONS

1. Hailey, K.L., Li, S., Andersen, M.D., Roy, M., Woods, V.L., Jennings, P.A.. (2009) "Pro-Interleukin (IL)-1β Shares a Core Region of Stability as Compared with Mature IL-1β While Maintaining a Distinctly Different Configurational Landscape: A Comparative Hydrogen/Deuterium Mass Spectrometry Study" (2009) *J. Biol. Chem.* **284** 26173-26148.

ABSTRACT OF THE DISSERTATION

The Folding/Functional Landscape of the
Interleukin-1 Family

by

Kendra Lynn Hailey

Doctor of Philosophy

University of California, San Diego, 2010

Professor Patricia A. Jennings, Chair

Interleukin (IL)-1β is one of the "master" cytokines that initiates the innate immune response. IL-1β is a tightly regulated signaling molecule, and requires a delicate balance between its on/off states to maintain homeostasis in the organisms that produce it. Local and system-wide deleterious effects are seen when the actions of IL-1β are thrown off-balance. Therefore, there are multiple mechanisms that exist to keep this cytokine in check, from

transcription to degradation. In this study, we characterize the native state of the inactive precursor form of IL-1β, pro-IL-1β. Little detailed structural information is known about pro-IL-1β, despite the extreme importance of IL-1β as an immune system modulator. We find that pro-IL-1β is an extended, loosely packed confirmation with respect to the well-folded mature protein. The presence of the N-terminal region in pro-IL-1β prevents the C-terminal region, the eventual mature protein, from functioning by binding IL-1RI. With a combination of proteolysis and deutermium exchange mass spectrometry, we show that while pro-IL-1β is in a different conformation that the mature protein, an area important in the kinetic refolding pathway of the mature protein is protected from both proteolysis and deuterium incorporation into the amide backbone. Thus, pro-IL-1β is primed for quick-conversion into the mature form once the appropriate combination of signals is received by the cell producing it. IL-1β is also regulated extracellularly. It has co-evolved with a competitive inhibitor, IL-1 receptor antagonist (IL-1Ra). Both IL-1β and IL-1Ra bind IL-1RI, but only IL-1β elicits a cell-signaling response. Despite sharing only 30% sequence identity, IL-1β and IL-1Ra share the same tertiary structure, the β-trefoil fold. Since the structures between the agonist and antagonist are conserved, we would also like to know if their folding behavior and stability pathways are conserved as well. The dominant view of protein folding is the energy landscape theory, where protein sequences are designed well enough to fold on a "minimally-frustrated" funnel-shaped landscape. While minimizing frustration, or energetic traps on the landscape on-route to the native state leads robust and faster folding, areas within a structure that are functionally important have been shown to add frustration into a folding pathway. Therefore a balance must be struck between maintaining a functional protein that folds well. Recent minimalist Cα, or Go-model simulations of IL-1β determined that a region in IL-1β important for function (the β-bulge) added topological frustration into folding landscape for

this protein, where contacts formed early in the folding trajectory must be unmade and remade again late in the native state formation. As predicted from these theoretical simulations, removal of this area abolishes most of the frustration on the folding landscape. Since IL-1Ra lacks the β-bulge, we undertook equilibrium and kinetic folding studies to determine if indeed the folding of IL-1Ra is faster than that of IL-1β. We find that IL-1Ra, while maintaining the similar thermodynamic stability, folds faster from the I → N transition, indicating a less-frustrated landscape. Go-model simulations of IL-1Ra folding revealed a region of frustration in the vicinity of the loop between strands 11 and 12 of the protein, not in IL-1β. This area is in close proximity the receptor binding sites of both IL-1Ra and IL-1β. Folding and biological activity studies mutations made to this area in IL-1Ra, along with two other functionally important areas were undertaken. These studies revealed new insights into the functional landscape of IL-1Ra that could not be inferred by inspection and comparison of the structures of unbound/bound IL-1Ra and IL-1β to IL-1RI alone. Finally, the newest member of the IL-1 family of proteins, IL-33, contains a C-terminal β-trefoil structural motif. Early in vivo functional studies indicate it has a unique functional landscape as compared to all other family members. We undertook a combined folding and structural study of the β-trefoil region of IL-33, and show it is slightly destabilized and faster folding as compared to wt IL-1Ra and IL-1β in the same conditions.

Chapter 1

General Introduction

The interleukin (IL)-1 family of proteins consists of extracellular cytokines and antagonists that regulate the immune system(1-4). As of today there are 11 members, including the recently classified IL-33(5). Their main functions range from initiating the innate immune response (IL-1α and IL-1β), to stimulating the production of INF-γ in the cell-mediated immune response (IL-18) to mediating the Th2-imune response (IL-33), by binding their respective target extra-cellular receptors. Both IL-1α and IL-33 have dual roles as transcription factors in their much-longer precursor forms(4,6-8). These agonist activties of the IL-1 family are balanced by other family members that have antagonist activities. The first natural competitive inhibitor, IL-1Ra, was discovered in the urine of rheumatoid arthritis patients(9). IL-1Ra binds the type-1 IL-1 receptor (IL-1RI) and acts as a competitive inhibitor of IL-1α and IL-1β initiated signaling(10-12). Other antagonists of IL-1 familiy activities bind the cytokine and prevent it from binding its target receptor (sIL-1RI and II, IL-18BP, sST2)(1,13).

When the balance between agonist and antagonist family members is disturbed, a variety of deleterious effects can occur, leading to both acute and chronic disease states. For example, IL-1β is one of the cytokines responsible for propagating sepsis, when the immune response to a pathogen challenge has gone systemic, overwhelming and shutting down functions critical for maintaining system life(14-16). In addition, chronic over-production of IL-1β leads to joint degradation, inflammatory bowel disease, diabetes, atherosclerosis, Alzheimer's disease, cancer and cancer metathesis(14-19). Therefore, tight-regulation of this proinflammatory cytokine is critical in health and survival from disease.

The proinflammatory cytokine IL-1β and its competitive inhibitor IL-1Ra have co-evolved to bind the same extracellular receptor, IL-1RI. These two cytokines were reported to be the product of a gene duplication 300 million years ago, and have identical gene structure (number of exons and introns)(20-22). However, IL-1Ra is expressed as a combination of exons 1, 5, 6, 7 while IL-1β is expressed as 2 - 7(22). Exon 1 codes for the classical ER/Golgi secretory sequence of IL-1Ra. Interestingly, the gene for IL-1β also contains this exon, but it is not included when IL-1β is transcribed into mRNA. Exons 2 - 4 of IL-1β encode its N-terminal precursor domain, and truncated versions of these 3 exons are also present but not transcribed in the gene for IL-1Ra. Finally, the cytokine portion of both proteins is contained in exons 5 – 7.

IL-1β and IL-1Ra both share the same tertiary fold, the β-trefoil. These two structures align well, with as RMSD of 1.264 Angstroms when aligned in PyMOL(23). The β-trefoil consists of three repeating βββloopβ structural motifs, or trefoils (1, 2 and 3), that form a six-stranded barrel capped on one end by a six-stranded cap (Figure 1-1). The main deviations in overall structure between the two proteins are the loop between strands 4 and 5, the charged loop between strands 7 and 8, and the longer N-terminus of IL-1Ra(24,25). These differences map back to the different receptor binding sites of IL-1β and IL-1Ra (Figure 1-2). As shown in Figure 1-2, both IL-1β and IL-1Ra have an A-site, and the agonist IL-1β has a much more extended B-site(26,27). Structural analysis of the respective protein/receptor complexes led to the proposal that interactions with the B-site are responsible for the

conformational change in the IL-1β-IL-1R1 complex that recruits IL-1AcP, thus initiating signaling.

Although IL-1β and IL-Ra are structurally homologous, they share limited sequence identity (26-30%)(21). The majority of sequence identity maps to the strands involved in the observed kinetic folding intermediate in IL-1β(28), shown in Figure 1-3a. Surprisingly, only 5 residues out of the two A-sites (25 residues for IL-1β and 21 residues for IL-1Ra) are conserved between two proteins, but the general hydrophobicity/hydrophilicity of Site A is similar. Interestingly, the pattern of sequence conservation over species differences is different (Figure 1-3b). In IL-1β, only a select few residues in trefoil 1 are conserved, in strands or in a loop important for the A-binding site (3 residues conserved between IL-1Ra and IL-1β). The sequence is highly conserved between strands 4 and 11 (more than trefoil 2), with areas of high variability within this region mapping to connecting loops. The residues conservation is again diminished in trefoil 3, with identically conserved residues limited to pockets shown to be important for structural reasons (F146) or functional reasons (D145). In contrast, IL-1Ra maintains a very-well

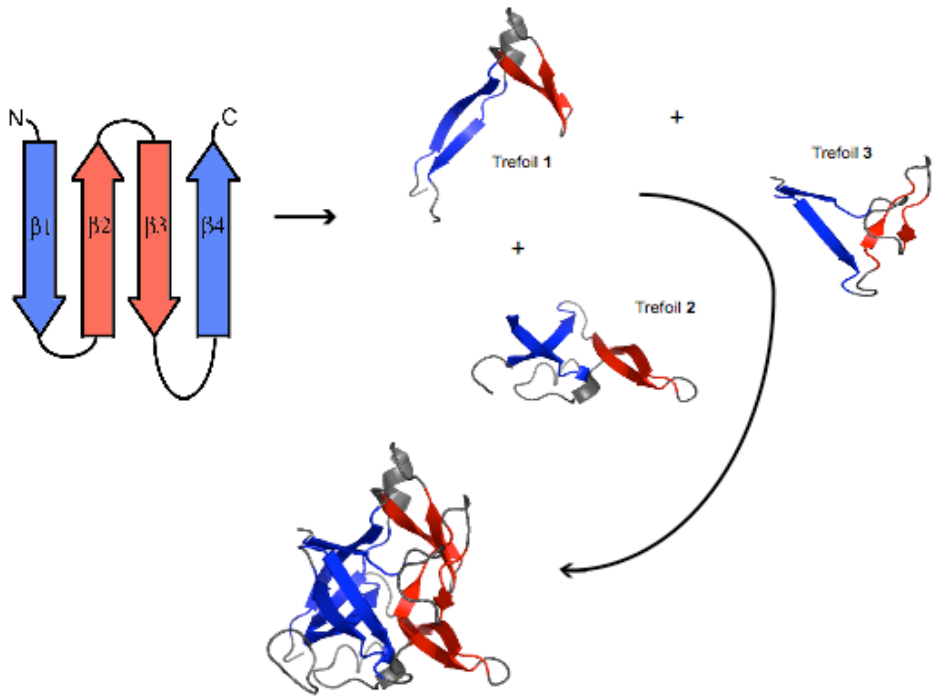

Figure 1-1: The β-trefoil fold. The β-trefoil fold consists of a triplet repeat of a βββloopβ structural motif, shown in the 2D cartoon representation in the top left corner. These individual units fold to form a trefoil unit (upper right corner), and three trefoil units fold into a six-stranded barrel with a six-stranded cap (bottom). The strand colors in the 2D cartoon representation are indicative as to where they eventual end up in the tertiary structure.

conserved region encompassing strands 1-3 of trefoil 1 (Figure 1-3c). Only pockets of conserved residues exist between strands 4 and 5, most notably on either side of the tight β-turn between the two strands. Conservation picks up again in strand 6, in an area overlapping well with IL-1β. The area between strands 7 and 9 is again limited to smaller regions, including several highly conserved residues in charged loop found in both proteins. Strand 9, the hydrophobic turn, and strand 10 are well-conserved, and overlap well with IL-1β. Finally, the area adjacent to and strand 12 is well-conserved in the sequence, unlike the analogous region in IL-1β. Therefore, the sequence conservation patterns are distinct between IL-1β and its competitive inhibitor IL-1Ra, even though they bind the same receptor.

Along with a competitive inhibitor, IL-1β is regulated in a number of other ways. Every step from transcription to receptor binding has a check-point. IL-1β is not constitutively-expressed and is only transcribed in response to an immune challenge(29). A second messenger, such as lipopolysacchride (LPS) from bacterial cell walls, is required for translation of the precursor protein (Schindler, JBC, 1990). Additional signals are necessary to process the inactive precursor protein into the active, mature cytokine, and for its release into the extracellular environment. Once in the extracellular environment, soluble receptor analogues sIL-1RI and sIL-1RII can effectively trap IL-1β and prevent it from binding cell-surface IL-1RI. A decoy cell surface receptor, IL-1RII, also sequesters free IL-1β(30,31).

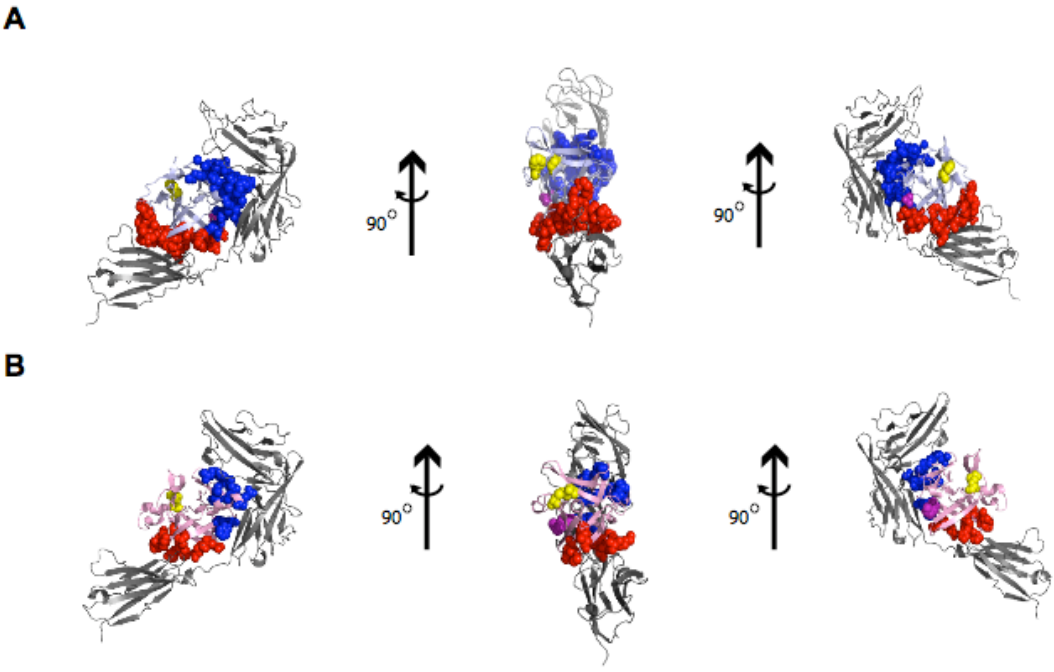

Figure 1-2: The A and B receptor binding sites for IL-1β and IL-1Ra. Shown here are three views of crystal structures of IL-1RI bound with either IL-1β (A) or IL-1Ra (B) (PDB:1ITB and 1IRA, respectively)(26,27). The sites are colored blue for Site A and red for Site B in both cases. Functionally relevant sites, residues 145 and 117/116 in IL-1β and IL-1Ra, respectively, are also labeled by color (145 is yellow, 117/116 is violet).

Figure 1-3: Sequence conservation over IL-1β and IL-1Ra families. The sequences of human IL-1β and IL-1Ra were aligned and the relative conservation is shown in (A) (refs). The available mammalian sequences for both proteins from the National Center for Biotechnology Institute (NCBI) were aligned (in their mature forms, 153 residues for IL-1β and 152 residues for IL-1Ra) and the alignments are shown in (B), IL-1Ra, and (C), IL-1β using Jpred(32). Residues that are not conserved between IL-1Ra and IL-1β, but are important for function, are indicated by red arrows.

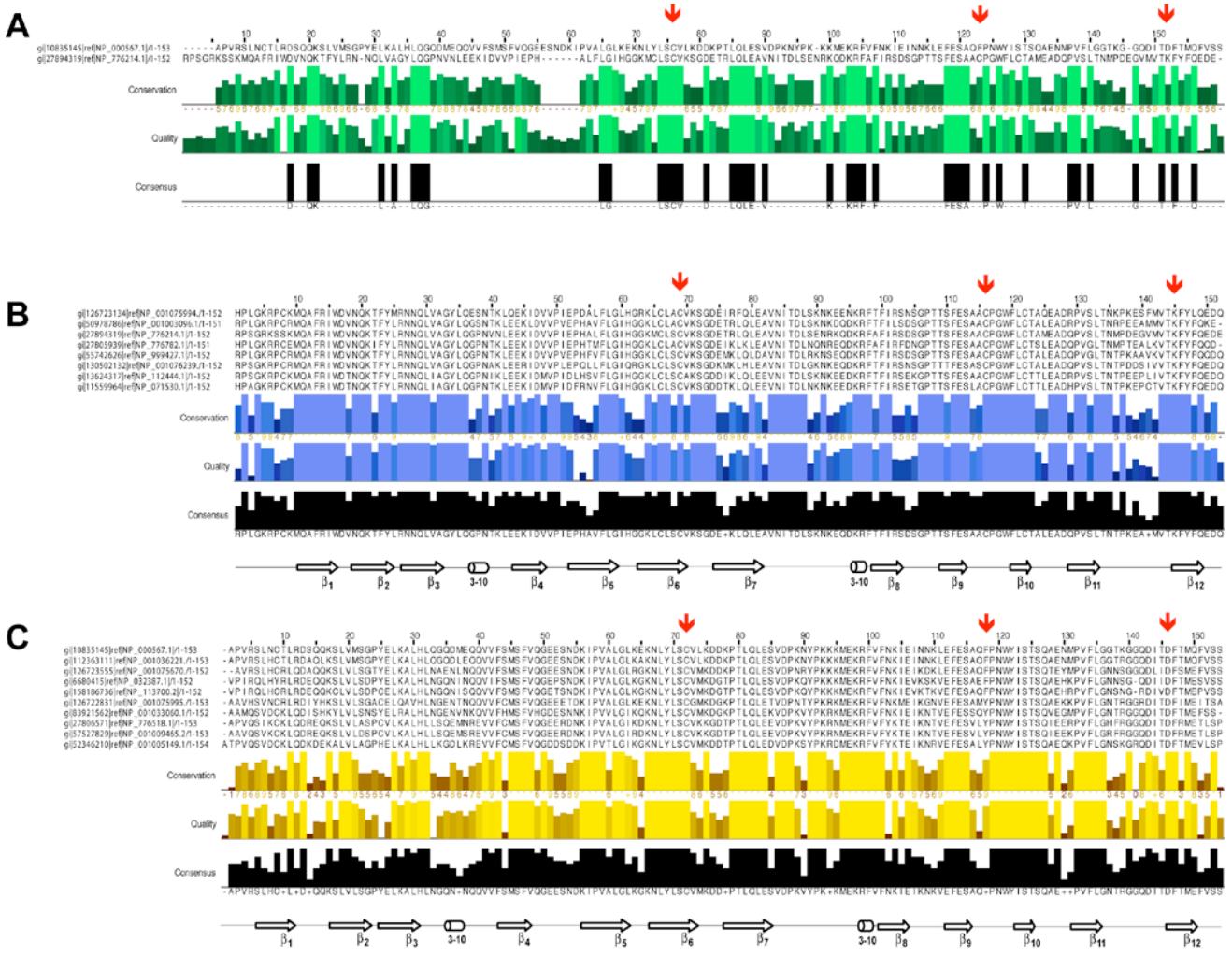
A
B
C
Conservation
Quality
Consensus
β1
β2
β3
3-10
β4
β5
β6
β7
β8
β9
β10
β11
β12

In this thesis, the roles of two modes of IL-1β regulation are explored as well as preliminary characterization of the newest identified member of this family, IL-33. The first regulatory feature studied is the nature of the precursor state of the protein. Little structural information is currently available on the precursor, or pro-IL-1β, protein. Using the combination of the classical biophysical techniques of fluorescence spectroscopy and circular dichroism, sizing methods such as size-exclusion chromatography and pulsed-field gradient (PFG) NMR, enzymatic digests, and the high-resolution structural characterization techniques of 2D ^{1}H-^{15}N NMR spectroscopy and deuterium-exchange mass spectroscopy (DXMS), the native state of pro-IL-1β can be characterized. In addition, the folding and functional landscape of the antagonist protein IL-1Ra will be explored using mutagenesis, stopped flow and manual mixing kinetics, equilibrium denaturation titrations, biological activity assays, and ^{1}H-^{15}N NMR spectroscopy. These studies will help determine how information is communicated across the protein and how that impacts activity.

In 2005, Schmitz and coworkers identified the newest IL-1 family member, IL-33(33). IL-33 was identified first as a nuclear protein up-regulated in response to brain hemorrhage in canines (DVS-27), and then again as a constitutively expressed nuclear protein in high-endothelial venules in lymphoid tissue (NF-HEV)(34,35). A study searching for distant β-trefoil family members to serve as yet-unidentified ligand for the orphaned IL-1 receptor family member ST2 finally identified IL-33 as it is currently known(33). The functions of IL-33 are now the subject of intense scrutiny

from 2007 until today. To date, IL-33 has been shown to participate as a key initiator of the Th2-adaptive immune response, be responsible for asthma, anaphylactic shock, parasitic infections and allergic inflammation(36,37). IL-33 also has protective functions in the cardiovascular system, preventing apoptosis in cells and associated heart failure after a myocardial infarction (heart attack)(38). Most recently, IL-33 has been shown to attenuate sepsis in mice(39). Already, IL-33 participates in and is responsible for a wide-range of acute and chronic activities *in vivo*, analogous to its older cousin IL-1.

In this study, we use the combined approach of fluorescence and CD spectroscopy to study the equilibrium and kinetic folding behavior of β-trefoil region of IL-33. We also use 2D ^{1}H-^{15}N NMR spectroscopy to determine the amide backbone fingerprint of wt and mutant IL-33, as well as the stability of the amide backbone to deuterium exchange. A point mutant of IL-33, D68A, is used to determine resistance to enzymatic processing in the β-trefoil region. Finally, a unique mode for purification of IL-1 family members IL-1β, IL-1Ra and IL-33 will be discussed.

Clearly, the IL-1 family is a large target for the pharmaceutical industry. IL-1Ra has been an FDA-approved drug (Anakinra) for rheumatoid arthritis since 2001(40). Other anti-IL-1 therapies undergoing clinical trials include anti-IL-1β monoclonal antibodies and an IL-1RI – IL-1RAcP - IgG fusion protein (IL-1 Trap, or Rilonacept)(41,42). These therapies target Cryopyrin-Associated Periodic Syndrome (CAPS), gout, and most recently Type-2 diabetes(17,43-46). Along with rheumatoid

arthritis, IL-1Ra (Anakinra) is being tested as a therapeutic for Type-2 diabetes and Familial Cold Urticaria. However, this is only a small number of targets for anti IL-1 therapy, since abberant IL-1 activity is involved with a much larger number of acute and chronic disease states, including cancer. Along with anti-IL-1, IL-33 will undoubtedly become a drug target in some form, as evidenced by the explosion of studies characterizing its protective and destructive activities(1). Therefore, it is of high importance that the folding and functional properties of these proteins are fully characterized, since this information can then be used to improve on existing therapies or create new ones. Taken together, the information gathered here on the IL-1 family of cytokines will help build a better foundation for future protein design studies, with the goal of improving human health.

Chapter 2

General Methods

INTRODUCTION

The folding and functional landscapes of the IL-1 family members IL-1β, pro-IL-1β, and IL-1Ra were characterized using a combination of classical biophysical techniques, biological assays, and hydrogen/deuterium (H/D) exchange mass spectrometry. Along with expression and purification of the wild-type (wt) proteins, a large number of point mutations and loop insertions were generated and purified. The *Escherichia coli*/pET vector system and robust FPLC methodology allowed for the facile acquisition of large amounts of pure protein. All materials and methods reported here are used throughout the rest of this thesis; any exceptions are noted within the pertinent chapters.

MATERIALS AND METHODS

Expression and Purification IL-1 Family Members

All point mutants described were made based on the Stratagene Quick-Change guide (ref). The expression and purification of mature IL-1β and point mutants were performed as described previously(47). The N-terminal aminopeptidase activity in *E. coli* leads to production of three isoforms of IL-1β, which differ in their N-terminus residue (1-Met, 1-Ala, 1-Pro). Therefore, isoform-specific mature IL-1β was obtained with additional purification step. The raw IL-1β fractions were pooled and extensively dialyzed into 20 mM sodium acetate, 1 mM EDTA, pH 5.2, and injected onto a Resource-S cation exchange column (GE Healthcare). Two isoforms of mature IL-1β, 1-Ala and 1-Pro (N-terminus), eluted as single peaks with a gradient of 30-50%

buffer B (100 mM sodium acetate, 1 mM EDTA, pH 5.2) over 200 mL at 1 mL/min. The 1-Ala fractions, which correspond to the active form *in vivo*, were pooled and the isoform identity was confirmed by MALDI mass spectrometry. All experiments were performed using the 1-Ala isoform of mature IL-1β, as this reflects the native mature protein produce by caspase-1 processing of pro-IL-1β.

Recombinant human pro-IL-1β wt protein (and mutants) were prepared using the following procedure. The cDNA encoding the E6 isoform (IMAGE:3875593) was subcloned into a pET24-d(+) vector (Novagen) and transformed into *E. coli* BL21(DE3) cells (Novagen). Cells were grown in luria broth (LB) at 37 °C to an OD_{600} of 0.6, and protein expression was induced with the addition of IPTG (1 mM final concentration) . The temperature was reduced to 30 °C, and the cells were harvested after 4 hours. The harvested cultures were spun at 6238 x g for 30 min, and the cell pellets were suspended in lysis buffer (25 mM Tris, 2 mM EDTA, 5 mM DTT and 1 mM PMSF at pH 6.8). The cells were lysed by sonication at 4 °C, and then spun at 13,000 rpm for 30 min. The soluble pro-IL-1β was made 25% saturated by ammonium sulfate, then precipitated by spinning at 20,201 x g for 30 min. The resulting pellet was suspended in buffer A (25 mM Tris, 2 mM EDTA and 5 mM DTT at pH 6.8) and extensively dialyzed. The dialyzed protein was spun at 20,201 x g rpm for 30 min, filtered by a 0.22 μ filter, and injected onto a HiTrap-Q anion exchange column (GE Healthcare). Pro-IL-1β eluted as a single peak using a linear gradient of 200 - 400 mM NaCl over 250 mL at a flow rate of 3.0 mL/min. The pro-IL-1β

fractions were pooled and concentrated, then injected onto a 26/20 S-200 size-exclusion column (GE Healthcare) equilibrated with buffer A (with 200 mM NaCl added) at a flow rate of 2.5 mL/min. Purity was assessed by SDS-PAGE (>95%).

The cDNA for human interleukin-1 receptor antagonist (IL-1Ra) isoform 1 was obtained from Open Biosystems (GenBank number NM_173842). The DNA corresponding to the mature secreted form (residues 26-177 of the precursor protein) was amplified by PCR, restriction digested and ligated into the pET-24a expression vector (Novagen). The ligated DNA was transformed into *E. coli* DH5α competent cells (Novagen) and insert-containing DNA purified from isolated colonies was verifed by sequencing (Eton Bioscience). The insert-containing vector was transformed into *E. coli* BL21 (DE3) competent cells (Invitrogen). An LB culture was inoculated with these cells and grown at 37 °C until they reached an OD_{600} of 0.6. Protein expression was induced by adding 1 mM IPTG (final concentration) and the temperature was reduced to 30 °C. The cells were harvested after 4 hours by centrifuging at 6238 x g for 10 min. The media was carefully decanted, and the resulting pellets were suspended in a total volume of 80 mL of 25 mM ammonium acetate, pH 5.2, 1 mM EDTA and 1 mM PMSF. The resulting supernatant was extensively dialyzed into 25 mM ammonium acetate, pH 5.2, 1 mM EDTA (Buffer A). The dialyzed protein was spun again at 20,201 x g for 20 minutes, and supernatant was filtered by 0.2 μ filter. The filtered protein was injected onto a HiTrap-S HP cation exchange column (GE Healthcare) equilibrated with Buffer A. The protein eluted as a single peak between a gradient of 30-70% B over 100 mL (Buffer B is 750

mM ammonium acetate, pH 5.2, 1 mM EDTA). The purity of the protein was asessed by SDS-PAGE. All IL-1Ra point mutations were prepared using the same procedure. Additional chromatography steps were performed as needed.

Uniformly ^{15}N-enriched samples of pro- and mature IL-1β were grown using M9 minimal media salts, with 99% [^{15}N] ammonium sulfate (Isotec) at 2 g/L (Isotec).

Protein concentrations were determined by measuring the A_{280} on a UV-Vis spectrometer (Bio-Rad). The extinction coefficient for wt IL-1Ra is 15460 L cm^{-1} mol^{-1}, calculated by the method described in Gill and Von Hippel (ref). All proteins were exchanged into 10 mM 2-(N-morpholino)ethanesulfonic acid, pH 6.5, 90 mM NaCl, 1 mM EDTA buffer (1xMES) unless noted otherwise.

Circular Dichroism (CD) Spectroscopy

The spectra for near- and far-UV were recorded on an Aviv-2 Circular Dichroism Spectropolarimeter at 25 °C in a 0.1 cm pathlength quartz cuvette. Each sample was at 0.2-0.3 mg/ml (final concentration) in 1xMES, over a range of guanidine-HCl concentrations. The samples were equilibrated at least 24 hr at room temperature. The averaging time at each wavelength was 5 s, and experiments were performed in triplicate.

Equilibrium Titrations

Equilibrium unfolding/refolding titrations were monitored using tryptophan fluorescence intensity, average fluorescence wavelength, and circular dichroism spectroscopy. For the unfolding titrations, protein samples were prepared in the range of 0.1 - 0.4 mg/ml in a buffer solution (10 mM MES, pH 6.5, 90 mM NaCl, 1 mM EDTA). Protein samples were diluted to varying final denaturant concentrations and equilibrated overnight. The excitation wavelength used was 293 nm, and the emission spectra were collected from 300 to 450 nm on a FluoroMax-2 or 4 spectrophotometer (Horiba Jobin-Yvon) or an Aviv-2 Circular Dichroism Spectropolarimeter at 25 ˚C. The refolding titrations were prepared by unfolding the protein in 4 M guanidine-HCL and equilibrating overnight. Protein samples were diluted to varying final denaturant concentrations and equilibrated overnight. The data were fit according to the parameters and equations listed in **Data Fitting and Analyses** section of this chapter.

Equilibrium denaturation titrations measured by CD were performed as follows. Samples were prepared as for the fluorescence experiments, and measured in the far-UV range as described in the **Circular Dichroism (CD) Spectroscopy** section. The data were fit according to the parameters and equations listed in the **Data Fitting and Analyses** section of this chapter.

Manual-Mixing Folding Kinetics

Relaxation times greater than 20 s were measured using manual mixing techniques. Unfolding experiments were initiated by adding native protein stock into

a cuvette to a final Gdn-HCl concentration in the range of 1.5 – 4.0 M. Refolding experiments were initiated by diluting unfolded protein at 2.2 – 4.0 M Gdn-HCl to final denaturant concentrations ranging from 0.6 – 1.2 M. The final protein concentrations ranged from 0.1 to 0.3 mg/ml. Kinetic rates were determined from the observed time dependent change in fluorescence emission at 343 nm (excitation wavelength of 293 nm) on a Fluoromax-2 or 4 spectrophotometer. All data was fit according to the methods described in the **Data Fitting and Analyses** section of this chapter.

Stopped-Flow Refolding Kinetics

Relaxation times less than 20 s were measured using stopped-flow methods. Refolding experiments were initiated by a 1:11 dilution of unfolded protein stock in 2.2 M Gdn-HCl into varying final denaturant concentrations ranging from 0.2 – 0.8 M. Final protein concentrations were in the range of 0.1 – 0.3 mg/ml. The excitation wavelength was at 293 nm, and emission was collected through a >320 nm cut-off filter. Stopped-flow kinetics of the time dependent change in fluorescence was measured using a Pi-Star stopped flow instrument (Applied Photophysics). All data were fit according to the methods described in the **Data Fitting and Analysis** section of this chapter.

DXMS Operation

The instrument set-up was previously described (48-50). All flash-frozen samples were thawed and run using the conditions determined during fragmentation optimization.

Optimization of Fragmentation Conditions

The initial conditions for the sample composition and instrument parameters were determined before starting the exchange time-course experiments. The instrument set-up was previously described (48-50). A 5 μL stock of mature IL-1β or pro-IL-1β was diluted with 15 μL 1xMES and quenched with 30 μL of 0.5% formic acid, 16.6% glycerol and 3.2 M guanidine-HCl (quench buffer) at 0 °C. The samples were immediately flash-frozen in liquid nitrogen and stored at -80 °C. The samples were later thawed at 0 °C and run at 100 μL/min on a pepsin-66 column, generating peptides. The peptides were separated using a C18 reversed-phase column (Vydac) running a gradient of 5-45% 5%TFA/acetonitrile over 30 min before injecting onto the LCQ mass spectrometer (Thermo LCQ Classic, Thermo Finnigan). The peptides were identified using MS1 and MS2 data. The fragmentation conditions were deemed appropriate by assessing quality of generated peptides and amount of peptide coverage over the full-length protein.

Deuterium On-Exchange Experiments

The exchange time-course experiments for pro-IL-1β and 1-Ala mature IL-1β were all performed simultaneously at 25 °C with the following procedure. A full time-course experiment was initiated by adding 100 μL of protein in 1xMES (pH 6.5) to 300 μL of the equivalent deuterated exchange buffer for a final $\%D_2O$ of 75%. Deuterated 1xMES was prepared by using D_2O and adjusted to a pD* of 6.1 with DCl. The exchange was monitored over the course of 24 hours, at the intervals of 0.1, 1, 5, 15, 60, 120, 480, and 1440 min. Aliquots (20 μL) from the master reaction were removed and quenched in pre-chilled HPLC vials containing quench buffer (30 μL). The vials were sealed and flash-frozen, then stored at -80 °C. The in-exchange control consisted of the protein added directly to the pre-chilled deuterated and quench buffers, then followed immediately by the normal sample preparation procedure. The back-exchange control was determined by incubating the samples in 0.5% formic acid in D_2O with varying concentrations of Gdn-DCl (0 M, 2.0 M and 4.0 M, Cambridge Isotopes) for 24 or 48 hours. All samples were injected and run on the instrument with the same conditions listed in the fragmentation optimization section. Data for the exchange time courses was acquired in the MS1 mode.

Sequence Identification of Peptide Fragments

The most-likely identity of the parent peptide ions was determined using the SEQUEST software program (Thermo Finnigan, Inc.) and the MS1 and MS2 data. The quality of each peptide was monitored by individually examining each measured

isotopic envelope spectrum for the entire exchange time course. The deuterium content was calculated for each time point by using specialized software as previously described(49,50).

Enzymatic Digestion Assays

The chymotrypsin A and caspase-1 (Sigma) digests of pro- and mature IL-1β were performed in the following manner. Master reactions were made containing 200 μL substrate at 15 μM in 1xMES buffer. The reactions were carried out at 30 °C. After adding the enzyme, time points were taken by quenching the reaction by adding each aliquot to 2xgel running buffer (200 mM Tris-HCl, 10% glycerol, 2% SDS, 0.5% bromophenol blue and 10% β-mercaptoethanol) and flash-freezing in liquid nitrogen. Reactions with chymotrypsin quenched with the addition of the protease inhibitor PMSF (1 mM) to the gel running buffer showed no difference in the amount of substrate cleaved when compared to no PMSF added (data not shown). The substrate cleavage was monitored over time by change in band intensity on a Coomassie-stained, SDS-polyacrylamide gel. The enzymes were added based on the number of units necessary to digest the total amount of substrate in 15 min in the case of chymotrypsin and 1 hour in the case of caspase-1.

Data Fitting and Analyses

Fitting of the fluorescence-detected equilibrium data was done as described previously (refs). Equilibrium unfolding/refolding titrations were fit using a two-state model of unfolding (ref). The average wavelength and normalized fluorescence intensities as a function of final denaturant concentration were both fit. Pro-IL-1β fluorescence was followed using Trp 108 and Trp 236 (Trp 120 in the mature protein numbering). IL-1Ra fluorescence was followed using Trp 17 and Trp 120. The average wavelength was calculated using Equation 2.1:

$$\lambda_{average} = \frac{\sum_{300-450nm} \lambda * I_{\lambda}}{\sum_{300-450nm} \lambda} \qquad (2.1)$$

where λ is the wavelength of light in nm and where Iλ is the intensity at that wavelength.

Equilibrium unfolding and refolding data was fit in Matlab (Math Works) using the two-state model shown in Scheme 1:

$$N \leftrightarrow U \tag{2.2}$$

where N is the folded species and U is the unfolded species (ref). The apparent fraction of the unfolded form, F_{NU}^{app}, populated at a given concentration of denaturant is used to calculate the apparent free energy of N, ΔG_{NU}^{app}, in Equation 2:

$$F_{NU}^{app} = \frac{e^{\frac{-\Delta G_{NU}^{app}}{RT}}}{1 + e^{\frac{-\Delta G_{NU}^{app}}{RT}}} \tag{2.3}$$

where R is the gas constant and T is temperature (ref).

The free energy of stabilization (ΔG_{NU}^{app}) and cooperativity of the folding transition (m) of wt and mutant proteins were determined using Equation 3:

$$\Delta G_{NU}^{app} = \Delta G_{NU}^{H_2O} - m([D]) \tag{2.4}$$

where $\Delta G_{NU}^{H_2O}$ is the free energy of unfolding in the presence of no denaturant and [D] is the concentration of denaturant.

Manual mixing and stop flow fluorescence data were fit using Equation 4 and the Marquardt algorithm and globally(51,52).

$$A(t) = \sum^{i} A_i e^{\frac{t}{\tau_i}} + A(\infty) \tag{2.5}$$

The number of kinetic processes, *i*, amplitude of the process A_i, relaxation time τ_i, and signal value at equilibrium A(∞) were calculated using Matlab (Math Works) and GraphPad Prism (GraphPad Software, Inc.). The fit quality was determined by the random dispersion of residuals and the X^2 (chi-squared) values. The relaxations times reported here are the inverse of the observed rate constant, which is not directly equivalent to the intrinsic rate constant of a chemical process.

The number of deuterons incorporated into each peptide over time was calculated using the method of Zhang and Smith in Equation 5:

$$Deuterium(\#) = \frac{m(P) - m(N)}{m(E) - m(N)} \times MaxD \tag{2.6}$$

where m(P), m(N) and m(E) are the centroid values for the partially deuterated peptde, the non-deuterated peptide and the equilibrated fully-deuterated peptide, respectively. MaxD is the maximum deuterium incorporation possible for each peptide, assuming the first two deuterons of each peptide are lost due to end effects, and subtracting the number of prolines in the peptide sequence(50).

Chapter 3

The Native-State of Pro-IL-1β

ABSTRACT

Pro-IL-1β is a 269-residue precursor protein produced in the cytosol upon cell stimulation, but becomes active as an extracellular cytokine in the shorter, 153-residue mature form. Preliminary studies of pro-IL-1β in vitro revealed that eventual mature protein undergoes a significant change in stability upon processing of the N-terminus by a wide-range of enzymes(53-56). However, no detailed characterization of pro-IL-1β has been performed until now, because of the difficulties associated with purifying significant quanties of the protein for structural analysis. The mechanisms associated with the production and processing of the precursor protein are significant in targeted drug therapies as the recognition of inflammatory processes in orchestrating the poor prognoses associated with disparate diseases ranging from cancer to diabetes grows(57,58). Therefore, after overcoming the problems associated with isolation of the purified protein, we explored how the presence of the precursor domain modulates the function of the eventual mature protein by first characterizing the native state of pro-IL-1β.

INTRODUCTION

IL-1β is a pluripotent cytokine responsible for a multitude of immune responses to host invasion (ref-dinarello). It is synthesized as a 269-residue precursor protein (pro-IL-1β) in the cytosol upon cell stimulation, but only acts as an extracellular cytokine in the shorter, 153-residue mature form. The mature form is generated after secondary stimulation with a distinct signal that initiates processing and secretion of the protein(59,60). Mature IL-1β is a potent cell-signaling activator with full immune response requiring <10 IL-1R sites occupied per cell, in many cases(14). This extreme potency has coevolved with tight regulation of the mature protein via multiple mechanisms, including the inability of pro-IL-1β to bind the receptor and elicit an immune response(10). Thus, there is growing interest in understanding how the pro-protein is stabilized prior to processing and release of the active cytokine in response to inflammation/injury(61-63).

While the structure and function of IL-1β has been an area of active research since its discovery, little is known about the structure /function and folding of pro-IL-1β. The N-terminal 116 residue pro-domain contain no known localization sequences, no post-translational modification sites, and has no known function to date, other than destabilizing/inhibiting the activity of IL-1β. Indeed, the cellular half-life for pro-IL-1β is approximately 2.5 hours, while the mature protein is very protease-insensitive(64). The cytosolic proprotein is processed to the mature form after assembly of the newly identified inflammasome, an intracellular scaffolding platform necessary for the activation of interleukin converting enzyme (ICE or caspase-

1)(63,65-67). Once activated, ICE cleaves pro-IL1β at two conserved cutsites, D27|G28, and D116|A117 upon stimulation of macrophages and monocytes(68). While pro-IL1β is also is readily cleaved by a number of other proteases including chymotrypsin, proteinase K, and matrix metalloproteases, ICE activation is thought to be the predominant mechanism for generation of mature IL-1β. Thus, understanding the mechanism of processing by ICE and the role the precursor domain plays in regulating the structure and activity of this cytokine is of intense interest.

Precursor domains are used throughout nature to modulate the functions of their respective eventual mature domains. Many enzymes are synthesized as inactive zymogens, so that they can be translocated to the desired areas within or outside the cell in an inactive state, preventing any deleterious effects of their active function. For example, the non-specific protease pepsin is synthesized as the inactive precursor pepsinogen, then exported into the interior of the stomach and activated by high concentrations of HCl(69). There are also examples of proteins that have precursor domains acting as chaperones, removed after the eventual mature domain has folded correctly and becomes active. Examples of these proteins include bacterial enzymes subtilisin and alpha-lytic protease and the mammalian protein bovine trypsin inhibitor(70-72). Finally, precursor domains are responsible for localization within the cell and for export out of the cell. An example of this type of precursor domain can be found in the IL-1 family, secreted IL-1Ra has an N-terminal, 22-residue precursor sequence that directs it to the classical ER/Golgi secretion pathway(9). Despite significant interest in targeting pro-IL1β and its cleavage products for

therapeutic control, molecular insights into the role the precursor domain plays in regulating the structure, folding and subsequent function of the cytokine is not readily available.

The current work uses a number of biophysical techniques to characterize the native state and processing of pro-IL-1β. The fluorescence-detected studies of the pro-protein indicate that the tryptophans are sequestered from solvent in the native protein and that the protein undergoes a cooperative unfolding transition upon denaturation(73). However, comparison of the thermodynamic stabilities of the pro- and mature proteins indicates that the pro-protein is 4.3 kcal/mol less stable than the mature cytokine. A combination of size-exclusion chromatography (SEC) and pulsed field gradient (PFG) NMR experiments reveal that the pro-protein exists in a loosely compact conformation under native conditions. Comparison of the heteronuclear ^{1}H-^{15}N HSQC of the pro- and mature proteins reveals that the protein is not in a single, well-defined conformation prior to processing and likely exists as an ensemble of inter-converting states. Finally, analysis of the enzymatic processing of pro-IL-1β and mutant proteins D27A and D116E reveals that ICE cleavage is not sequential as previously thought, and does not require conformational changes subsequent to initial cleavage for full processing to the mature form(68). Taken together, our studies indicate that the prodomain inhibits the formation of the stable, mature cytokine and that pro-IL-1β is a cooperatively folded, but destabilized protein that is readily available for processing to the active cytokine upon protease exposure.

SPECIAL METHODS

Heteronuclear NMR

The ^{1}H-^{15}N heteronuclear single-quantum coherence spectra of pro- and mature IL-1β were collected on a Bruker DMX spectrometer with an operating frequency of 800 MHz equipped with a gradient probe. The 500 μM sample was exchanged into 90 mM NaPO4, pH 6.8, 50 mM KCl buffer, and 10% final volume of D_2O was added. The ^{1}H dimension was directly referenced to DSS.

Pulsed-Field Gradient NMR

All experiments were collected on a Bruker DMX 500.13 Hz spectrometer equipped with a standard 5mm triple-resonance gradient probe. The spectrometer was calibrated before each experiment on a sample of 99.9% D_2O as described(74). A standard BP-LED pulse program was used(75), equipped with a rectangular shaped gradient pulse for sample gradient calibration. The total pulse length δ (pulse length 2x) was set to 2600 μs in the Z direction, and 3250 μs in the X and Y directions. The diffusion delay Δ was set to 0.05 s for all directions, and the gradients were calibrated over the range of 5-95% strength in 5% increments, with the signal reaching zero by <95%.

Pro-IL-1β (300 μM) was exchanged into 30 mM d^3-Bis-Tris, pD 6.5, 90 mM KCl, in 99.9% D_2O (Isotec), with and without the addition of 2.0 M Gdn-HCl (equilibrated for 24 hrs). The pulse sequence used was a BP-LED program with an added WATERGATE sequence for water suppression(74). The acquisition

parameters δ and Δ were calibrated for each sample in the X, Y and Z directions. Typically, δ was set to 5800 - 6000 μs for X and Y directions and 4800- 5200 μs for the Z direction, and Δ was set to 100-110 μs. The data were acquired in a pseudo 2D fashion to allow for changing the gradient strength. The gradient strength was increased incrementally, first by 1% steps for the first 15 steps (5-20%), then in 5% increments until at 95%. The total number of data sets was 31 for each experiment, with the number of real points set at 2048 and spectral width set to 14 ppm. All experiments were collected at 298K.

Data Processing and Analysis

The D_2O diffusion gradient calibration was performed as reported previously(74), yielding the established diffusion coefficient of 1.90 e^{-5} cm^{-2}/s(76). The diffusion data for the pro-IL-1β samples was processed using the SpinWorks program(77). The baseline for each spectrum was corrected by integrating a region of the spectrum absent of signal, then subtracting it from area calculated for the protein. The signal from the aliphatic region of the protein spectrum was integrated for the diffusion coefficient calculations, since the amide region was susceptible to artifacts owing to the presence of Gdn-HCl or exchange processes. The normalized integral volumes, or signal intensity I, were fit to Equation 5:

$$I = I_0 e\left[-(\gamma G\delta)^2 D\left(\Delta - \frac{\delta}{3} - \frac{\tau}{2}\right)\right] \qquad (3.1)$$

where I_0 is the initial intensity, γ is the gyromagnetic ratio (26750 (gauss*cm)$^{-1}$), G is the gradient strength, δ is the length of the gradient pulse, Δ is the length of the diffusion delay, τ is the length of the gradient recovery delay (300 μs), and D is the diffusion coefficient. The resulting diffusion coefficients in the X, Y and Z directions were calculated and converted to hydrodynamic radius (r_h) by using the following relationship:

$$r_h^{\text{Protein}} = \frac{D_{BPTI}}{D_{\text{Protein}}}(r_h^{BPTI}) \qquad (3.2)$$

The protein bovine trypsin inhibitor (BPTI) was used as an external control to account for changes in viscosity in the sample upon addition of Gdn-HCl. The hydrodynamic radius values were calculated based on the published hydrodynamic radius of 15.2 Å (78) and experimentally determined D of 1.64E-06 for BPTI(74).

RESULTS

IL-1β is synthesized as a 31 kD proprotein and remains a soluble, inactive species in the cytoplasm until cleaved and secreted from activated macrophages and monocytes(29). Unlike the intracellular pro-IL-1α protein which can bind the receptor, pro-IL-1β cannot but instead, the pro-region of IL-1β is proposed to maintain the mature region of the sequence in a partially folded (intermediate) configuration that is

secretion competent(10,11,53). Detailed analysis of the structure, stability and processing of pro-IL-1β have been hampered in the past by the lack of sufficient quantities of protein and/or the degradation of the precursor protein during isolation(79). We overcame these problems and can now produce and purify large quantities (tens of milligrams in a single prep) of the pro-IL-1β. A key development in our purification strategy was the finding that both pro- and mature IL-1β could be recovered from *Escherichia coli* cells by simple osmotic shock (see Chapter 2). This feature limits the exposure of the pro-protein to non-specific protease degradation and greatly reduces our purification time. The proprotein is not amenable to X-ray nor NMR structure determination methods and we focus here on lower resolution methods that give us insight into the structure of pro-IL-1β and the effect of the N-terminal 116 residues on the conformation and stability of the C-terminal 153 residue protein.

Pro-IL-1β Displays a Relatively Compact Native-State and Non-cooperative Folding

Our first approach to determining whether or not the native state of pro-IL-1β was in an unfolded conformation was to characterize the solution behavior of the purified protein. Pro-IL-1β can be expressed as a soluble protein in the *E. coli* BL21 (DE3) strain (Invitrogen) in mg/l amounts following the procedure detailed in the Materials and Methods chapter of this thesis (Chapter 2) and analyzed by SEC. In general, unfolded proteins have larger hydrodynamic radii due to the random-coil like behavior, and are therefore excluded from the column matrix. Smaller proteins elute later due to diffusion into the pores of the matrix(79). The SEC chromatograph of

pro-IL-1β is given in Figure 3-1. The protein elutes as a single, well-resolved peak at 72 mL after the void volume (100 mL for a S-200 column (GE Healthcare)). By comparison, carbonic anydrase MW standard (Sigma, 29 kDa, elutes at 94 ml, Figure x) under the same conditions. If pro-IL-1β was indeed unfolded, it would elute much earlier as the matrix of the SEC column separates based on hydrodynamic radius (r_h). These initial studies suggest that pro-IL-1β is expanded relative to what is expected for a 31 kD protein but folded into a loosely compact structure.

Since pro-IL-1β appeared to be in a collapsed state by the low-resolution sizing method of SEC chromatography, equilibrium unfolding studies were performed (as described in the Materials and Methods chapter of this thesis). All experiments were performed on a FluoroMax-2 fluorescence spectrometer at 25 °C. Since there

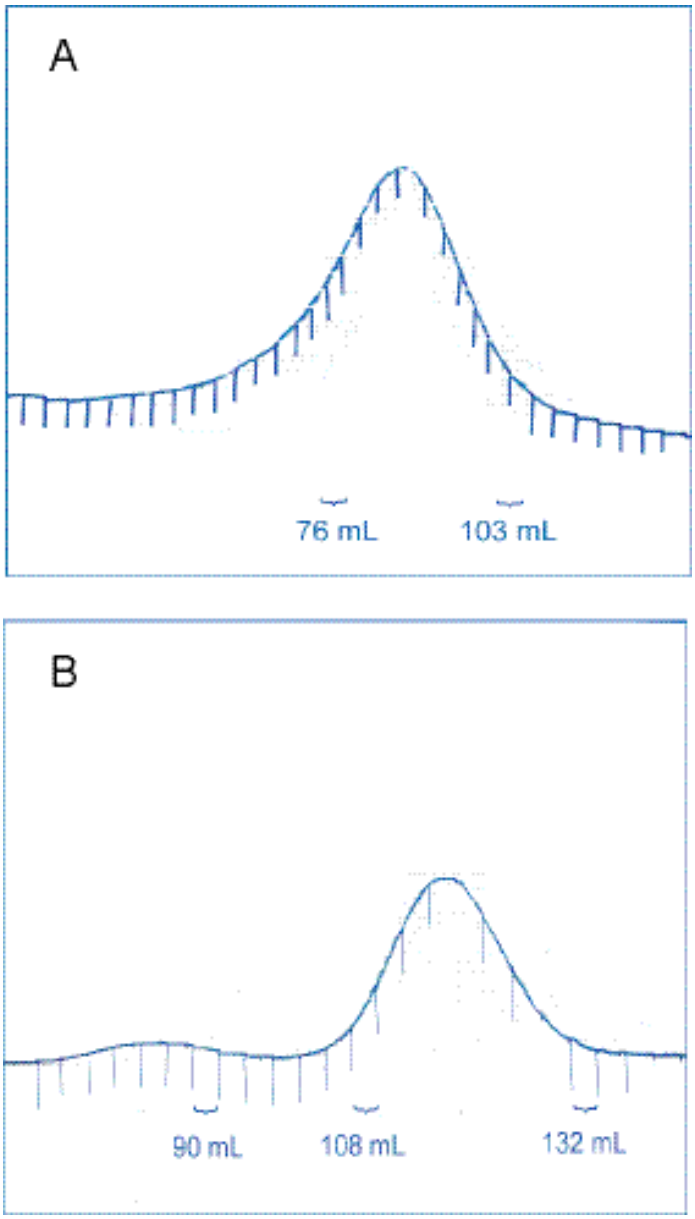

Figure 3-1: Size-exclusion chromatograms for (A) pro-IL-1β and (B) carbonic anhydrase. Pro-IL-1β and carbonic anhydrase were run on a S-200 size exclusion column under the same buffer conditions and at the same flow rate. The elution volumes are indicated on each chromatogram, subtracting the 100 mL void volume of the column.

are two tryptophans in the pro-IL-1β sequence (W108 and W236), the excitation wavelength was set at 293 nm and the emission was measured in the range of 300-450 nm. The fluorescence spectra of native pro-IL-1β is shown in Figure 3-2. The observed maximum intensity signal over the range of 300 – 450 nm with an excitation wavelngth 293 nm indicates that there is an increase then decrease of fluorescence, which is also exhibited to a larger degree by the mature protein. An overlay of the fluorescence spectra for one representative titration is given in Figure 3-2. The normalized fluorescence intensity was plotted as a function of final Gdn-HCl concentration and is given in Figure 3-3. For comparison, the results obtained for mature IL-1β are plotted in Figure 3-3. The data were fit to a 2-state model as described (Materials and Methods), and the resulting ΔG and m values are listed in Table 1.

Since the two tryptophan residues of pro-IL-1β reside one each in the N-terminal (W108) and C-terminal (W236) domains of the protein, W108L and W236L and W236F mutants were made. The W108L mutant was purified as the wt protein. Interestingly, the W236 mutants were either insoluble (W36L) or unstable (unpublished observations). An overlay of the fluorescence spectra of W108L as a function of denaturant concentration is and the resultant equilibrium unfolding curve is given in Figure 3-4. The ΔG and m-values are given in Table 3-1. We observe that there is no difference in stability for the W108L mutant.

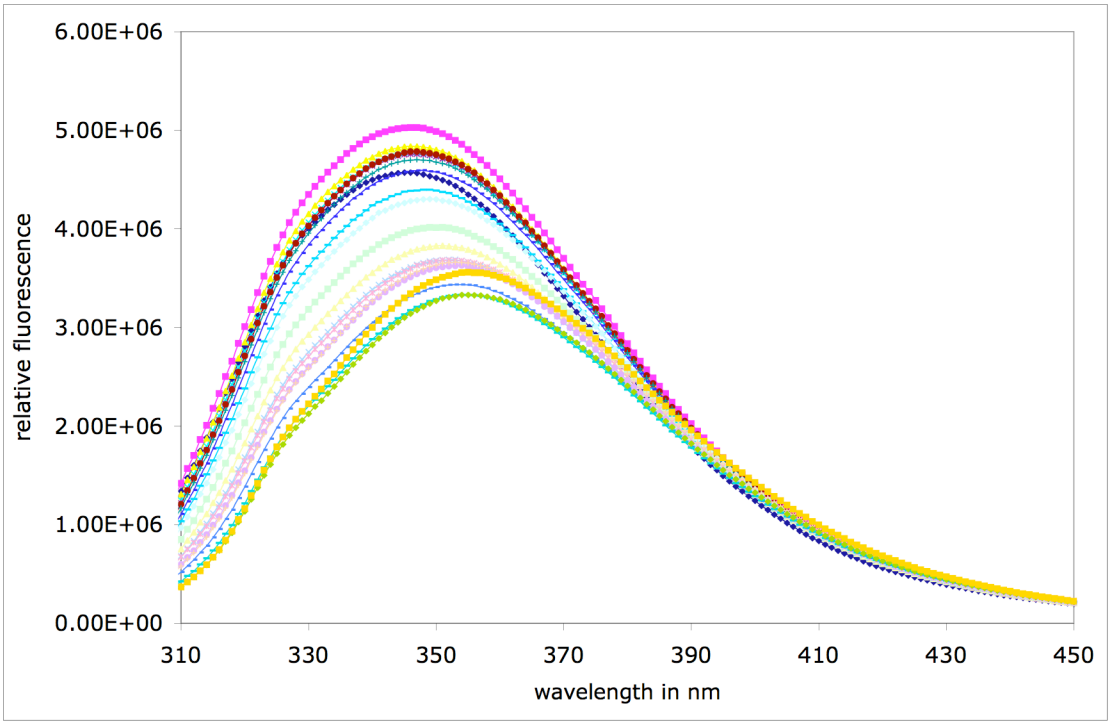

Figure 3-2: Overlay of the fluorescence spectra from an equilibrium unfolding titration of pro-IL-1β. Fluorescence spectra were collected over a wavelength range of 300 – 450 nm, over a range of denaturant concentrations at an excitation wavelength of 293 nm. The emission maximum of the two Trp residues of pro-IL-1β (108 and 236) is red-shifted with increasing concentrations of denaturant (354 to 363 nm), indicating a change in the local environment of the tryptophan indole ring. The fluorescence intensities were normalized and used to calculate the thermodynamic stability of pro-IL-1β.

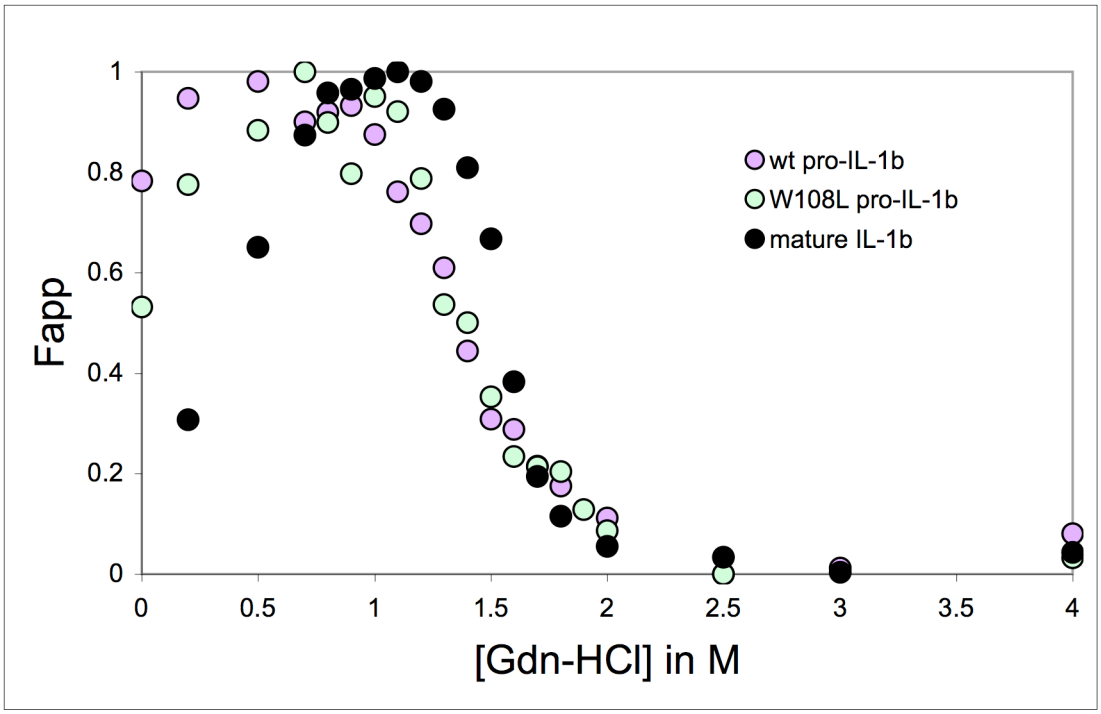

Figure 3-3: Equilibrium titration curve overlay of pro- and mature IL-1β, and W108L mutant of pro-IL-1β. The normalized fluorescence intensities from equilibrium unfolding titrations of pro- and mature IL-1β over 0 – 4 M Gdn-HCl are shown here. The curve was fit to a 2-state model of folding (U → N) to determine the stability (ΔG) and the cooperativity (m-value) of the transition.

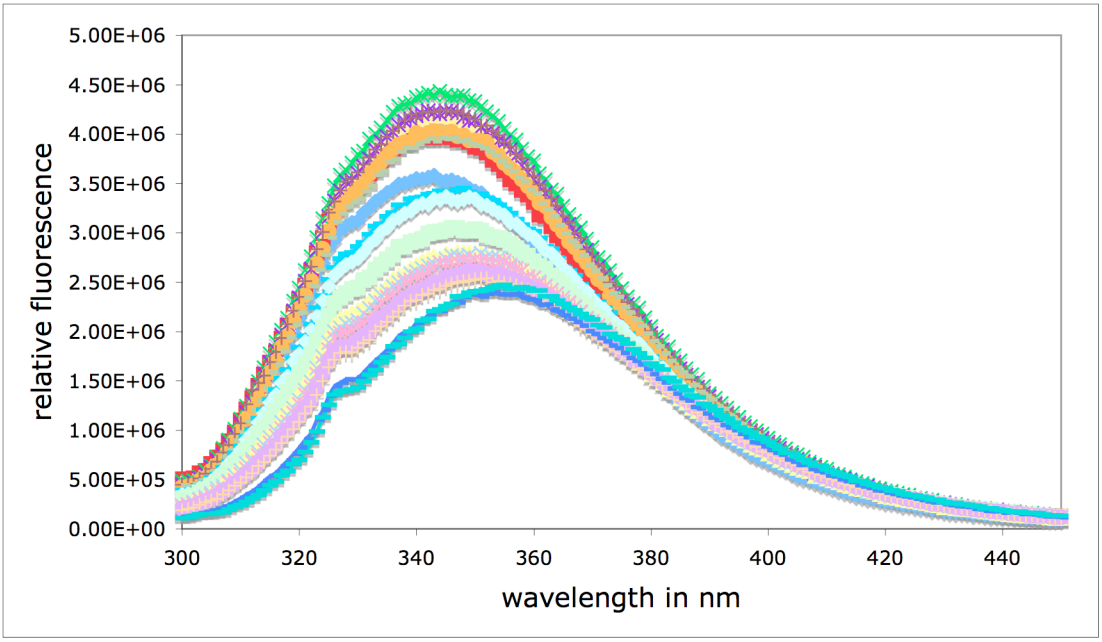

Figure 3-4: Overlay of the fluorescence spectra from an equilibrium unfolding titration of W108L pro-IL-1β. Fluorescence spectra were collected over a wavelength range of 300 – 450 nm, over a range of denaturant concentrations at an excitation wavelength of 293 nm for the W108L mutant of pro-IL-1β. The emission maximum of the lone remaining Trp residue of pro-IL-1β (236) is red-shifted with increasing concentrations of denaturant (352 to 362 nm), indicating a change in the local environment of the tryptophan indole ring. The fluorescence intensities were normalized and used to calculate the thermodynamic stability of W108L pro-IL-1β.

Table 3-1: Thermodynamic parameters for wt and W108L pro-IL-1β and mature IL-1β

	ΔG_{NU}[a,b] (kcal*mol^{-1})	$\Delta\Delta G_{NU}$[a,b] (kcal*mol^{-1})	m-value[a,b] (kcal*mol^{-1}*M^{-1})	C_m[c] (M)
Wt pro-IL-1β	3.5 ± 0.6	-3.8 ± 0.4	2.5 ± 0.4	1.4
W108F pro-IL-1β	3.8	-3.5	2.7	1.4
Mature IL-1β	7.3 ± 0.1	0	4.9 ± 0.1	1.5

Changes in folding parameters between pro-IL-1β and mature IL-1β. The equilibrium data were fit using MATLAB in order to obtain equilibrium parameters for folding, ΔG_{NU}. Changes in ΔG_{NU} ($\Delta\Delta G_{NU}$) were obtained using mature IL-1β as a reference. m-value indicates changes in the accessible surface area upon folding and indicate cooperativity of the folding transition.

[a]Equilibrium transition data were evaluated using a two-state model.

[b]Data were obtained by calculating the average fluorescence intensity and calculating the relative fluorescence intensity in terms of F_{app} as a function of [Gdn-HCl].

[c]C_m values are determined by dividing ΔG_{NU} by the m-value.

Structural Heterogeneity of Native Pro-IL-1β is Apparent by 2D Heteronuclear NMR

2D ^{1}H-^{15}N heteronuclear single-quantum coherence (HSQC) spectra are used routinely by protein biochemists to show how well a protein is folded before structure determination(80). The spectra show each backbone amide resonance (except for proline) as a single crosspeak for well-ordered proteins(80). The peak intensity, and line shape of each peak is dependent upon the surrounding environment as well as chemical exchange processes such as inter-conversion between stable states. The HSQC of mature IL-1β displays well-resolved amide resonances with a large amount of chemical shift dispersion, characteristic of the extended β-strand network within the protein (Figure 3-5a). In contrast to this observation, the HSQC spectrum of pro-IL-1β displays poorly resolved peaks with limited chemical shift dispersion (Figure 3-5b). These spectral signatures indicate an overall lack of well-ordered secondary structure and a heterogeneous native state in the proprotein.

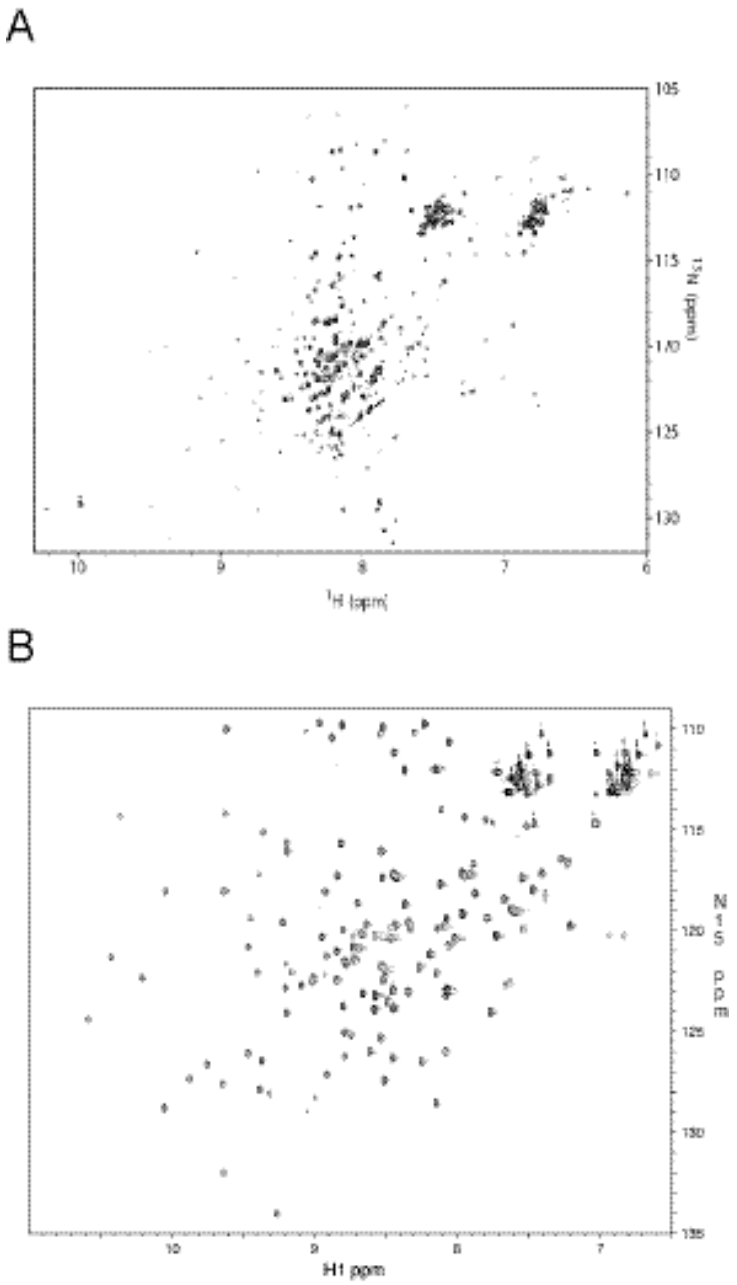

Figure 3-5: ^{1}H-^{15}N HSQC spectra of pro- (A) and mature (B) IL-1β. The HSQC experiment provides a "fingerprint" of the amide backbone and select side-chain residues of ^{15}N- isotopically labeled proteins. The spectrum for pro-IL-1β (A) exhibits the characteristics of a highly-dynamic, flexible native state, showing broad resonances and lack of peak dispersion. The spectrum of mature IL-1β (B) is indicative of a well-ordered, β-structure, with good peak dispersion and signal. This indicates that the structure of the mature domain within the pro-IL-1β sequence is significantly altered.

PFG-NMR Analysis of Pro-IL-1β Reveals a More Extended Structure for the Native State

The hydrodynamic radius of a protein gives a snapshot of the average dimensions of its conformational ensemble in solution(81). The hydrodynamic radius (r_h) is dependent on the translational diffusion of the protein in solution. This relationship is given by the Stokes-Einstein Equation:

$$r_h = \frac{k_B T}{6\pi\eta D} \tag{3.3}$$

where D is the diffusion coefficient, T is temperature, k_B is the Boltzmann constant, and η is the viscosity of the solution(82). There is a well-studied relationship, or power law, between sequence length and r_h for compact, globular proteins and for highly denatured, random-coil like proteins(81,82). Recently, a power-law for intrinsically disorder proteins (IDPs) was described by Marsh, et. al(82). Intrinsically disordered proteins (IDPs) are suggested to differ from the typical random-coil conformations observed in high denaturant concentrations in that they contain a number of charged residues and prolines, which can confer some local elements of ordered structure. Therefore, these proteins are predicted to be more compact than random coil, but much less compact that a folded, globular protein.

The PFG-NMR methodology was implemented on a Bruker DMX 500.13 MHz spectrometer by a former graduate student from our lab, Dr. Nicole K. Kruse(74). She measured the diffusion coefficients of mature IL-1β over a range of Gdn-HCl concentrations, effectively generating the equilibrium unfolding curve for this protein(74). Using BPTI as an external viscosity standard, she determined the hydrodynamic radius of mature IL-1β is 21.89 ± 0.30 Å in 0M and 42.41 ± 0.46 Å at 2M Gdn-HCl at pH 6.5 and at 308K. A plot of the observed average aliphatic peak intensities from representative data sets at 0 and 2M Gdn-HCl are given in Figure 3-6. The fit of the data to the single exponential model as described the methods section in this chapter is also given in Figure 3-6. The compaction factors (C) were also calculated, using Equation 3.4:

$$C = \frac{r_h^D - r_h}{r_h^D - r_h^N} \qquad (3.4)$$

where r_h^N is the predicted radius for the native protein based on sequence, r_h^D is the predicted radius for the denatured protein based on sequence length, and r_h is the measured radius. The power law used to determine r_h of a native, globular protein with N residues is:

$$r_h^N = 4.92N^{0.285} \quad (3.5)$$

and the power law for the r_h of denatured protein, or a random-coil is:

$$r_h^D = 2.33N^{0.549} \quad (3.6)$$

These constants were determined from experimentally-determined r_h values available in the literature(81,82). A new power law for IDP was determined by Marsh, et. al, yielding the equation:

$$r_h^{IDP} = 2.49N^{0.509} \quad (3.7)$$

Since IDPs are more compact than a true random coil, there is a divergence from the traditional native and denatured power laws(82,83). The theoretical r_h values for pro-IL-1β using all of the above power laws are also located in Table 3-2.

A

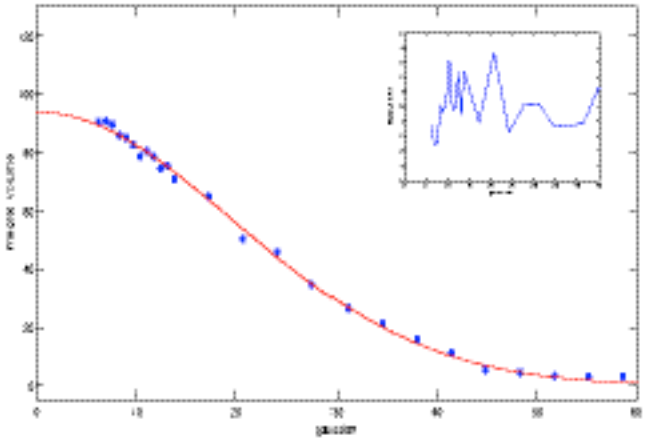

B

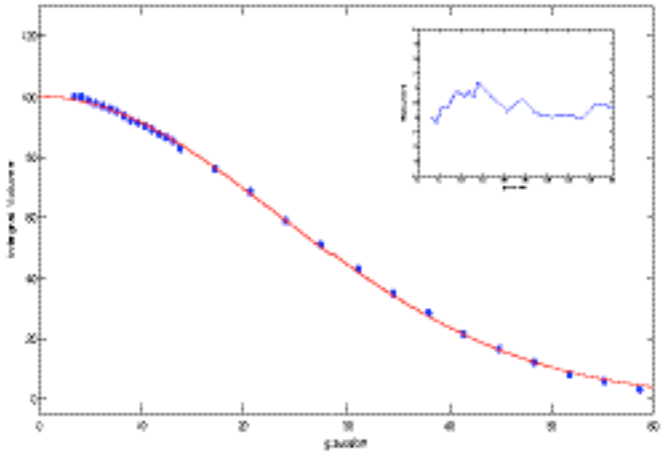

Figure 3-6: PFG decay curves for pro-IL-1β in 0M (A) and 2M (B) Gdn-HCl. The average aliphatic peak intensity for pro-IL-1β is plotted over the range of gradient pulse strengths (5 – 95%). The data was fit to Equation 3-1 to obtain the diffusion coefficient of pro-IL-1β at two Gnd-HCl concentrations. The residuals of each fit are shown in the insets.

Table 3-2: Experimental and predicted r_h of pro- and mature IL-1β

	$r_h^{[0M]}$ [a] (Angstroms)	$r_h^{[2M]}$ [a] (Angstroms)	r_h^{N} [b] (Angstroms)	r_h^{IDP} [b] (Angstroms)	r_h^{D} [b] (Angstroms)	C_f [c] (Angstroms)
Wt pro-IL-1β	29.7 ± 0.1	44.9 ± 1.7	24.1	48.2	53.6	0.81
Mature IL-1β	21.9 + 0.3	42.4 + 0.5	20.6	n.d.	36.9	0.92

Changes in hydrodynamic radius between pro-IL-1β and mature IL-1β. The data were fit using MATLAB to Equation 3.1 in order to obtain the diffusion coefficient, D. The r_h values were determined by using the published value BPTI using Equation 3.2.

[a]Experimentally determined r_h values at 0M and 2M Gdn-HCl for mature IL-1β is reported in (nicole's thesis).

[b]Theoretical r_h values were determined using Equations 3.5, 3.6 and 3.7, and a chain length of 269 residues for pro-IL-1β and 153 residues for mature IL-1β.

[c]C_f values were determined by using Equation 3.4.

Pro-IL-1β Cutsite Mutants Show Preference for First Cutsite by Caspase-1

Pro-IL-1β is processed *in vivo* by the cystiene protease caspase-1(56). Cystiene proteases recognize and cleave after an aspartate residue (P_1 position in the protease recognition motif). Caspase-1 belongs to the pro-inflammatory side of the caspase family, whereas the other side is pro-apoptotic (including caspase-3 and 7)(84). Caspase-1 recognizes two Asp residues in the pro-IL-1β sequence, D27 and D116 (thornberry). The consensus recognition motif in the N-terminus-$P_4P_3P_2P_1 \mid P_{1'}P_{'}$-C-terminus motif for caspase-1 is -YEVD | GW-(85). The sequence and placement of cutsites in pro-IL-1β is illustrated in Figure 3-7, along with a schematic of how the mature protein may be generated by caspase-1.

The enzymatic digest assays of wt pro-IL-1β and the D27A and D116E mutants were performed as described in Chapter 2 of this thesis. Representative gels of the enzymatic cleavage reactions are shown in Figure 3-8a,b,c for wt, D27A and D116E, respectively. The wt pro-IL-1β time course shows the appearance of the longer 28 kD species first, followed by the 17 kD mature protein and 11 kD truncated N-terminal species. The D27A gel shows after a slight lag the appearance of the 17 kD mature protein, along the 14 kD N-terminal region. The D116E gel shows quick conversion of the full-length protein into the 28 kD cleavage product.

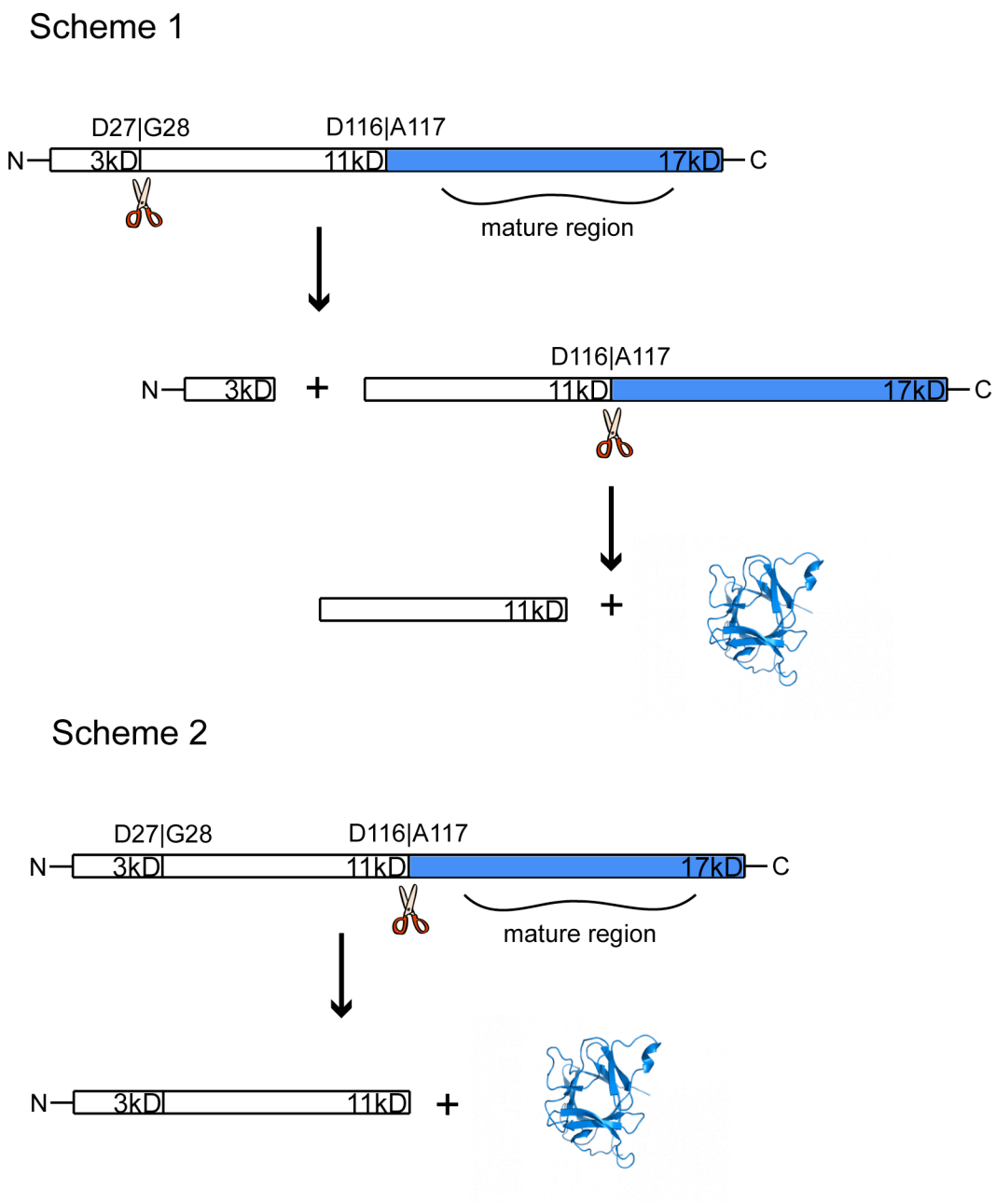

Figure 3-7: Schematic for the caspase-1 cleavage sites in pro-IL-1β. Scheme 1 shows cleavage at cutsite 1 (D27) first, generating a 3 kD piece and a 28 kD piece. A second cleavage event at cutsite 2 (D116) generates an 11 kD piece and a 17 kD piece that folds mature protein. Scheme 2 shows the cleavage products after cleavage at cutsite 2 takes place first, generating a 14 kD piece and the mature protein. Only the 3 kD, 11 kD, 17 kD and 28 kD pieces have been detected *in vivo*.

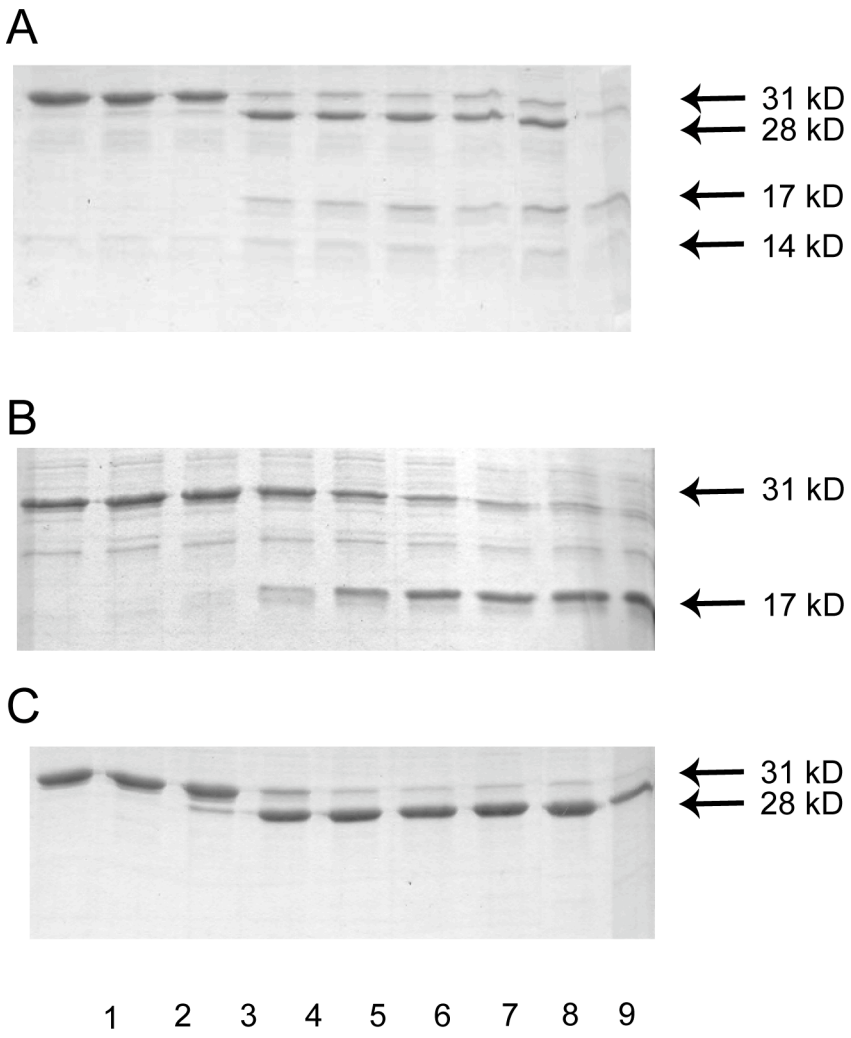

Figure 3-8: Representative gels of wt, D27A and D116E mutants of pro-IL-1β cleavage by caspase-1. (A) In the wt pro-IL-1β caspase-1 digestion reaction, a band at 28-kD accumulates before the appearance of the 17-kD band for the mature protein, indicating cutsite 1 is preferentially recognized and processed first. (B) The D27A mutant cleavage profile indicates that it is not necessary for pro-IL-1β to be first cleaved at cutsite 1 in order for caspase-1 to gain access to cutsite-2. (C) The 28 kD species is readily generated from the cleavage of the D116E mutant. The numbers 1-9 indicate control (no enzyme), 0 sec (directly into quench), 5, 15, 30, 60, 120, 240, 1440 min, respectively, for all three gels.

DISCUSSION

The Life-Cycle of Interleukin-1β is Tightly Regulated

IL-1β initiates a long list of cellular responses, both positive and negative. The main recognized function of IL-1β is to initiate the innate immune response to a variety of pathogenic or stress-related challenges(2,3,15). Misregulation of this potent cytokine leads to deleterious effects that are global (sepsis) and local (tissue remodeling, growth factor stimulation, protease upregulation, metabolite regulation) that lead to various disease states(15,16,43). IL-1β gene transcription, translation, post-translational processing and secretion are highly-regulated, decoupled processes(29,62,86). While monocytes and macrophages are responsible for producing the majority of mature IL-1β, other cell types also translate and express the gene in varying degrees. The expression and secretion of the active cytokine are also cell-type dependent(29,62).

Due to its universal influence on a broad range of cells, the life-cycle of IL-1β is controlled at multiple steps. Synthesis of IL-1β as an inactive, protease-sensitive precursor protein provides one check-point for the cycle. The intracellular half-life for pro-IL-1β is ~2.5 hours(29,64), which is considered to be in the rapid turnover category(87). *In vitro*, pro-IL-1β is extremely sensitive to protease degradation and must be handled using multiple protease inhibitors (Hazuda, observations), whereas mature IL-1β is highly protease-resistant(53,79). Hazuda, et. al outlined several hypothesis for why the mature cytokine is kept in this precursor form. They

postulated that the precursor may provide a folding nuclei for the mature protein, differing protease lability of the pro- vs. mature form may control the duration of its activity, and additional processing of the precursor to active cytokine may put limits on the time and place of its activity(53). Recent studies including NALP-3 inflammasome activation of caspase-1 and the subsequent processing of pro-IL-1β have shown that the processing and secretion are closely timed, there is little to no intracellular build up of the mature species(46,63,66,67,88,89). Coupling the short half-life of pro-IL-1β and the secondary signal required for activating caspse-1 to process it into the mature form and its subsequent exit from the cell, there is only a small window for cells to introduce active, mature IL-1β into the extracellular environment.

Pro-IL-1β is in an Extended Conformation Relative to Mature IL-1β

Earlier studies of pro-IL-1β showed evidence of a conformational change upon protease activation(53). This conformational change is responsible for activating the C-terminal region of the protein. In order to determine initial state of the C-terminal domain is in before it processed into the mature domain, it is necessary to first characterize the precursor protein. Our initial size exclusion chromatography results indicated that pro-IL-1β is expanded relative to what would be expected for a compact, globular protein of 31 kD. The diffusion coefficients of mature IL-1β at 0M and 2M Gdn-HCl were measured previously. These values were used to determine the r_h to be 21.9 $\pm$ 0.3 Å in 0M and 42.4 $\pm$ 0.5 Å at 2M Gdn-HCl. In contrast, the r_h values

for pro-IL-1β were found to be 29.7 $\pm$ 0.1 Å and 44.9 $\pm$ 1.7 Å for 0M Gdn-HCl and 2M Gdn-HCl, respectively. The predicted r_h values calculated using the power law relationship are given in Table 3-2.

The predicted value of r_h for a protein of pro-IL-1β's size without denaturant is less (24.06 Å). The assumption using the globular protein power-law relationship is that the protein is well-folded and compact (with a compaction factor = 1)(90). Another power-law for intrinsically disordered proteins, or IDPs, was compiled from available literature data and formulated by Marsh, et. al(82). IDPs are proteins that are extended but not fully denatured. These proteins lack a hydrophobic core for folding, but their sequences contain charged residues or prolines. These residues confer a collapse in the random-coil structure(82). Since pro-IL-1β does contain regions of highly charged residues in the precursor and mature sequence (residues preceding and near Cutsite 1, D27, a conserved acidic region, 98-105, the region encompassing the β-bulge in the mature protein, 163 – 171, and the region corresponding to the basic 90's loop in the mature protein, residues 200-215). Using the IDP power-law, pro-IL-1β would have an r_h value of 48.16 Å. Finally, the denatured protein power-law prediction for pro-IL-1β is 53.6 Å. Taken together, the hydrodynamic radius of native pro-IL-1β lies between a compact, globular protein and an intrinsically disordered protein on the power law scale.

The compaction factor for the mature protein is 0.92 (Table 3-2). The slight deviation from the native power-law is most-likely due to the nature of the hydrated structure of mature protein(91). The compaction factor for pro-IL-1β is 0.81 (see

Table 3-2). Compaction factor variances are seen when proteins undergo conformational changes upon a binding event. For example, the Apo version of Ca^{+2}-binding protein calmodulin has a compaction factor of 0.75, while the bound version has a compaction factor of 1.0(90). Since r_h is a measurement of the average conformation in solution, the conformation of pro-IL-1β is likely to be extended as compared to the mature protein. This more extended, or looser confomation most likely contributes to the differences in protease sensitivity between pro- and mature IL-1β, since more recognizable cutsites are exposed to non-specific proteases like chymotrypsin. Both sequences of pro- and mature IL-1β have cutsites throughout their sequences, both only pro-IL-1β is susceptible to being cleaved (Chapter 4).

^{1}H-^{15}N 2D NMR Spectra of Pro-IL-1β as Compared to Mature IL-1β Shows Lack of Ordered Structure

^{1}H-^{15}N HSQC spectra provide a fingerprint of the backbone and side-chain amides in solution. Folded and well-structured proteins generally give well disperse peaks in the amide region of the spectrum with chemical shifts ranging from 10.5 to 6.5 ppm (ref). In general, when proteins go from the native state to unfolded, the chemical shifts collapse to the middle of this amide region. While the chemical shifts of unfolded proteins have collapsed, their line shape is sharp and peaks are intense (Wright). HSQC spectra of proteins during a refolding reaction display significant line-broadening due to structural fluctuations on the μs-ms timescale, making peaks appear less intense (Dyson, PNAS). However, resonances corresponding to the native

structure start to appear, and peaks start to display chemical shift dispersion. Instead of unfolded, the spectrum of pro-IL-1β displays the characteristics of a protein during a refolding reaction. Although there is significant peak overlap in the middle of the spectrum, weak peaks seen in the wider range indicate the existence of structure, as in a folding intermediate (or ensemble) (ref). In contrast, the HSQC spectrum of the mature protein (Figure 3-6) has well-resolved, intense peaks indicative of its highly-ordered, stable structure.

Pro-IL-1β Has a Less Cooperative Unfolding Transition as Compared to Mature IL-1β

Proteins that fold via a highly cooperative, 2-state equilibrium folding trajectory displays a large-denaturant dependence, or m-value. In the case of mature IL-1β, the equilibrium unfolding/refolding trajectory has been well-established to be highly cooperative and 2-state (Jennings lab refs). In contrast to this, non-cooperative transitions are broader or less sharp, and therefore exhibit less denaturant dependence for unfolding (lower m-value). This indicates a partially-folded or flexible protein, or a heterogeneous native state. Since the SEC chromatogram of pro-IL-1β did not show the protein eluting as two peaks, the non-cooperativity in the folding transition most likely arises from the partially folded and dynamic nature of its native state. The thermodynamic stability (ΔG_{NU}) of pro-IL-1β is also diminished, indicating there is a less energy added into the pro-IL-1β native state upon folding.

Caspase-1 Can Access Both Cutsites in Full-Length Pro-IL-1β

Caspase-1 cleaves pro-IL-1β in two places, after D27 and D116 of the N-terminal prodomain. All of the cleavage products outlined in Figure 3-7 have been detected in cells and extracellularly (refs). Processing *in vivo* shows that caspase-1 firsts generates the 28 kD piece. Over time, the mature protein appears, along with the 11 kD piece. Swaan, et. al, proposed that processing at the first cutsite (D27) was necessary, leading to a conformational change in the protein making the second site (D116) accessible. In order to test this model, two cutsite mutants were made, D27A (cutsite 1) and D116E (cutsite 2). Running analogous caspase-1 cleavage reactions side-by-side with the wt protein, we show that the 28 kD product appears before the 17 kD piece in the wt protein. However, in the cutsite 1 mutant, the 17kD piece appears in the same timeframe as the 28 kD product in either the wt protein or D27A mutant, demonstrating that the accessibility of D116 is not dependent on cleavage at D27 first. Interestingly, all of the wt protein is converted first to the 28 kD species before the build-up of the 17 kD mature protein. This may be due to a preference for the first cutsite by caspase-1 perhaps indicating this area of the precursor protein is exposed. As discussed in Chapter 1, the N-terminal region of pro-IL-1β has less conservation than the mature region. Both caspase-1 cutsites are conserved over species, especially in mammals. Therefore, it is possible that the small, 3 kD piece may have its own function, requiring processing by caspase-1 to release it. Further *in vivo* studies are required to determine if this is true.

CONCLUSION

The presence of the N-terminal precursor region greatly impacts the eventual mature region in IL-1β. Solution NMR and SEC methods show that pro-IL-1β is in a dynamic, expanded conformation, differing greatly from the compact, well-ordered structure of the mature protein. 2D-NMR, fluorescence and equilibrium denaturation titrations indicate that even though the protein is an a loosely packed confirmation as compared to the mature protein, there is some residual structure that remains, most likely in the eventual mature region. Further investigation is required to determine how much of the eventual mature region is folded, and what conformation(s) it maintains while in the presence of the precursor region.

Chapter 4

Pro-IL-1β Shares a Core Region of Stability as Compared with Mature IL-1β While Maintaining a Distinctly Different Configurational Landscape: a Comparative Hydrogen/Deuterium Exchange Mass Spectrometry (DXMS) Study

ABSTRACT

Interleukin-1β (IL-1β) is a master cytokine involved in initiating the innate immune response in vertebrates (3). It is first synthesized as an inactive 269-residue precursor (pro-interleukin-1β, or pro-IL-1β). Pro-IL-1β requires processing by caspase-1 to generate the active, mature 153-residue cytokine. In this study, we combined hydrogen/deuterium exchange mass spectrometry, circular dichroism spectroscopy, and enzymatic digestion comparative studies to investigate the configurational landscape of pro-IL-1β and the role the N-terminus plays in modulating the landscape. We find that the N-terminus keeps pro-IL-1β in a protease-labile state while maintaining a core region of stability in the C-terminal region, the eventual mature protein. In mature IL-1β, this highly protected region maps back to the area protected the earliest in NMR studies characterizing an on-route kinetic refolding intermediate. This protected region also encompasses the two important functional loops that participate in the IL-1β/receptor binding interface required for biological activity. We propose that the purpose of the N-terminal precursor region in pro-IL-1β is to suppress the function of the eventual mature region while keeping a structurally and also functionally important core region primed for the final folding into the mature protein's native, active state. The presence of the self-inhibiting precursor region provides yet another layer of regulation in the life cycle of this important cytokine.

INTRODUCTION

Nearly all cell types respond to IL-1β, in a very sensitive manner, via the binding of it to the interleukin-1 receptor type 1 (IL-1RI) (92). While essential in the immune response, overproduction of IL-1β can lead to both acute (sepsis) as well as chronic (rheumatoid arthritis, atherosclerosis, obesity, diabetes) disease states (15). Thus, the expression, activation and secretion of this cytokine are tightly controlled (16). Although many cell types express IL-1β, it is predominately produced and secreted by monocytes and macrophages (3). The protein is synthesized as a biologically inactive 269-residue precursor molecule, pro-IL-1β, and the 153-residue active, mature IL-1β is generated from the C-terminal domain. The processing of the proprotein involves the recently discovered NALP-1 and NALP-3 inflammasomes, that are responsible for activating procaspase-1 (66). The inflammasome function is integral in wound repair as well as for combating infection (46,88,93,94).

In vivo, the 31-kD pro-IL-1β precursor is processed to the active C-terminal 17-kD form by the interleukin-1 converting enzyme, caspase-1 (56,95). Caspase-1 is a cysteine protease that recognizes two cleavage sites in pro-IL-1β, the D27↓G28 and D116↓A117 peptide bonds (Figure 4-1a). These cleavage sites are conserved across mammals (96-98). The activation pathway is believed to proceed with cleavage first at D27↓G28 (Site 1) followed by D116↓A117 (Site 2). These processing events lead to the generation of the mature, active IL-1β from the C-terminal domain of pro-IL-1β (99). After cleavage, the mature protein is exported via a cell-specific non-classical pathway {Rubartelli, 1990 #20}. The events leading from caspase-1 activation to

active IL-1β secretion are poorly understood and constitute an area of active research (63,100-103).

The native structure of IL-1β is classified as a beta-trefoil. The global protein fold contains three pseudo-symmetric βββloopβ motifs that coalesce to form a six-stranded barrel with three hairpins that form a six-stranded cap closing one end of the barrel (Figure 4-1b) (104). Mature IL-1β refolds relatively slowly (105), accessing multiple routes including a major route with a detectable intermediate population (28,106). Recently, this slow folding has been attributed to repacking of a functionally important loop (the β-bulge) in the mature protein (Figure 4-1bi) (107-109). Although much information is known about the structure, folding and function of mature IL-1β, there is little information available on pro-IL-1β, despite the central importance of this molecule in mediating critical inflammatory processes (79,110,111). What is known is that the presence of the N-terminal 116 amino acids results in a highly protease-sensitive protein with no biological activity (61). Folding of mature IL-1β is believed to occur after cleavage of pro-IL-1β *in vivo*. Therefore, structural analysis of the precursor is essential for a better understanding of the role the precursor region plays in regulating folding events leading to the generation of the eventual mature protein.

The crystal structure of pro-IL-1β has not been determined, despite ca. 25 years of intensive efforts directed towards this goal, as a result of the dynamic nature of this molecule (112-114). Therefore, we used structure sensitive methods to

compare pro-IL-1β in reference to the mature protein. Optical methods in combination with hydrogen/deuterium exchange mass spectrometric analysis (DXMS) and enzymatic digestion were used to investigate how the N-terminal precursor region modulates the properties of the C-terminal mature domain. DXMS is a well-established technique for characterizing proteins refractory to standard crystallographic or NMR structure determination techniques (115-117). Taken together, our results indicate that the N-terminus inhibits the folding to the fully active trefoil structure in the C-terminal region, but maintains the protein in a conformation that is primed for efficient folding upon release after caspase-1 cleavage.

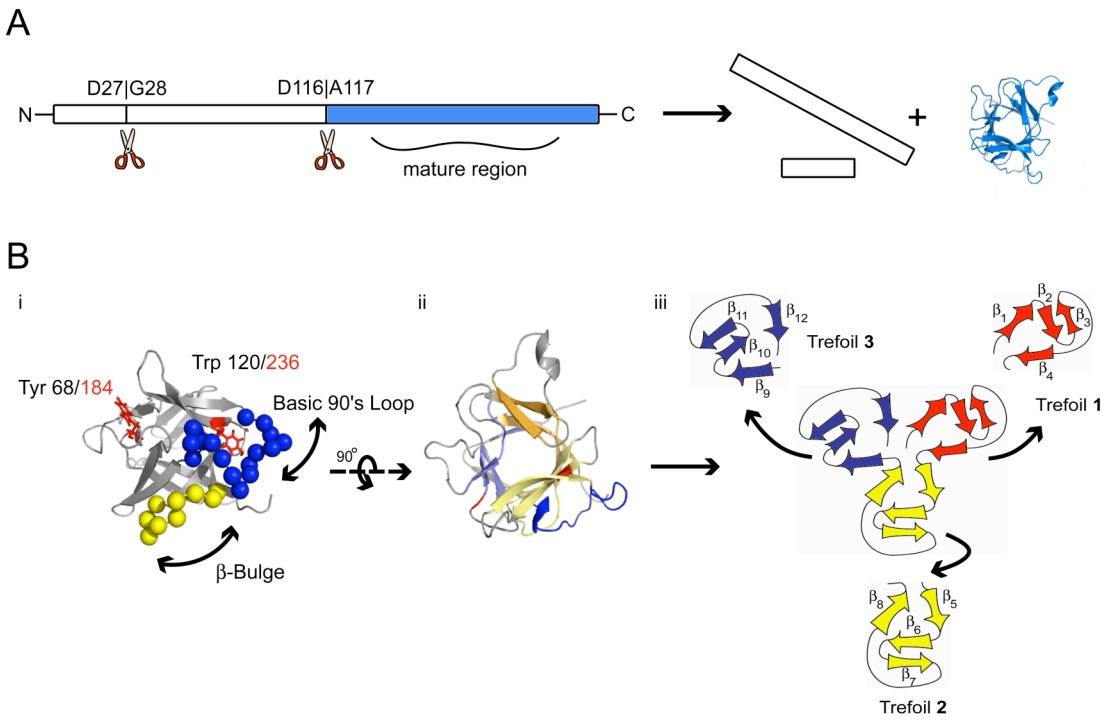

Figure 4-1: A cartoon schematic prointerleukin-1β processing by caspase-1. (A) The two caspase-1 cleavage sites are labeled by residue/number. The products for the cleavage scenario are represented as smaller blocks, and the final mature protein as the actual 3-D structure shown in blue (PDB:6I1B, (23)). (B) i. Important features are highlighted on the structure of mature IL-1β. Residues Tyr 68 (residue 184 in pro-IL-1β) and Trp 120 (236 in pro-IL-1β) are indicated by a red side chain stick representation. The two loops important for binding at third Ig-domain of the receptor are indicated by blue spheres (the basic/hydrophobic 90's loop which encompasses residues 85-99 in mature and 201 - 216 in pro- IL-1β) and yellow spheres (the β-bulge, residues 46-53 and 162-169). The numbering corresponds to mature and pro-IL-1β, respectively. ii. After rotating the structure 90°, the individual trefoils are labeled by color (trefoil 1 in orange, trefoil 2 in yellow, and trefoil 3 in blue). The structural features described in i. maintain the same coloring. iii. The 2-D splay diagram of the trefoils labeled by color as in ii. Showing the three-fold symmetry of the secondary structure elements.

RESULTS

Generation of Mature IL-1β via Proteolysis

Human pro-IL-1β was cloned, expressed and purified as described in Materials and Methods. It is processed to the fully active mature protein by caspase-1 *in vivo*. In addition, a range of other proteases can cleave pro-IL-1β to generate mature proteins of varying activities (53-55,110,111,118). To investigate the properties of our expressed protein, we performed a series of proteolysis experiments on the recombinant pro-IL-1β. Figure 4-2a shows the time course for *in vitro* processing of the protein with caspase-1 as detected by SDS-PAGE analysis. The bacterially expressed full-length proprotein migrates as a single, 31-kD band as expected from the amino acid sequence. Upon addition of caspase-1, a band at 28-kD accumulates, consistent with the expected molecular weight of the protein upon cleavage at the D27 | D28 site. Subsequent processing to the mature, 17-kD protein is observed with time, demonstrating that the recombinant pro-IL-1β holds the correct conformation to be processed by caspase-1 as observed *in vivo*. Comparative studies of the chymotrypsin sensitivity of pro- and mature IL-1β are presented in Figures 4-2b and 4-2c, respectively. Shown by SDS-PAGE analysis, pro-IL-1β is efficiently cleaved by chymotrypsin to generate a 17-kD product that is protected from further digestion as is observed for the mature folded IL-1β. These results are consistent with facile generation of mature folded protein from pro-IL-1β as there are many chymotrypsin recognition sites within the C-terminal 17-kD domain.

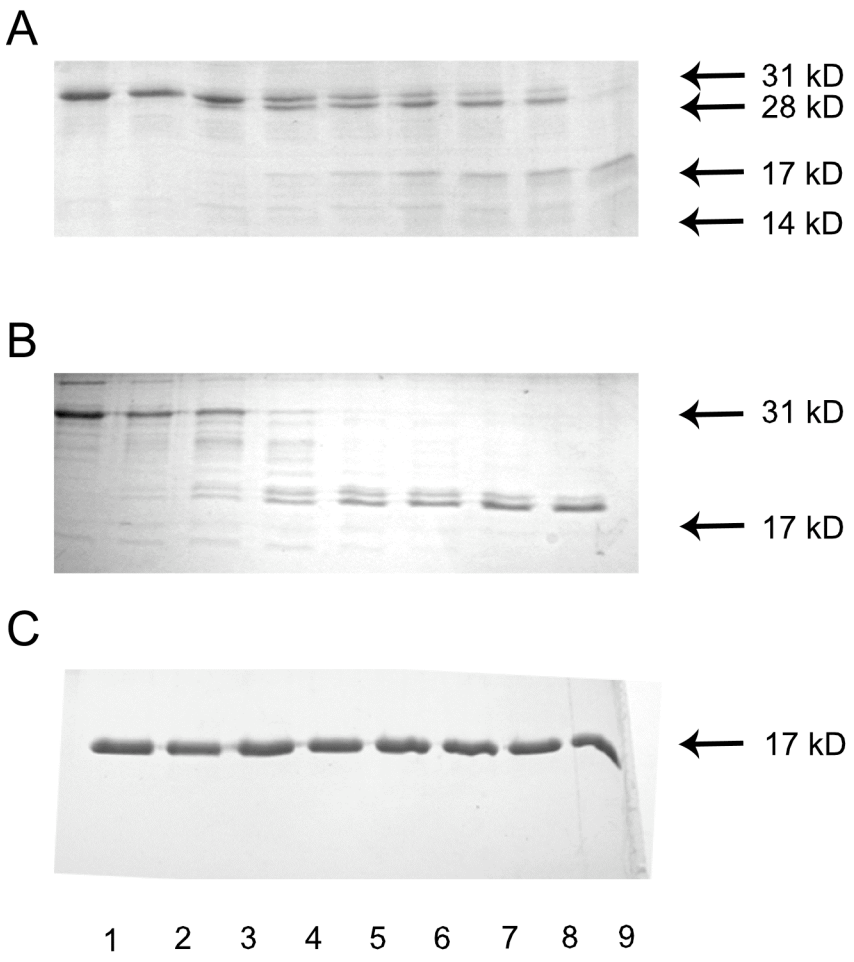

Figure 4-2: Generation of mature IL-1β via proteolysis. (A) An SDS-PAGE gel showing the time course for processing of pro-IL-1β by caspase-1. A band at 28-kD accumulates before the appearance of the 17-kD band for the mature protein, indicating Site 1 is preferentially recognized and processed first. Here, the numbers 1-9 indicate control (no enzyme), 0 sec (directly into quench), 5, 15, 30, 60, 120, 240, 1440 min, respectively. (B) An SDS-PAGE gel showing the time course for processing of pro-IL-1β by catalytic amounts of chymotrypsin. As is evident in the analysis, pro-IL-1β is efficiently cleaved by chymotrypsin to generate a 17-kD product that is protected from further digestion. (C) Control. Mature folded IL-1β is protected from further digestion. These results are consistent with facile generation of mature folded protein from pro-IL-1β. The numbers 1-9 for (B) and (C) correspond to the control (no enzyme), 0 sec (directly into quench), 1, 5, 15, 30, 60, 120 min, respectively.

CD Spectroscopy Demonstrates Less Secondary Structure in Pro-IL-1β Compared to Mature IL-1β

Although CD spectra of proteins containing α-helix secondary structure exhibit characteristic signatures, CD spectra of β-sheet proteins are highly variable (119). There is only a weak intrinsic signal for the twist in the beta-sheet and side-chain signals such as those associated with disulfide bonds and/or exciton interactions easily complicate spectra and make secondary structure interpretation difficult (120). Nonetheless, comparison of the CD spectra of folded/unfolded states of pro- and mature IL-1β can give information about structural features in reference to each other.

Representative spectra of pro- and mature IL-1β in the presence and absence of denaturant are shown in Figure 4-3. There is a large difference between the spectra of the native precursor and mature proteins and between the spectra of folded and unfolded precursor protein in the far-UV wavelength range. The difference between spectra of the pro- and mature proteins in the presence of denaturant is minimal, and consistent with denatured random coil. The unfolded spectra of pro- and mature IL-1β almost have the same overall shape and mean residue ellipticity. In the near-UV range of the spectra (Fig. 4-3 inset), only the spectra of native mature IL-1β is consistent with the presence of well-ordered aromatic side-chains. There are two maxima with positive mean residue ellipticity at approximately 270 and 300 nm. An earlier study attributes the majority of the near-UV signal to Trp 120 and Tyr 68 in mature IL-1β

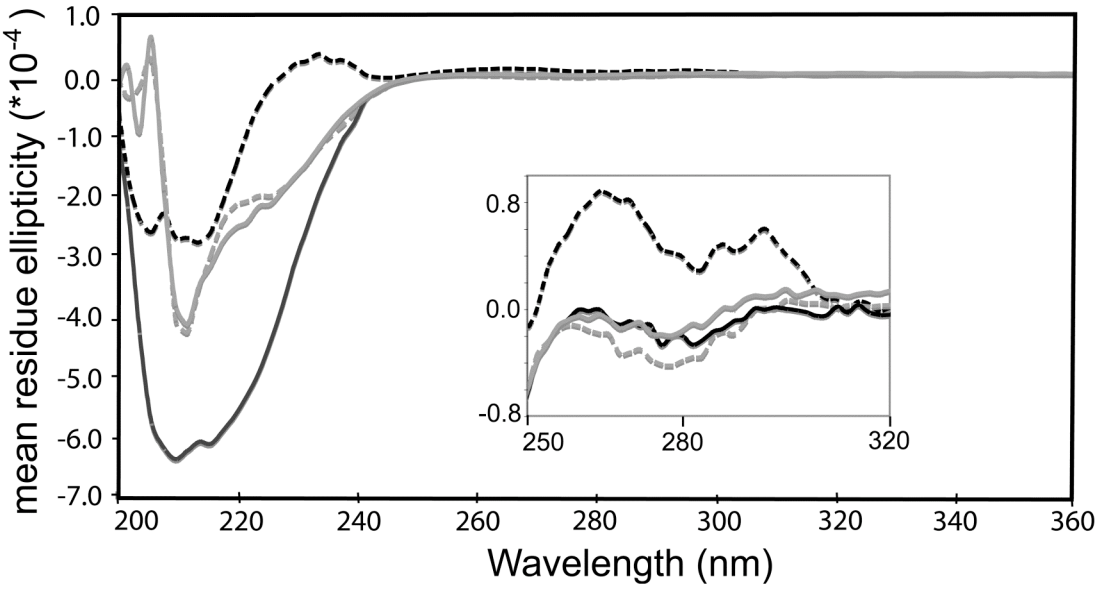

Figure 4-3: Comparison of native pro- and mature IL-1β indicates the generation of additional ordered tertiary structure upon cleavage. The far and near UV circular dichroism (CD) spectra of native and unfolded pro- and mature IL-1β are shown. There is a very large distance between the spectra of the native pro- and mature proteins in the far UV-range (solid and dashed black lines, respectively), but the spectra of the pro- and mature proteins in the presence of denaturant is minimal (solid and dashed grey lines, respectively). In the near UV-range of the spectra (inset), only the spectra of native mature IL-1β is consistent with the presence of well-ordered side-chains, while both pro-IL-1β spectra is similar in this region to unfolded mature IL-1β.

(Trp 236 and Tyr 184 in proIL-1β) (121). The native pro-IL-1β spectrum lacks the same signal intensity. This indicates either a lack of ordered side chain packing, the presence of a nearby quenching moiety or the cancellation of the aromatic side chain signals (119).

Mass Spectrometric Studies of Pro-IL-1β Structure and Stability Relative to Mature IL-1β

H/D solvent exchange experiments require optimal sample conditions for pepsin digestion and minimal deuterium back-exchange (48-50). These conditions were achieved by using a 3.2 M guanidine-HCl, 0.8% formic acid quench buffer solution (final pH 2.5) for all samples (see Materials and Methods). As mature and pro-IL-1β are stable at the low pHs necessary for optimal quenching of the H/D exchange, the addition of denaturant was necessary to generate good quality peptides by pepsin cleavage of the full-length proteins. Quenched samples were kept at -80 °C until analysis. The resulting pepsin fragmentation maps for a typical experiment for both pro- and mature IL-1β are displayed in Figure 4-8 (122), labeled in black and bold red sequence numbering, respectively. The conditions described generated 71 good quality peptides covering 91% of the pro-IL-1β sequence and 102 good quality peptides covering 100% of the mature IL-1β sequence in a representative data set.

The mass spectra of a non-deuterated and fully-deuterated peptide generated from mature IL-1β (V72-L82) are given in Figure 4-8 (inset) to illustrate the deuterium incorporation into the peptide backbone over time after exposure to D_2O. We observed a range of exchange speeds from fully exchanged before the first time point (10 s) to highly protected from exchange after the longest time point (1440 min, or 24 hours) for peptide fragments generated from both pro- and mature IL-1β. The average number of deuterons incorporated was calculated for each peptide at each time point (39-41). Log plots of the observed deuteron incorporation as a function of time for representative directly overlapping peptides are given in Figure 4-4a. There are two categories of peptides, those sharing the identical sequence composition between pro- and mature IL-1β (eg. mature IL-1β peptide 9-19 and pro-IL-1β peptide 125-135), and those that do not. The N-terminal of pro-IL-1β (residues 1-116) is, of course, absent in mature IL-1β. In addition, there is altered protease sensitivity between the two proteins resulting in different peptide coverage maps. Figure 4-4b illustrates directly overlapping peptides over the exchange time course using the color block schematic representation of %max deuterons incorporated. The coloring scale for the %max deuterons incorporated for the peptides over time is also indicated.

The overall relative protection profiles of amide protons against H/D exchange for the N-terminal region of pro-IL-1β (4-5a), and the C-terminal region of pro- and mature IL-1β (4-5b) are depicted in color blocks. The blocks representing the pro-IL-1β C-terminal sequence are located directly above the corresponding analogous

sequence of the mature protein for ease of comparison. The N-terminal region of pro-IL-1β (residues 1-116) show minimal protection and stability overall, with a very few scattered areas of moderate protection (Figure 4-5a). Areas of moderate protection include a conserved stretch of aromatic and acidic residues (95 - 105), a stretch of residues (50-70) with predicted secondary structure, near cutsite 2, and residues 77 - 80. Areas with no protection at all, ie. exchanging faster than the first time point (10 seconds), include cutsite 1 and the area surrounding Trp 108 (pro-IL-1β numbering).

The C-terminal region of pro-IL-1β, residues 117-269, (which correspond to 1-153 of the recombinant mature protein) shows substantially more protection overall compared to the N-terminal region. There are a number of areas of moderate to high protection, with pockets of little to no protection (Figure 4-5b). The turn before and at the start of strand 2, the loop between the first 3-10 helix and start of strand 4, the region covering strands 5-7, strand 8, and the region covering strands 9 and 10 display high protection from exchange (note that these strands correspond to the secondary structure seen in structure of the mature protein). Interestingly, 3 of the 4 protected turns mark the barrel-to-cap transition and the other is between two strands of the barrel. Regions of moderate protection include the area near cutsite 2, the region covering strands 2 and 3, the basic loop between strands 7 and 8, and the region preceding and including strand 11. Areas of little to no protection include strand 1, the loop between strands 3 and 4, the β-bulge (loop between strands 4 and 5), and the region covering strands 11 and 12 (the C-terminus).

Mature IL-1β shows the most protection and stability overall (Figure 5B, bottom set of color blocks). As compared to the C-terminus of pro-IL-1β, the biggest difference lies in trefoil 1 (residues 1-45). Mature IL-1β shows more solvent-exchange protection and hence more secondary and tertiary structure here than the corresponding region in pro-IL-1β. Well-protected areas in mature IL-1β are comprised of the region covering strands 1-3, the sequence preceding strand 4 and strand 4, the region covering strands 5-7, the region covering strands 9-11, and a small pocket preceding strand 12. These areas correspond well with the most protected residues seen by H/D exchange NMR, that correspond in a residue-specific manner to the β-sheet secondary structure of the β-trefoil (91,123,124). Areas of moderate protection include the beginning of strand 1, the basic 90's loop, and strand 12. The least protected areas include the N- and C-termini, the loop between strands 11 and 12, the loop between strands 3 and 4, and the β-bulge loop.

Figure 4-4: Representative log plots showing deuteron incorporation over time for analogous peptides between pro- and mature IL-1β. (A) The red circles correspond to the pro-IL-1β peptide, and the blue circles correspond to the exactly matching peptide in mature IL-1β. Both the pro- and mature sequence numbering is indicated in each plot. The data represents an H/D exchange time course under the same conditions for each protein. Time points were taken at 10, 60, 300, 900, 3600, 28800, and 86400 seconds. The color blocks representation of %max deuterons incorporation over time for the directly overlapping peptides between pro- (top) and mature (bottom) are displayed in (B) Each block represents an exchange time course for one peptide, analogous to the log plots in (A). The %max deuterons incorporated for each for each time point in each block is colored according to the key located at the bottom right of the figure. The red numbers correspond to the mature and the black numbers to the precursor sequence, and the three trefoil subunits are indicated by brackets. The secondary structure of the mature protein calculated from the NMR structure (PDB:6I1B) is represented by open arrows (β-strands) and cylinder (3-10 helix) below the mature blocks.

A

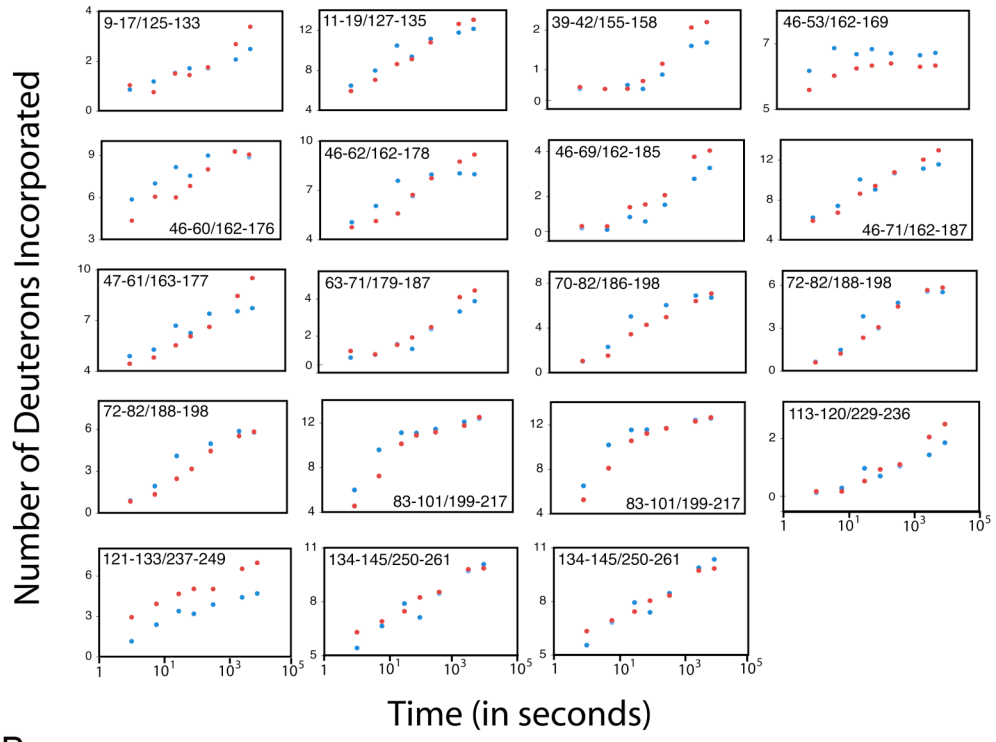
Number of Deuterons Incorporated
9-17/125-133
11-19/127-135
39-42/155-158
46-53/162-169
46-60/162-176
46-62/162-178
46-69/162-185
46-71/162-187
47-61/163-177
63-71/179-187
70-82/186-198
72-82/188-198
72-82/188-198
83-101/199-217
83-101/199-217
113-120/229-236
121-133/237-249
134-145/250-261
134-145/250-261
Time (in seconds)

B

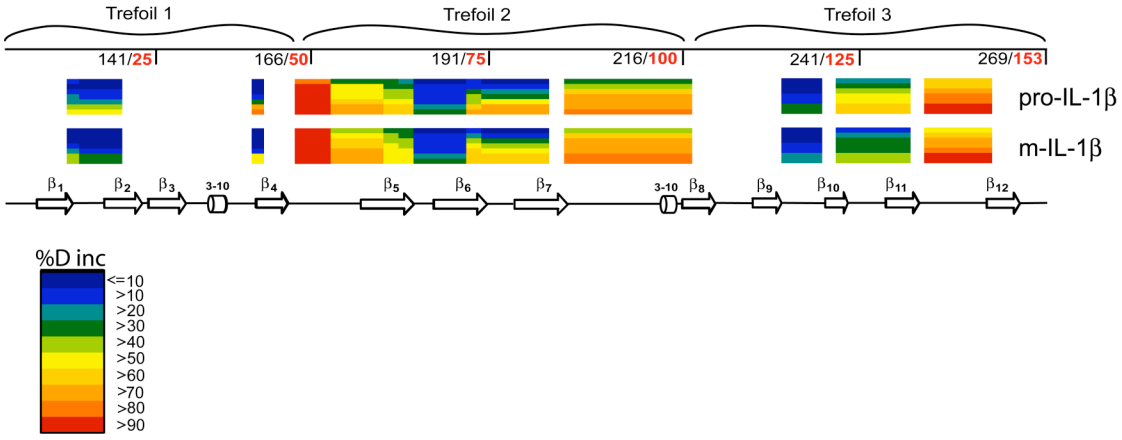
Trefoil 1
Trefoil 2
Trefoil 3
141/25
166/50
191/75
216/100
241/125
269/153
pro-IL-1β
m-IL-1β
β1 β2 β3 3-10 β4 β5 β6 β7 3-10 β8 β9 β10 β11 β12
%D inc
<=10
>10
>20
>30
>40
>50
>60
>70
>80
>90

Figure 4-5: Color-block schematic of %deuterium incorporation over time, representing relative amide solvent exchange protection in a full set of generated peptides. Relative protection of peptides against solvent exchange in (A). the N-terminal region of pro-IL-1β, (B) side-by-side comparison of the C-terminal region of pro-IL-1β, which corresponds to mature IL-1β (top row), and mature IL-1β (bottom row). Each block represents a peptide or a group of overlapping peptides of the entire exchange time course, and each time point is colored by the %max deuterons incorporated for that peptide. The level of protection is indicated by the coloring of that peptide over the entire time course, and the coloring scheme key is located at the far right of the figure. Due to the existence of many overlapping peptides, some peptides can only be partially represented. The protein sequence is indicated by the black line located above the blocks, and the sequence numbering in black corresponds to the pro-IL-1β sequence and in red for the mature protein sequence. Areas of high protection are generally <10-30% exchanged, areas of moderate exchange are >30%-80% exchanged, and areas of little to no protection are >80-100% exchanged over the duration of the experiment. The areas with the most significant differences in protection between pro- and mature are bracketed by red arrows. Areas in both panels of Figure 4-5 with no blocks indicate the absence of an available probe in that region, and the secondary structure of the mature protein is indicated in open arrows below the blocks in (B).

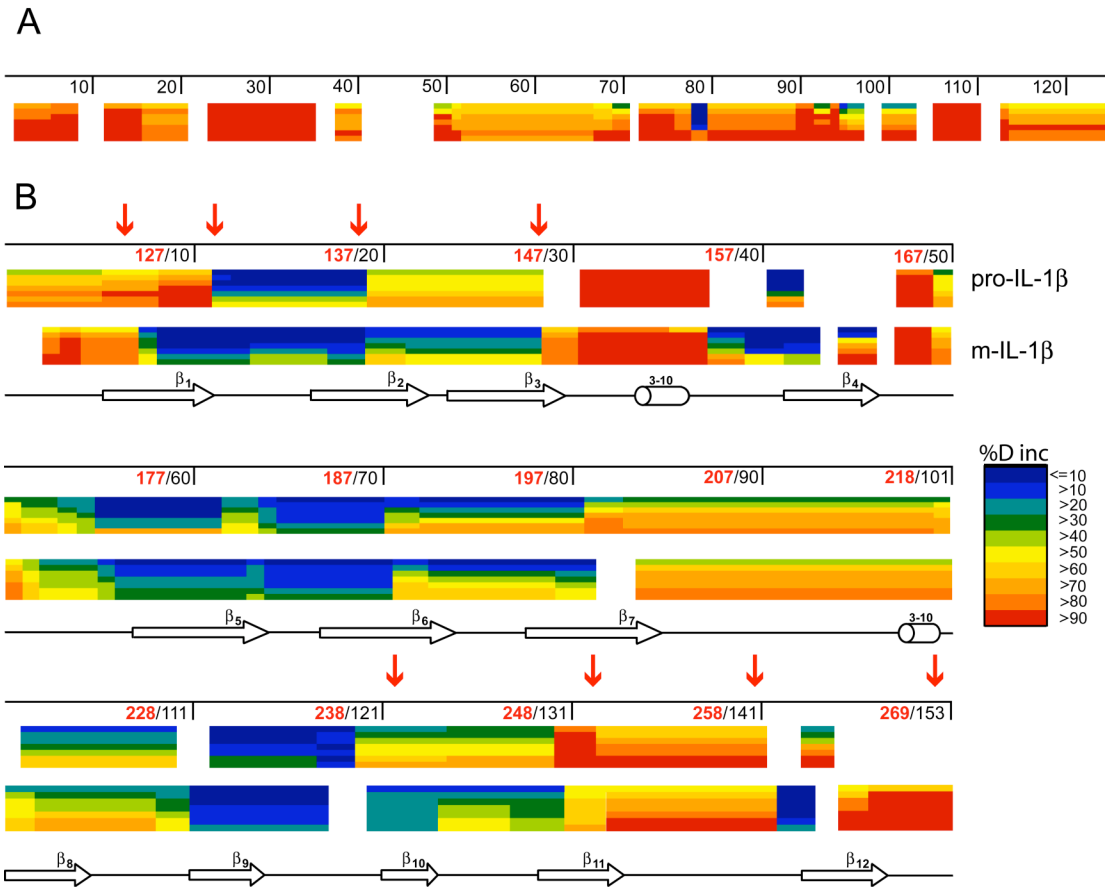
A
10
20
30
40
50
60
70
80
90
100
110
120
B
127/10
137/20
147/30
157/40
167/50
pro-IL-1β
m-IL-1β
β1
β2
β3
3-10
β4
%D inc
<=10
>10
>20
>30
>40
>50
>60
>70
>80
>90
177/60
187/70
197/80
207/90
218/101
β5
β6
β7
3-10
228/111
238/121
248/131
258/141
269/153
β8
β9
β10
β11
β12

DISCUSSION

Proteins over a wide array of fold and functional families are synthesized as larger precursor molecules (72). Many enzymes, including caspase-1, exist as larger inactive precursors known as zymogens before being activated (56). Precursor regions may also act as chaperones, facilitating the folding of the eventual mature protein as in the case of bovine pancreatic trypsin inhibitor (125). Some proteins would not fold without the presence of their precursor domain. The prodomain of α-lytic protease is thought to reduce the conformational entropy of the active region thereby acting as a folding catalyst, allowing the mature protein to bypass the large kinetic folding barrier between it and its native state (70). Precursor domains also act as intracellular targeting sequences, as in the case of the outer-mitochondrial Fe-S cluster protein mitoNEET (126), or as extracellular targeting sequences, as with interleukin-1 receptor antagonist (IL-1Ra), the first identified naturally occurring antagonist (9).

The cytokine IL-1 family members contain the same fold, the β-trefoil. The antagonist for IL-1, IL-1Ra, also shares the same fold. This protein contains a short N-terminal precursor segment (24 residue) that acts as a recognition sequence directing it towards the endoplasmic reticulum (ER) for secretion via the classical ER/Golgi pathway (9). The agonist members of the IL-1 family, IL-1α, IL-1β, IL-18 and IL-33, are synthesized as much larger precursor molecules (1). All of these family members are secreted via a non-classical pathway, which is dependent on cell type for the respective protein. The functions of these precursor domains are still being

investigated. The most well-characterized to date is the N-terminus of pro-IL-1α, (processed by calpain to the mature form (127)) which contains a nuclear localization sequence and can act as a transcription factor with or without the C-terminal region (8,128). IL-1β and IL-18 are processed by caspase-1. The C-terminal mature forms of IL-1β, IL-18, and IL-33 all bind IL-1RI-family receptors in order to activate their respective signaling cascades (1).

The N-terminal precursor domain for IL-1β contains no known localization sequence and has no assigned function. Only limited information about the structure and function of pro-IL-1β is available. A pull-down assay showed that when in the folded native state, mature IL-1β does not interact with the N-terminal sequence alone, suggesting that the conformational change after removal of the precursor sequence in one or both of the regions prevents further interaction (110). The expression, translation, processing and secretion of mature IL-1β are tightly controlled events that require intricate networks of stimuli to occur. Recent work has shown how the inflammasome precisely orchestrates caspase-1 activation as a timely and unique response to a multitude of environmental and pathogenic assaults (46,63,88,94). Along with the inflammasome, due to the potency of IL-1β as a key initiator of the innate immune response, the presence of a self-inhibiting precursor region adds yet another layer of regulation for this powerful cytokine.

Pro-IL-1β is a Protease Sensitive Precursor Molecule

Pro-IL-1β can be processed to a fully-active molecule by a range of other proteases in addition to caspase-1. Recognition sites for enzymes such as chymotrypsin and proteinase K are found throughout the entire sequence. Previous cleavage studies indicate that the precursor is more protease-sensitive along the entire polypeptide length (N-C) including the section that becomes mature IL-1β, whereas mature IL-1β is protease-resistant under the same brute-force conditions (1:10 enzyme:substrate) (53,61,79,99,111). We performed experiments where we added chymotrypsin in catalytic amounts (1:1000 enzyme:substrate), and found that the enzyme preferentially acts on the N-terminal cutsites of pro-IL-1β, thus allowing the C-terminal region time to fold into the protease-resistant β-trefoil of IL-1β prior to complete digestion (Figure 4-2b). In this caspase-1 digest study, cutsite 1 (D27↓G28) is accessed first and preferentially cleaved before cutsite 2 (D116↓A117) (Figure 4-2A). These findings suggest that even in the presence of the N-terminus, the C-terminus is still protected from degradation, although not to the same degree as the final folded, mature protein. Therefore, pro-IL-1β is more protease labile state than the mature protein, but once separated from the prodomain after processing, the C-terminal region is primed to fold quickly and within a certain time frame into the final native conformation.

Optical Studies Indicate Differences in Native Structure

Circular dichroism spectroscopy is used to characterize a protein secondary structure. The signature of the native mature IL-1β spectrum displays the characteristic positive intensity between 230-240 nm, whereas the spectrum of native pro-IL-1β lacks this characteristic (Figure 4-3). However, pro-IL-1β contains regular secondary structure as there is a large change in signal upon the addition of denaturant. The spectra of mature and pro-IL-1β overlay in the presence of added guanidine-HCl (2 M), both showing the loss of regular secondary structure upon exposure to denaturant (Figure 4-3). The local environment around the aromatic side chains in native pro-IL-1β is different than that observed in the native mature protein, as indicated by the lack of a strong near-UV signal from 250-320 nm (Figure 4-3 inset). While the possibility exists for the cancellation of the well-defined peaks of Trp 236 (120) and Tyr 186 (68) by aromatics located throughout the precursor sequence, it is more likely that the local environment around these residues has changed, consistent with lack of change in signal with and without the presence of denaturant. Indeed, the lack of intensity in this region is consistent with having more highly mobile side chains in pro-IL-1β versus the mature protein. More mobile side chains may be a result of the ability of the proprotein to sample locally unfolded states versus the more structured mature protein. This conformational heterogeneity can also account for the decreased resistance to protease degradation seen in the enzyme cleavage assays, and decreased protection seen in the H/D exchange analysis presented here. Taking the lack of stability in the overall exchange profile of the 116 N-terminal residues in pro-

IL-1β into account, it is likely most of the secondary structure seen in the spectrum is found in the C-terminal region.

The N-terminus Region of Pro-IL-1β (Residues 1-116) Displays Only Limited Regions of H/D Exchange Protection

The majority of the amide protons within the N-terminal region of pro-IL-1β are 70-100% exchanged for deuterons in the first minute of solvent exposure to D_2O (Figure 4-5a). The peptide covering the first caspase-1 cutsite (D27 | G28) is fully exchanged within 10 seconds. The calculated average exchange half-life for the polypeptide at this pH and temperature is less than 1 second (129,130). The peptides covering the second cutsite (D116 | A117) still show some protection after 24 hours. Therefore, we propose that the first cutsite is recognized first, consistent with the degree of solvent exposure, as it is more exposed and easier to access. There is also no solvent exchange protection of the peptide covering Trp 108, the only tryptophan residue in the N-terminal region of pro-IL-1β. This would facilitate preferential cleavage by chymotrypsin, since the enzyme recognizes aromatic residues in the P1 position of its substrate recognition sequence.

The N-terminal region does contain two pockets of moderate protection, one located at residues 95-105 and the other at residues 77-80. Residues 95-105 are highly conserved over mammalian species of IL-1β and also between IL-1β and IL-1α. This

is particularly interesting because most of the sequence conservation between species lies within the C-terminal region (residues 117-269), and there are few regions in the N-terminal region (residues 1-116) of pro-IL-1β that are conserved over mammalian species (97,131). Residues 95-105 consist of alternating acidic and hydrophobic residues, and are complementary to the basic 90's loop (residues 201-216) between strands 7 and 8 as identified from the structure of the mature protein (104). The other pocket of moderate protection is the peptide that covers residues 77-80. There is neither predicted nor observed secondary structure in this region, but Val 79 and Pro 80 are highly conserved residues in higher mammals. Hence the lower rate of deuterium exchange may be the result of amino acid type rather than from ordered structure. These residues do not suffer an anomalously high exchange rate (130). Residues 77-80 may be consistent with turn or secondary N- to C-terminus interactions, thus stabilizing them from exchange. A region of some limited protection (residues 45-75) encompasses two smaller regions of highly conserved residues (49-53 and 61-73), and also lies within an area with predicted secondary structure. Interestingly, these moderately protected areas of predicted secondary structure also appear in the secondary structure prediction for pro-IL-1α (32).

The C-terminal Region of Pro-IL-1β (Residues 117-269) Displays Decreased Amounts of Protection Relative to Mature IL-1β Overall, but Maintains a Core Region of Stability

Figure 4-5 shows the peptides generated from the N-terminus of the proprotein (5A) and the region of pro-IL-1β that corresponds to the mature protein and the peptides of the mature protein (5B). Overall, the C-terminal region of pro-IL-1β, that corresponds to the mature protein, is less protected from exchange, which implies less stable secondary and tertiary structure overall for the IL-1β sequence within the intact precursor protein (see top row vs. the bottom of blocks). For ease of discussion, all structural elements referred to are that of mature IL-1β, and we are not implying these elements exist in pro-IL-1β here. The main differences between the top and bottom sets of blocks are within the residues corresponding to the first and third trefoil units of mature IL-1β (refer to Figure 4-1B). The peptide covering the area representing the turn between strands 1 and 2 (125-135, 9-19, pro- and mature IL-1β numbering) structure is the most protected area in trefoil 1 region (117-162, 1-45) of pro-IL-1β. In mature IL-1β, peptides starting in the middle of strand 1 up until the loop after strand 3 (8-28) display a high amount of solvent protection. This is expected because of the hydrogen bonds between the anti-parallel β-strands 2 and 3, and 1 and 12 (barrel) stabilize the backbone amide protons to solvent exchange. Strand 12 in mature IL-1β shows less protection relative to the other strands due to fraying at the C-terminal end of the barrel, as seen by NMR (91). In pro-IL-1β, the highest protection from exchange in this region is the portion corresponding to the turn between strands 1 and 2, and strand 2 itself (125-135, 9-19). Overlapping residues (12-20) are protected from exchange after 48 hours as observed by H/D NMR in the mature protein (123). Either pro-IL-1β structure preserves these turn contacts, or the steric bulk of the N-

terminal region helps limit solvent exchange in the C-terminal region. In pro-IL-1β, there is limited protection of residues 259-264 (corresponding to β-strand 12) relative to a close region in the mature protein (143-146). This drop in protection can be explained as either the lack of hydrogen bonding between strand 12 and 1 of the barrel, or a more highly mobile state. The area covering strands 9 and 10 in trefoil 3 is well protected in both proteins (217-249, 101-133), although the pro-1L-1β peptides show less protection relative to IL-1β approaching the C-terminus.

The main area of similarity in stability and protection for both proteins is in residues 162-217 of pro-IL-1β and residues 46-100 of mature IL-1β. In relation to the mature IL-1β structure, these residues correspond to the central trefoil unit or trefoil 2. This area is the most solvent protected area of pro-IL-1β and of mature IL-1β. The exchange profiles of the directly overlapping peptides in the majority of this region (strands 5 - 8, including the basic 90's loop) between proteins are very similar, differing by less than 10%max deuterons incorporated after 24 hours (Figure 4-4b). β-strands 6 through 10 in IL-1β (trefoil 2 and the leading edge of trefoil 3) were protected first during protein refolding as detected by pulse-labeling NMR (105). These strands comprise an on-route folding intermediate of IL-1β (28,106). Interestingly, the areas adjacent to the sequence corresponding to one of the two main functional loops, the β-bulge, are also highly protected in pro-IL-1β.

Overall, the areas in either the mature or pro-IL-1β that encompass the two important functional loops of the B-site, the β-bulge (residues 162-169 and 46-53 in

pro-, mature IL-1β), and the basic 90's loop (residues 201-216 and 85-99, respectively) are protected the most. The main differences in protection are in the N- and C-termini, where the eventual pro-IL-1β is significantly less protected than corresponding region in the mature protein.

Geometric Frustration During Folding is Linked to Function in Mature IL-1β

IL-1β binds the IL-1RI receptor in two distinct sites, the A-site and B-site, indicated in Figure 4-6 (27). The refolding of mature IL-1β is slow for globular proteins of its size, 17.4 kD (on the order of minutes or longer depending on conditions to the native basin). Experimental and theoretical studies show that this slow folding largely results from geometric frustration (91,107,108). That is, the requirements for a particular functional substructure within a fold may not be as fully evolved for efficient folding as the rest of the structure, because only a limited number of contacts will lead to optimal activity. Some of the geometric frustration in the refolding of mature IL-1β attributed to the β-bulge being packed into the correct conformation to interact with the receptor. Having the most geometrically frustrated but functionally-important areas of the protein in close proximity to their final position in the precursor domain would not only ensure that it folds correctly after processing, but also quickly. Simplified model simulations indicate there are multiple refolding routes accessible for mature IL-1β on its folding landscape (108,132). The preferred route has the barrel form first, while an alternate route has the receptor binding B-site

form before the barrel (109). The latter route has contacts involved in a "back-tracking" mode during folding, where contacts are initially made in and around the B-site, then unmade while other regions of the protein fold into place, before the B-site is finally able to take its final native structure. This back-tracking is attributed to geometrical complexity of packing the functionally important loop, the β-bulge (109). Having two or more competing routes frustrates the folding landscape of the mature protein. The addition of these proposed contacts between the N-terminal domain and the functional loop area could trap the C-terminal into a new well-defined local minimum, mimicking an intermediate state of the mature protein. This intermediate-like state may prevent the formation of the functional loops while keeping them close to a structure that can easily access the native fold. Then, removing the N-terminal portion of the protein allows it to proceed quickly to its final native fold, bypassing the back-tracking route. The precursor protein not only suppresses the receptor binding function of itself, but promotes quick access to the native basin for the mature protein by abrogating the geometrical searching process (a "fast-pass").

The Precursor Domain Suppresses the Folding and Function of the C-terminus

Peptide backbone ^{1}H-^{15}N resonances of mature IL-1β are well-resolved in HSQC spectra and studies on the effects of solvent conditions and/or mutations on the residue-specific stability of mature IL-1β to solvent exchange by 2D heteronuclear NMR spectroscopy have been quite useful (91,123,124). However, the 1H-15N

HSQC spectrum of pro-IL-1β has limited chemical shift dispersion and this characterization, combined with a fairly large molecular weight, results in amide backbone resonances that are poorly resolved. Data from light scattering studies, size-exclusion column chromatography, and 1D diffusion NMR spectra preclude the possibility of aggregation under our experimental conditions. Poorly resolved amide proton resonances for pro-IL-1β are the result of a more heterogeneous conformational native state ensemble than seen in the mature protein (133-136). Our results indicate the pro-IL-1β consists of a much more heterogeneous native state than the mature protein.

Both pro-IL-1β and the mature IL-1β have good peptide coverage and are highly amenable to DXMS analysis (Figure 4-8a). The pattern of relative protection for peptides represented in the block diagram in Figure 4-5b is consistent with residue-specific protection factors determined in previous hydrogen/deuterium exchange NMR studies of mature IL-1β (91). The NMR and mass spectrometry results agree for studies of mature IL-1β. Therefore, any differences observed in the amino acid sequence corresponding to residues 117-269 are owing to conformational/dynamic differences of this region within the proprotein.

Another indication of the difference in conformation of the mature region within the proprotein is the fact that the number of identical peptides generated during peptide cleavage for DXMS analysis is confined to a subset of peptides, despite overall good peptide coverage (Figure 4-8a). The distribution of identical peptides

varies by location within the sequence, with the majority located in the trefoil 2 region (see Figures 4-1b and 4-4). A direct comparison of exact peptides indicates a similar pattern of protection (Figure 4-4b). The more comprehensive analysis of the data using peptides generated from the same regions of the sequence, but with non-equivalent residue composition, indicates large differences between pro- and mature IL-1β (Figure 4-5b).

Owing to the increased size of pro-IL-1β relative to the mature protein, one may infer that the proprotein would show increased solvent exchange protection solely based on increases in steric, or bulk non-polar interactions (137). However, we discovered and as indicated in Figure 4-5b, the directly overlapping peptides between pro- and mature IL-1β are well-protected and show similar or reduced solvent exchange protection over time. Since the exchange protection along the β-strands and in the surface 90's loop hydrophobic mini-core has been (well documented by NMR studies of the mature protein) attributed to secondary structure interactions (anti-parallel β strand hydrogen bonding), this is likely the cause for protection in pro-IL-1β as well (138). The pro-IL-1β native state heterogeneity is most likely due to the mobility of the N-terminal 116 residues, since these residues have minimal stabilization to solvent exchange (Figure 4-5a).

The full-length precursor protein neither binds IL-1RI nor is active (139). Presumably the N-terminal region of the proprotein interacts with the C-terminal to prevent its biological functioning. The charge complementarity between the N-

terminal acidic/aromatic region (residues 95-105) and exposure of the C-terminal basic 90's loop (201-215 and 85-99, pro- and mature IL-1β) suggest this as a highly plausible interaction. Residues 95-105 are highly conserved and constitute one of the few regions of predicted secondary structure in the N-terminus. In mature IL-1β, the 90's loop is one part of the B-site binding interface with the receptor (Figure 4-6). Blocking this region would prevent the interaction between the 90's loop and receptor, thus preventing binding (Figure 4-7). An additional interaction between the N- and C-terminal regions of pro-IL-1β includes the acidic β-bulge (162-169, 46-53) and a conserved basic/hydrophobic region (residues 73-80), further blocking the B-site.

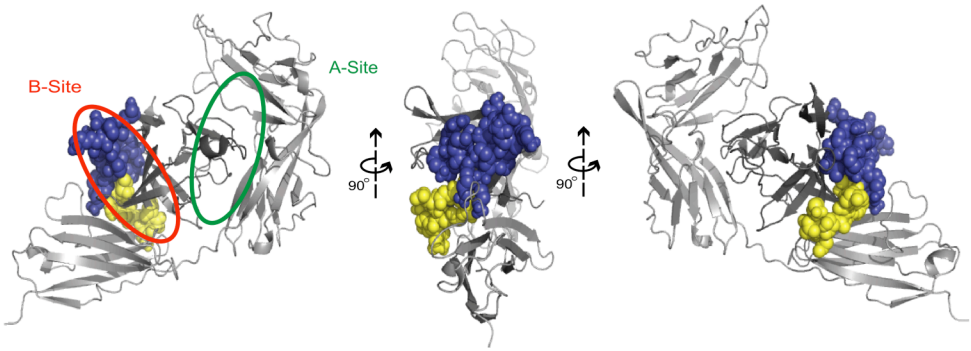

Figure 4-6: Receptor binding sites of IL-1β. The crystal structure of mature IL-1β bound to the extracellular domain of IL-1RI (PDB:1ITB) is colored in grey. The two discontinuous binding sites of IL-1β are indicated by a green (site 1) or red circle (site 2). Site 1 involves an interaction between IL-1β and the first two Ig-domains of IL-1R1. Site 2 involves an interaction between IL-1β and the third Ig-domain of IL-1R1. The two functional loops important to site 2 are the β-bulge, indicated in yellow, and the basic 90's loop, indicated in blue. The complex is rotated twice by 90º for ease of viewing. Binding at both receptor sites provides the scaffolding necessary to recruit the interleukin-1 receptor accessory protein (IL-1AcP) to make the active signaling complex. The crystal structure was rendered in Pymol (23).

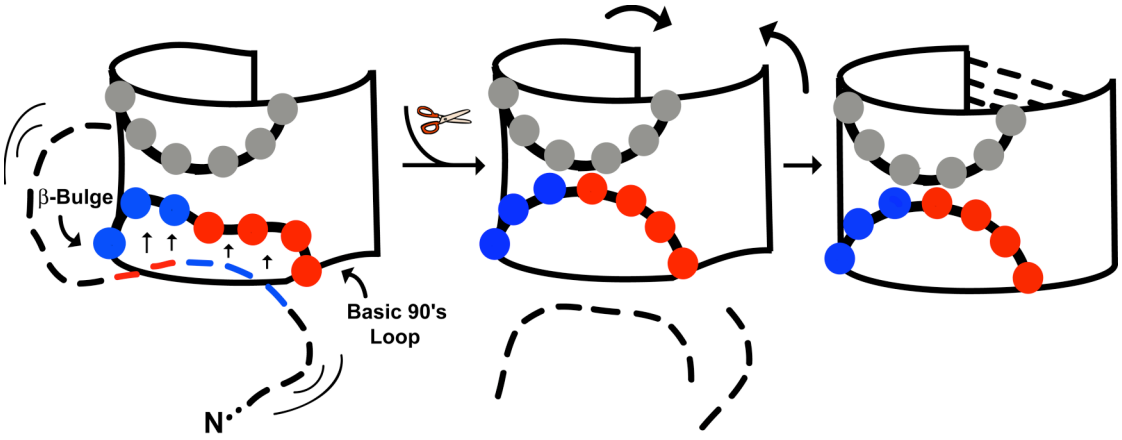

Figure 4-7: Model for pro-IL-1β N-terminal domain interaction with components of the C-terminus. A cartoon schematic representation of the precursor domain preventing the full barrel formation in the eventual mature domain is shown here. Initially, the basic/hydrophobic 90's loop (red circles) and the β-bulge loop (blue circles) of the C-terminal region and the acidic/hydrophobic (residues 95-105, blue dashes) and basic/turn portions (residues 73-80, red dashes) of the N-terminal region interact via side-chain/side-chain charge complementarity. This interaction between the two domains creates a "pinching" effect, destabilizing the barrel (as in the mature IL-1β structure). The effect is transmitted to the opposite end of the protein, preventing the ends of the barrel from coming completely together. Subsequently, the proprotein is cleaved by caspase-1 or another protease capable of generating mature IL-1β. After the precursor region is removed, the functional loops are revealed and the C-terminus is free to finish folding into the native state. The now fully-folded mature IL-1β is stabilized further from exchange.

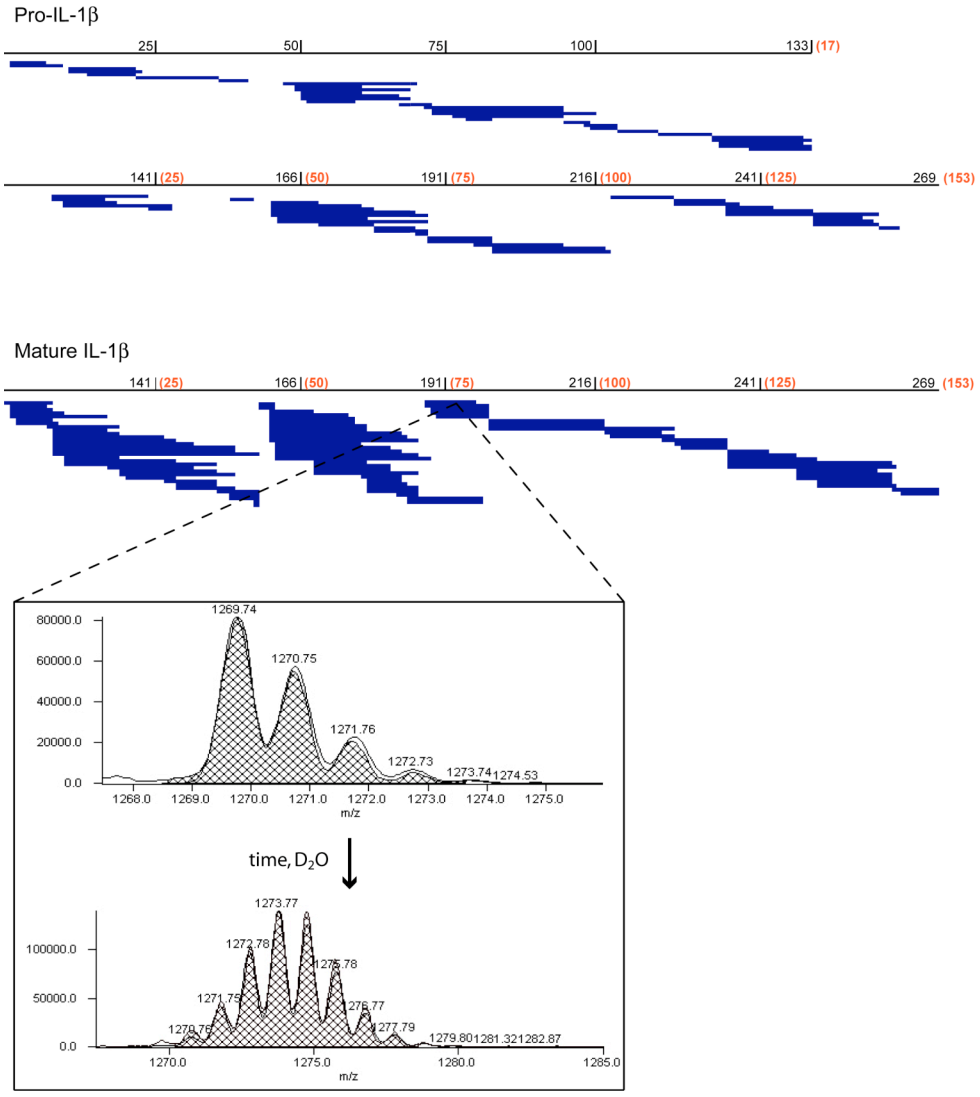

Figure 4-8: Peptide coverage maps of pro- and mature IL-1β. Representative peptide fragmentation maps for *A*. pro-IL-1β and *B*. mature IL-1β. Each blue block represents a unique peptide. The sequence is indicated by the black line above, with pro-IL-1β numbering in black and numbering in red corresponding to mature IL-1β. The peptides were generated by running quenched samples (at pH 2.5) over a pepsin column as described in the Materials and Methods section. Mass spectra of peptide fragment V72-L82 from mature IL-1β shown with and without deuteration (inset). The top panel shows actual and predicted isotope envelope for the non-deuterated peptide, and the bottom panel shows the fully-deuterated peptide. The shifting isotopic envelope to a higher m/z ratio indicates deuterium incorporation into the amide backbone.

Biological activity for the proprotein may also be precluded by the presence of limited secondary/tertiary structure and an overall destabilized N-terminal region may inhibit the trefoil 1 region from fully folding. Only one small area in pro-IL-1β corresponding to the residues of trefoil 1 in the mature protein is protected over the exchange time course (Figure 4-5b). These residues are most likely less stable to solvent exchange and in an altered conformation due to their proximity to the minimally protected, destabilized N-terminus. The first trefoil region may act to buffer the effects seen in the remainder of the C-terminal region (eventual trefoils 2 and 3) due to the conformational heterogeneity of the N-terminus. Only after the N-terminus is removed can these residues fully fold into the native mature structure.

CONCLUSION

Taken together with previous studies our current results lead us to propose that the presence of the conserved N-terminus of pro-IL-1β prevents the final folding to the native structure of this potent cytokine. This trait would block the function of the eventual mature protein, which is to bind IL-1RI (92). The overall destabilization allows the proprotein to be in a protease-labile state for quick processing while keeping the C-terminal area primed to fold quickly and correctly after cleavage. Only after the N-terminal region is fully removed can these residues be stabilized into their final native structure. If unneeded by the cell, pro-IL-1β can be quickly disposed of by proteases working alone or in concert without it erroneously escaping and eliciting destructive responses (16). Regulating IL-1β function in this layered, subtle fashion is

truly an example of how nature accomplishes the many finely-tuned complexities that constitute cell signaling.

Chapter 4, in part, is a reprint of the material as it appears in the Journal of Biological Chemistry 2009. Hailey, Kendra L., Li, Sheng, Andersen, Mette D., Roy, Melinda, Woods, Jr., Virgil L., Jennings, Patricia A. The dissertation author was the primary investigator and author of this paper.

Chapter 5

The Shared Folding Landscape of

IL-1Ra and IL-1β

ABSTRACT

The proinflammatory cytokine IL-1β and its competitive inhibitor IL-1Ra have co-evolved to bind the same receptor and maintain a regulatory balance. Both proteins share the same overall tertiary structure, the β-trefoil fold, with only 30% sequence identity. The folding landscapes of proteins appear to have evolved to be sufficiently smooth such that formation of the native state is facile and the routes accessed appear to be dominated by geometrical constraints. We have explored the hypothesis that barriers to efficient folding are likely areas necessary for function. Theoretical and experimental studies of the agonist IL-1β have shown that functionally important substructures within the protein impede efficient folding. In the current study, we use the combination fluorescence-monitored equilibrium denaturation studies and stopped-flow and manual mixing kinetics to explore the compare the folding landscapes of IL-1Ra and IL-1β.

INTRODUCTION

Interleukin-1β (IL-1β) is produced in response to infection, inflammation, and tissue damage. It is a pro-inflammatory, multifunctional cytokine that affects nearly all cell types. The role that the cytokine plays in the inflammatory cascade is complex and its activity is highly regulated(14,63,140). Interestingly, the IL-1 family is the only identified cytokine family known to have natural antagonist (a competitive inhibitor) proteins(9). IL-1ra, has no known agonist activity, and has the same overall fold as IL-1β. IL-1ra and IL-1β have coevolved to tightly regulate the activity associated

with IL-1 receptor. One key difference between the two structurally homologous proteins is in the region of the β-bulge (IL-1ra has a tight turn in place of the β-bulge found in IL-1β (Figure 5-1). IL-1β binds the IL-1 receptor (IL-1R) and triggers a signal cascade whereas IL-1Ra competes for the same site and inhibits signaling(10,11,141).

The IL-1R belongs to the immunoglobulin (Ig) superfamily characterized by three extra-cellular Ig domains (I, II, III), a single transmembrane spanning sequence, and a globular intracellular domain(26,27,142,143). In addition, a soluble form of the receptor (sIL-1R) arising from alternative splicing and comprising residues 1-311 of the IL-1R (Ig domains I, II and III) is found in the circulating blood stream and also acts to inhibit IL-1β signaling(10,30,144). The structures of the complexes of sIL-1R with IL-1β and IL-1ra have been solved and reveal a novel interaction motif for a cytokine (antagonist)-receptor complex where the three Ig domains wrap around the trefoil fold with a 1:1 stoichiometry(26,27,145). IL-1β has two known binding sites for the IL-1R, designated A and B (Figure 2). Site A binds the first two Ig domains on the receptor while site B interacts with domain III. IL-1ra maintains the interactions between Site A and the IL-1R, but differs in its interaction with Ig domain III. Comparison of the structures of the IL-1β/receptor and IL-1ra/receptor complexes has led to the proposal that binding to the B-site of IL-1β (not IL-Ira) induces a conformational change in the receptor which may help to trigger the signal cascade(26,27,145) (Figure 5-2).

Computational studies indicate that most of the B-site can be extracted from structural differences between the two proteins. In addition to the β-bulge the other major structural difference between the two proteins is a cap loop which is in contact with residue K145 in IL-1Ra. Replacing the corresponding tight β-turn of IL-1Ra with the functional β-bulge partially restores signaling activity in a K145D IL-1Ra mutant (146). Molecular dynamics (MD) simulations of a structure-based model of IL-1β have indicated that IL-1β folds slowly in simulations in part due to geometrical frustration as a result of contacts between the β-bulge (residues 48 through 53) and a cap loop (residues 92 through 94: the 90s loop). Replacing the β-bulge with the tight β-turn from IL-1Ra in hybrid model of IL-1β, simplifies the shape of the protein and reduces the barrier to folding(108,109,132). Thus, the presence of the functional B-site complicates folding(107).

In the present work, we explore the equilibrium and kinetic folding of the β-trefoil protein IL-1Ra and compare the results to those obtained for IL-1β. Surprisingly, our results indicate that two proteins have coevolved to the same thermodynamic stabilities despite a 70% difference in amino acid sequences (21). In addition, analysis of the denaturant-dependence of the folding kinetics indicates that

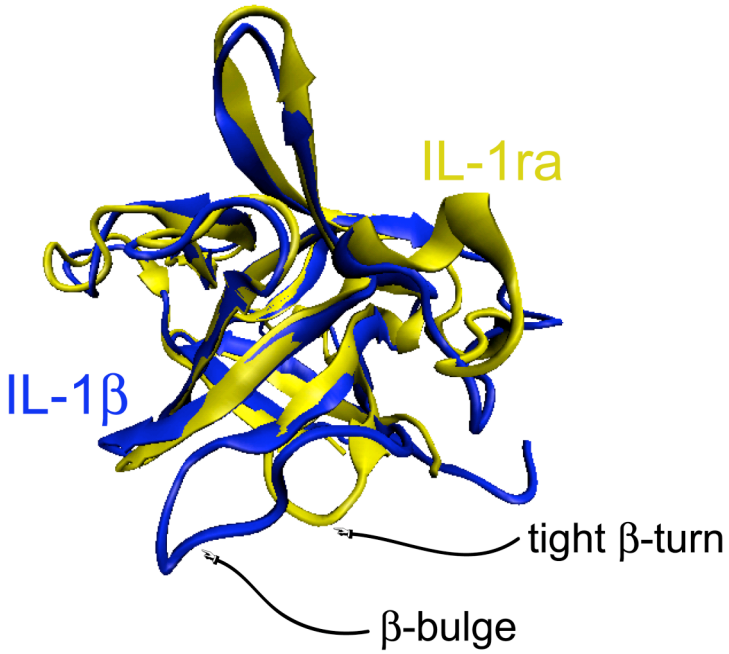

Figure 5-1: A structural overlay of IL-1Ra and IL-1β. The two proteins are remarkably similar except in the B-site of IL-1RI receptor binding, which includes the β-bulge of IL-1β.

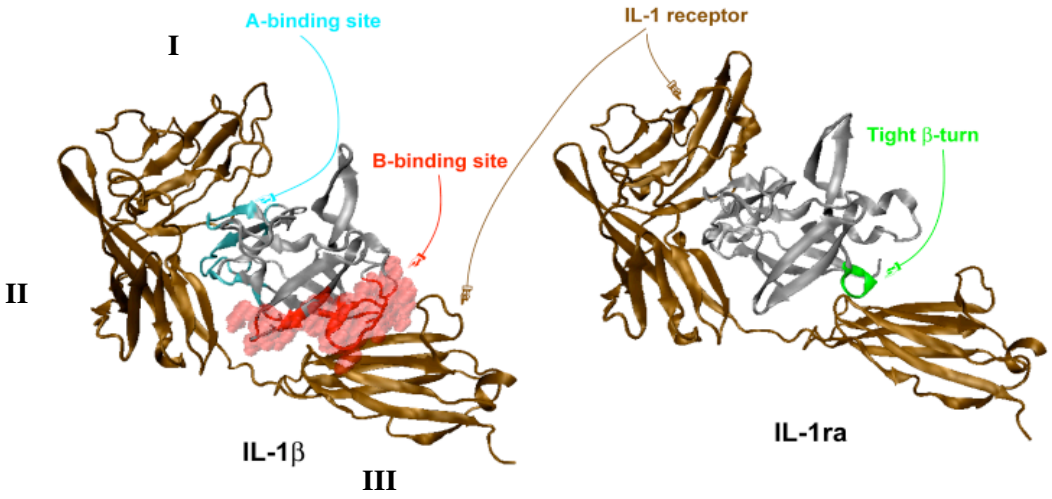

Figure 5-2: Comparison of IL-1β and IL-1Ra bound to the IL-1RI receptor. Ig domains I, II and III of sIL-1RI are labeled on the complex on the left for clarity. IL-1β is thought to induce a conformational change (helical structure in the linker between domains II and III and a 20° rotation of Ig domain III with respect to that observed in th IL-1RI complex of IL-1Ra) and binds the third domain of the receptor. In contrast IL-1Ra binds predominantly the first two domains.

the apparent stabilities of populated kinetic intermediates are within error. However, IL-1Ra is faster to both unfold and refold than IL-1β under all denaturant conditions. Taken together, our results support the predictions of structure-based simulations that IL-1Ra has a lower free energy barrier, a better-defined transition state and less trapping during folding than its signaling structural homolog IL-1β.

RESULTS

Equilibrium Unfolding

In order to compare difference between the thermodynamic stabilities of the IL-1Ra and IL-1β, equilibrium unfolding studies were undertaken. A comparison of the fluorescence emission spectra upon excitation at 293 nm of IL-1Ra in 0, 0.8 and 4M Gdn-HCl is given in Figure 5-3. The fluorescence emission maximum is at 343 nm in the folded protein, reflecting the sequestration of the Trp sidechain from solvent. Like IL-1β, IL-1Ra undergoes an initial increase in fluorescence intensity without a change in emission wavelength in low-level denaturants prior to unfolding. The fluorescence emission intensity is quenched and the maximum shifts to 353 nm in the unfolded protein (data not shown). A plot of the fluorescence detected equilibrium unfolding reaction for IL-1Ra compared to that obtained for IL-1β is given in Figure 5-3. The two-transitions are coincident. Fitting to a two-state model as described previously, the free energy of stabilization (ΔG) and the phase transition, m, for wild-type and mutant proteins was determined and is given in Table 5-1.

Table 5-1: Thermodynamic parameters for wt IL-1β and wt IL-1Ra

	ΔG_{NU}[a,b] (kcal*mol^{-1})	m-value[a,b] (kcal*mol^{-1}*M^{-1})	C_m[c] (M)
Wt IL-1Ra	8.1 ± 0.1	5.7 ± 0.1	1.4
Wt IL-1Ra + DTT	7.9 ± 1.1	5.5 ± 0.8	1.4
Wt IL-1β	7.3 ± 0.1	4.9 ± 0.1	1.5

Changes in folding parameters between wt IL-1β and wt IL-1Ra with and without 10 mM DTT. The equilibrium data were fit using MATLAB in order to obtain equilibrium parameters for folding, ΔG_{NU}. The m-value indicates changes in the accessible surface area upon folding and indicate cooperativity of the folding transition.

[a]Equilibrium transition data were evaluated using a two-state model.

[b]Data were obtained by calculating the average fluorescence intensity and calculating the relative fluorescence intensity in terms of F_{app} as a function of [Gdn-HCl].

[c]C_m values are determined by dividing ΔG_{NU} by the m-value.

Folding Kinetics

To ascertain whether the two homologous proteins have differences in their folding landscape as predicted(109), we performed a series of kinetic studies. The observed relaxation times, τ_1, plotted as a function of final denaturant concentration, are presented in Figure 5-4. Despite the similarities in thermodynamic stability of the two proteins, IL-1Ra unfolds almost an order of magnitude faster than IL-1β under all denaturant concentrations. Stopped-flow and manual mixing studies were performed to monitor the refolding reaction. IL-1Ra and IL-1β each exhibited three exponential phases during refolding, where τ_3 occurs on the millisecond timescale, τ_2 occurs on the millisecond to second timescale and τ_1 occurs in the on the tens of seconds timescale and can also be monitored by manual-mixing techniques(51,52,105). Plots of the relaxation times, as a function of final Gdn-HCl concentration are given and compared to those obtained for IL-1β in Figure 5-4. The initial collapse of the protein as monitored by τ_3 is within error of that obtained for IL-1β. However, the formation of the major intermediate species τ_2, is increased by a factor of 2 and the formation of the native protein, reflected by the slowest step in folding, τ_1, is reduced by a factor of 5.

IL-1Ra has the potential to form a disulfide bond between residues C116 and C69 in the native protein, which tethers the cap strand 7 to the hydrophobic loop between strands 10 and 11(25). In an effort to see whether the presence of the disulfide bond alters the observed thermodynamics or kinetics of folding, we

performed comparative studies of the folding of the protein in the presence and absence of added reducing agents (Figure 5-3, Table 5-1). The observed thermodynamics and kinetics of folding were unaffected, within error, to that obtained for the protein in the absence of reducing agent.

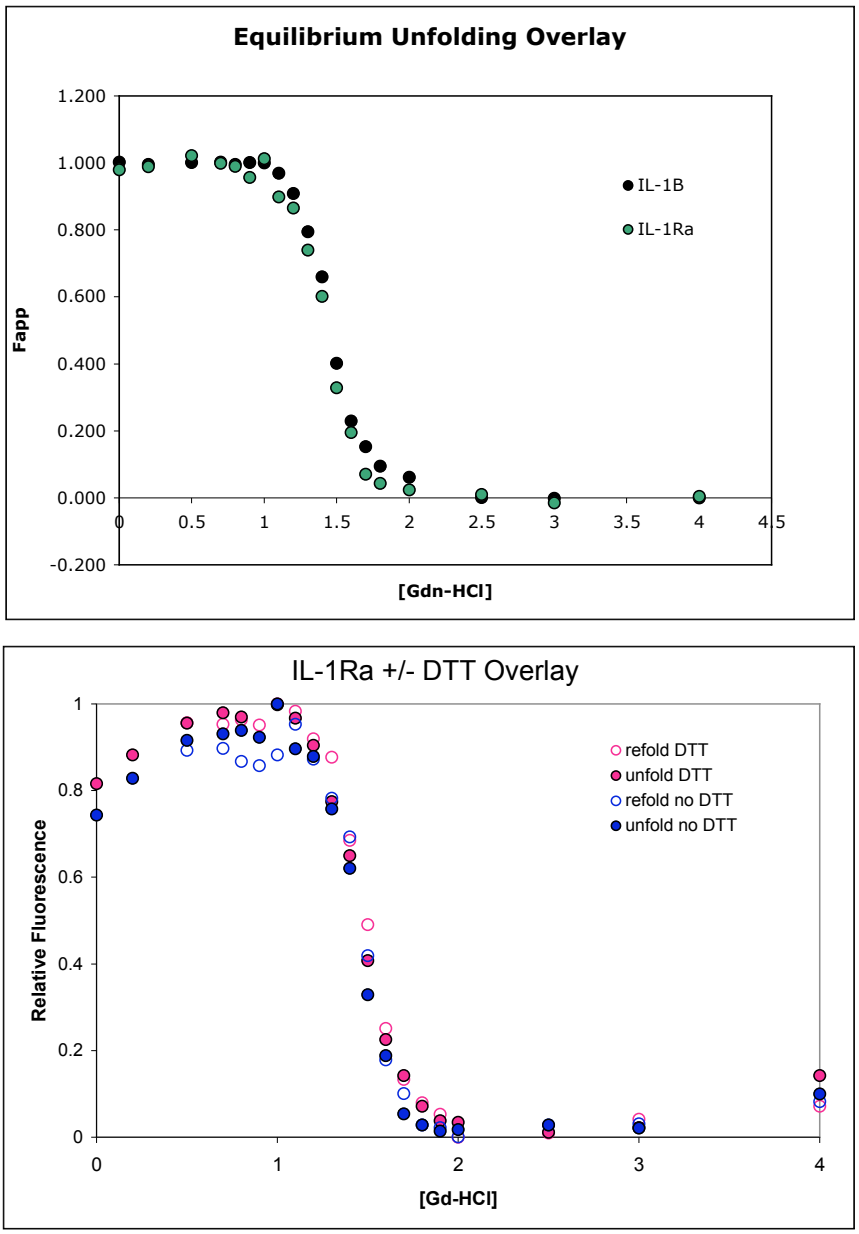

Figure 5-3: Equilibrium titration curve overlay of IL-1β and IL-1Ra with and without the presence of reducing agent. The normalized fluorescence intensities from equilibrium unfolding titrations of IL-1β and IL-1Ra (+/- 10 mM DTT) over 0 – 4 M Gdn-HCl are shown here. The curve was fit to a 2-state model of folding (U → N) to determine the stability (ΔG) and the cooperativity (m-value) of the transition.

DISCUSSION

Protein stability is oftentimes significantly impacted by amino acid changes within the sequence. In particular, for many proteins changes within the hydrophobic core are oftentimes accompanied by destabilization of the native fold, unless a particular variant fills a solvated cavity within the interior of the protein. Mutations in surface loops are generally well tolerated with respect to thermodynamic stability. In a major departure from these general findings, IL-1β shows dramatic shifts in stability upon mutation of surface residues and loops that are not associated with the core barrel or hairpin cap (28,124). In addition, changes in surface residues can alter torsion angles, environment and/or stability to H/D exchange in sites quite distant from the site of mutation (124). Given these findings and the fact that ca. ***70%*** of the residues are ***different*** between IL-1β and IL-1Ra, it is quite surprising that the observed thermodynamic stabilities of the two proteins are within error. IL-1β and IL-1Ra coevolved from the same gene to regulate the same receptor-signaling pathway 300 million years ago (21). Both proteins are protease resistant species, which may help to ensure their viability in extracellular compartments (64). It is possible that maintenance of the same thermodynamic stability of the protein offers a functional advantage in the balance between agonist and antagonist activities. It would be interesting to determine if this similar apparent stability is maintained across species, or evolved from lower to higher organisms.

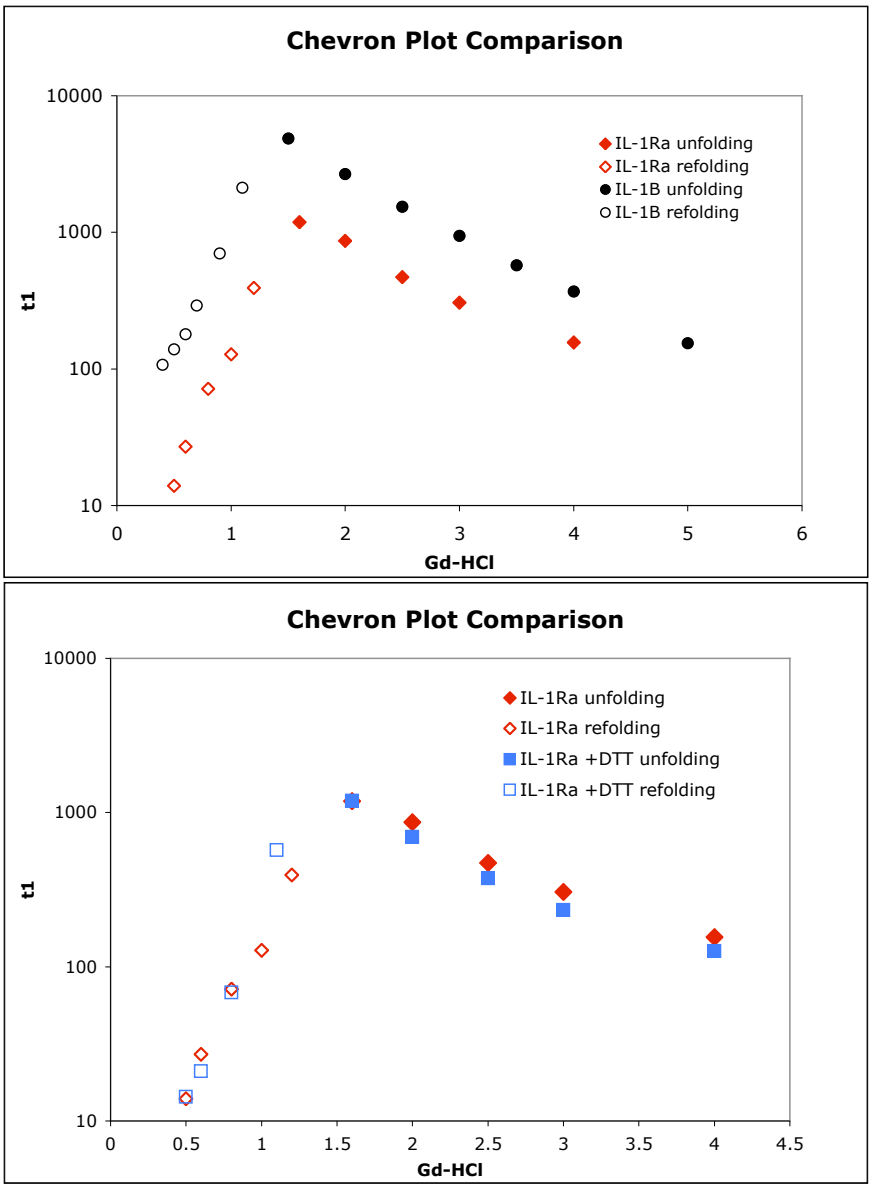

Figure 5-4: Chevron plots of IL-1β and IL-1Ra with and without the presence of denaturant. Each point on the chevron plot corresponds to the relaxation time of either an unfolding or refolding jump. Refolding jumps are initiated by adding protein unfolded in 2.2M Gdn-HCl to varying final denaturant concentrations (0.2 – 1.2), by following the change in tryptophan fluorescence using either by manual mixing or stopped flow. Unfolding jumps were initiated by adding native protein to varying final denaturant concentrations. The relaxation times are plotted vs. [Gdn-HCl] for () IL-1β, () IL-1Ra, and () IL-1Ra with the addition of 10 mM DTT.

Folding Barriers in IL-1Ra

Kinetic experiments were carried out in order to test predictions from theoretical studies of the folding of IL-1β and IL-1Ra. The results show clearly that the two proteins fold with the same number of relaxation phases, suggesting similar populations of intermediate species, but with significantly altered relaxation times. The slower rate of formation of the major intermediate species in IL-1Ra, as reflected by the t_2 relaxation time, suggests that the formation of the B-site in IL-1β may facilitate intermediate formation. However, these same contacts, when formed early, impede the closing of the barrel and formation of the final folded structure (108,132). Thus IL-1β backtracks, and disrupts these B-site contacts in order to access an alternative route to the native state. These native contacts are reformed upon barrel closure. The slower appearance of the intermediate in IL-1Ra is consistent with the reduced population of a partially folded intermediate species with contacts that impede folding and necessitate backtracking. In addition, the decreases in kinetic barriers to unfolding and refolding are in agreement with the hypothesis that the simpler the architecture of surface loops in IL-1Ra would lead to a more efficiently folded protein (109). Interestingly, the increased ease of formation of the IL-1Ra is perfectly balanced by the increased ease of disrupting the native structure and the relative stabilities of the native and intermediate species are similar in the two proteins.

CONCLUSION

Equilibrium and kinetic folding studies of IL-1Ra have shown that it maintains a similar thermodynamic stability to IL-1β despite its low sequence identity. Kinetic folding studies have revealed that the folding landscape is more efficient at getting to the native state than IL-1β, confirming that theoretical prediction that the important functional differences between the agonist/antagonist partners impart changes on their respective folding landscapes.

Chapter 6

The Shared Functional Landscape of

IL-1Ra and IL-1β

ABSTRACT

The proinflammatory cytokine IL-1β and its competitive inhibitor IL-1Ra have co-evolved agonist and antagonist signaling activities which helps maintain a regulatory balance. The folding landscapes of proteins appear to have evolved to be sufficiently smooth such that formation of the native state is facile and the routes accessed appear to be dominated by geometrical constraints. However, functionally essential regions (those involved in catalysis, binding etc.) are necessarily under different evolutionary constraint as they must maintain binding affinities and chemical reactivity towards their biological partners. While identifying residues necessary for catalytic activity within an active-site is reasonably facile, identifying protein-protein interaction surfaces and allosteric sites, *a priori*, is an active area of research. We have explored the hypothesis that barriers to efficient folding are likely areas necessary for function. Theoretical and experimental studies of the agonist IL-1β have shown that functionally important substructures within the protein impede efficient folding. In the current study, we use the combination of mutagenesis, fluorescence-monitored equilibrium denaturation studies, stopped-flow and manual mixing kinetics, biological assays, and ^{1}H-^{15}N 2D NMR to explore the functional/folding landscapes in the antagonist.

INTRODUCTION

IL-1β and IL-1Ra coevolved to bind IL-1R1 as an agonist and antagonist, respectively. Both contain a conserved receptor binding site, Site A, which engages

the first two Ig-domains of the receptor. These proteins diverge in function by the presence of an extensive second receptor-binding site in IL-1β, the B-site, which engages the third Ig-domain of the receptor (27). IL-1Ra also has a B-site, but it is much more limited, contacting only the loops of the third Ig-domain (26). The residues that make up the receptor binding sites in IL-1β and IL-1Ra with and without the receptor are shown in Figure 6-1. By comparing the binding B sites in crystal structures, one may infer that the extra residues that contact the receptor from the B-binding site in IL-1β induce a conformational change in the heterodimeric complex that is recognized by the third member of the IL-1 signaling complex, the interleukin-1 receptor accessory protein (IL-1RAcP) (145). The IL-1RAcP is structurally homologous IL-1RI, and is absolutely required for intracellular signaling (147). Only the IL-1β/IL-1RI complex can recruit IL-1RAcP to form a stable heterotrimeric complex (148). IL-1RAcP binding tightens the IL-1β/IL-1RI complex, and the intracellular scaffolding domains of the receptor protein complex initiate signaling cascades.

Misregulation of IL-1β leads to acute and chronic disease states in all areas of organism (15). Normal function between the two family members indicates that IL-1β and IL-1Ra production are coordinated after an immune challenge, with extra cellular concentrations of IL-1β peaking at ~ 2hrs, and IL-1Ra at ~3-6 hours after the initial challenge. Since it takes so little IL-1β to induce a response in target cells (~10 molecules/cell), IL-1Ra must be produced in great abundance in order to attenuate and control the biological effects of IL-1β (14). Indeed, IL-1Ra is

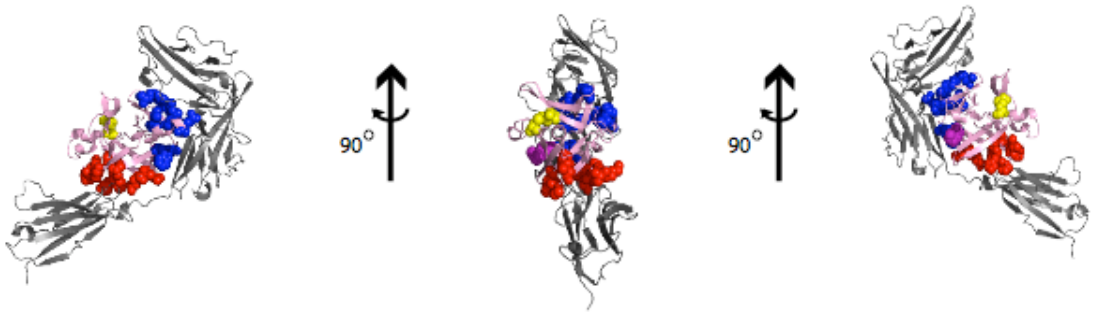

Figure 6-1: The A and B receptor binding sites for IL-1β and IL-1Ra. Shown here are three views of crystal structures of IL-1RI bound with either IL-1β (A) or IL-1Ra (B) (PDB:1ITB and 1IRA, respectively). The sites are colored blue for Site A and red for Site B in both cases. Functionally relevant sites, residues 145 and 117/116 in IL-1β and IL-1Ra, respectively, are also labeled by color (145 is yellow, 117/116 is violet).

produced in amounts 2-orders of magnitude greater than IL-1β (approximately 80 pg/mL vs. 6400 pg/mL) (14).

Recent theoretical simulation studies using structure-based models showed that functionally important features in IL-1β contribute to frustration on the folding landscape. Abolishing this region by deletion of the native β-bulge in both theoretical and experimental folding studies lowered the transition state barrier (theoretical) and increased the rate of refolding (experimental) without significantly altering the thermodynamic stability of the respective proteins (109). A biological assay assessing the function of this deletion mutant indicated that the function was reversed, changing IL-1β from an agonist to an antagonist molecule (Capraro and Hailey, unpublished results).

The functional landscapes of IL-1Ra and IL-1β are distinct, but shared, as they co-evolved to compete for the same receptor proteins. Since the observed frustration in the folding landscape is linked to function in IL-1β, we would like to determine if similar correlations can be identified in the antagonist IL-1Ra. Theoretical simulations have predicted frustration on the folding landscape of IL-1Ra (109). The current work uses a combination of equilibrium and kinetic folding studies, ^{1}H-^{15}N 2D heteronuclear NMR and biological assays to characterize the folding and functional landscapes of IL-1Ra and mutant proteins.

SPECIAL METHODS

Heteronuclear NMR

The ^{1}H-^{15}N heteronuclear single-quantum coherence spectra (HSQC) of wt IL-1Ra and mutants were collected on a Varian DMX spectrometer with an operating frequency of 500 MHz equipped with a triple-resonance probe. Samples in the range of 250 μM - 1 mM were exchanged into buffer containing either 25 mM NaPO4, 100 mM NaCl, pH 6.5 or 100 mM d^3 - NaOAc, pH 5.4, and 10% final volume of D_2O. HSQC spectra of the non-deuterated samples were recorded with a spectral width of 12.0 ppm in the ^{1}H dimension (centered at 4.63 ppm) and 32.0 ppm in the ^{15}N dimension (centered at 121.0 ppm). The number points acquired was 1024, with 64 increments in the ^{15}N dimension. The H/D exchange time course was initiated by equilibrating a 300 μL desalting column equilibrated in the 99.9% D_2O version of either buffer (pD* of 6.1 or 5.0, respectively). The exchange reaction was initiated by placing the protein on the column. After a period of 24 minutes, a series of 50 HSQC spectra were taken (with the identical parameters set for the non-deuterated samples). All spectra were recorded at 308K. The ^{1}H dimension was directly referenced to DSS. The collected spectra were processed and visualized with NMRPipe and NMRDraw, respectively (Delgano).

MEF Cellular Stimulation Time Course

3T3 immortalized MEF (mouse embryonic fibroblasts) were generated and maintained as described elsewhere (149). Cells were grown to approximately 100% confluency, then starved for 12-16 hours in 0.5% BCS/1xDMEM before stimulation with the appropriate concentration of cytokine. Cells were stimulated with wt and

mutant IL-1Ra in the starting concentration range of 1000 - 0.1 μg/μL. Wild-type IL-1β was used as a control in the range of 50 - 0.001 μg/μL (EMD). After cell stimulation, time points were taken at 10, 30, 60 and 90 minutes, with one plate set aside for the 0 minute time point.

Nuclear Extract Preparation and Electrophoretic Mobility Shitft Assay (EMSA)

A detailed description of the procedures is located in (Hoffmann, et. al). Briefly, time points were taken by washing the stimulated cells with cold 1xPBS + 1mM EDTA, which were then mechanically harvested and placed into a centrifuge tube. Cells were pelleted by spinning at 8000 rpm, and the supernatant was removed. The cells were resuspended in CE buffer and lysed by vortexing. The lysed cells were spun, and the supernatant was removed. The cell nuclei were resuspended in NE buffer and lysed by 3 freeze-thaw cycles, and then spun at 14,000 rpm. The supernatants were removed, and each complete time course and standard set were normalized by the Bradford assay. Normalized samples and standards were incubated in binding buffer and ^{32}P-labled probe (specific for NF-κB) for 15 min at room temperature before loading onto a 5% non-denaturing polyacyrlamide gel. After 2 hours at 200V, the gels were dried then placed in a storage phosphor cassette before visualizing on a Typhoon 9410 Variable Mode Imager (GE Healthcare). The bands were normalized based total amount of protein added, and the bands were quantified in ImageQuant (GE Helathcare).

RESULTS

Point and loop-insert mutants were constructed to investigate the functional folding landscape of IL-1Ra. The point mutants are C116F, K145D, and

C116F/K145D. The β-bulge sequence of IL-1β, QGEESN, was inserted between residues I52 and E53 of the tight turn in IL-1Ra, with addition of H54P. The point mutants were added to the β-bulge insert mutant, generating β-bulge/C116F, β-bulge/K145D, and the triple mutant β-bulge/C116F/K145D.

Equilibrium Unfolding

Equilibrium unfolding studies were undertaken to determine differences in thermodynamic stability between IL-1Ra and mutant proteins. IL-1Ra has two tryptophan residues, W16 and W120, that have been shown to be useful probes for fluorescence studies of equilibrium unfolding (150). The majority of the fluorescence intensity is emitted by W16, as W120 is in the analogous position in IL-1Ra as it is in IL-1β and has been shown to be quenched in the native protein (150). The equilibrium fluorescence-detected unfolding curves for the point mutants vs. wt IL-1Ra are shown in Figure 6-2a, and the β-bulge inset mutants vs. wt IL-1Ra in Figure 6-2b. The normalized fluorescence intensities were fit to a 2-state model as described in Materials and Methods to determine the free energy of stabilization (ΔG) and denaturant dependence of unfolding (m-value) for each mutant, given in Table 6-1. Replacing C116 with F slightly increased the stability of the protein, evident in the curve shift of the observed transition curve to higher denaturant concentrations than that observed for wt IL-1Ra. The K145D mutant also showed increased stability, and the C116F/K145D double mutant also showed a modest increase, as indicated from the ΔΔG values reported in Table 6-1. The β-bulge

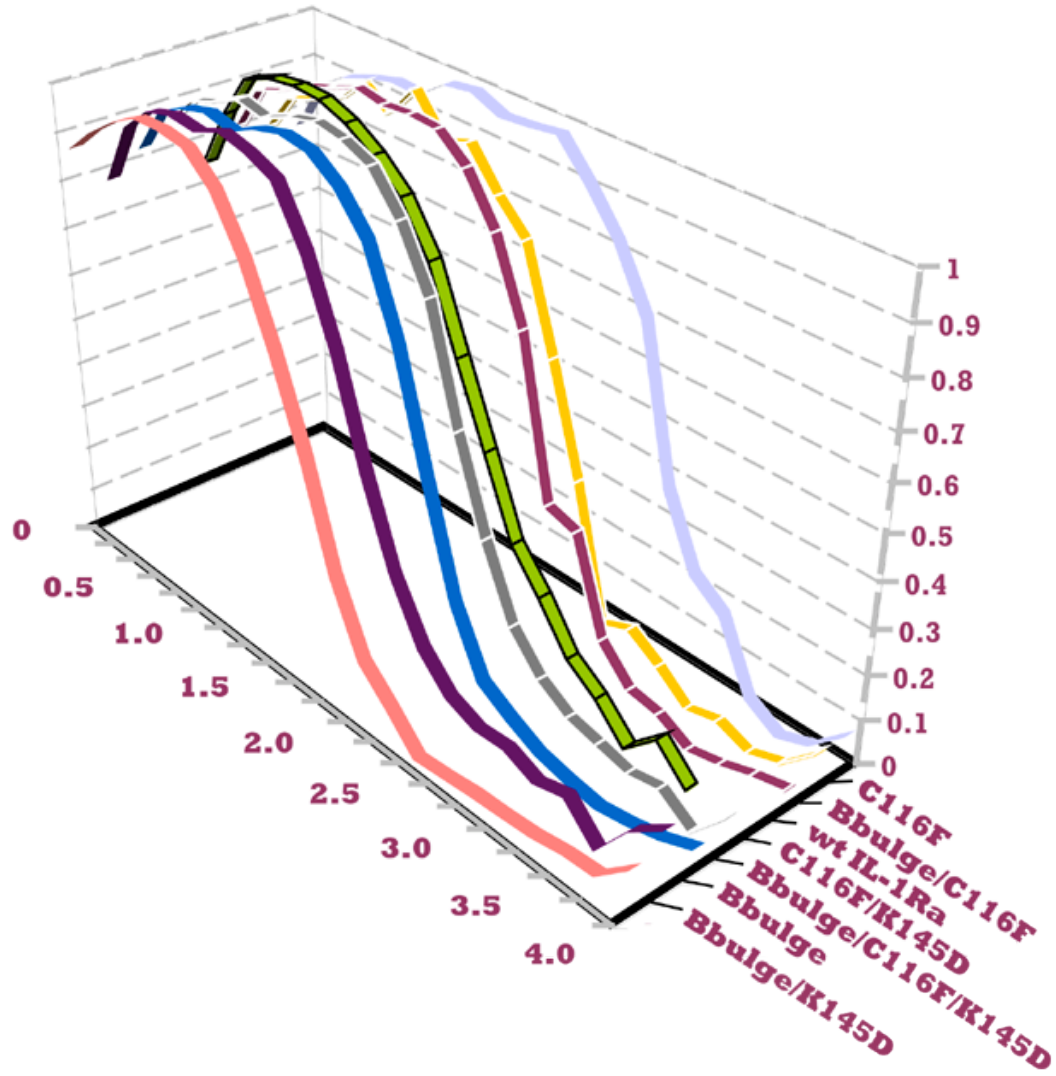

Figure 6-2: Equilibrium titration curve overlay of wt and mutant IL-1Ra. The normalized fluorescence intensities from equilibrium unfolding titrations of wt with C116F, K145D and C116F/K145D (A) and wt with β-bulge insert, β-bulge/C116F, β-bulge/K145D and β-bulge/C116F/K145D IL-1Ra are given. The fluorescence intensities were measured for each mutant over the range 0 – 4 M Gdn-HCl. All curves were fit to a 2-state model of folding (U → N) to determine the stability (ΔG) and the cooperativity (m-value) of the transition.

Table 6-1: Thermodynamic parameters for wt and mutant IL-1Ra

IL-1Ra	ΔG_{NU}[a,b] (kcal*mol^{-1})	$\Delta\Delta G_{NU}$[a,b] (kcal*mol^{-1})	m-value[a,b] (kcal*mol^{-1}*M^{-1})	C_m[c] (M)	ΔG_{NI}[d] (kcal*mol^{-1})	ΔG_{IU}[d] (kcal*mol^{-1})
Wt	8.1 ± 0.1	0	5.7 ± 0.4	1.4	4.9	3.2
C116F	9.3 ± 0.5	1.3 ± 0.5	5.6 ± 0.4	1.7	5.9	3.4
K145D	9.2 ± 0.7	1.2 ± 0.5	6.7 ± 0.1	1.4	5.4	3.9
C116F/K145D	9.0 ± 0.3	0.2 ± 0.4	5.8 ± 0.4	1.6	4.7	4.3
β-bulge insert	7.9 ± 0.2	-0.8 ± 0.2	5.8 ± 0.1	1.4	4.5	3.4
β-bulge/C116F	8.4 ± 2.3	0.3 ± 1.4	5.4 ± 1.5	1.5	4.1	4.3
β-bulge/K145D	7.1	-0.6	5.5	1.3	4.0	3.1
β-bulge/C116F/K145D	8.7 ± 0.1	0.8 ± 0.1	5.8 ± 0.1	1.5	3.8	4.9

Changes in folding parameters between wt and mutant IL-1Ra. The equilibrium data were fit using MATLAB in order to obtain equilibrium parameters for folding, ΔG_{NU}. Changes in ΔG_{NU} ($\Delta\Delta G_{NU}$) were obtained based on Equation 2.4. m-value indicates changes in the accessible surface area upon folding and indicate cooperativity of the folding transition.

[a]Equilibrium transition data were evaluated using a two-state model.

[b]Data were obtained by calculating the average fluorescence intensity and calculating the relative fluorescence intensity in terms of F_{app} as a function of [Gdn-HCl].

[c]C_m values are determined by dividing $\mathbf{\Delta G_{NU}}$ by the m-value.

[d]ΔG_{NI} was determined by using the slowest rate of refolding (k_1) and the unfolding rates over the range of denaturants. ΔG_{IU} was calculated by subtracting ΔG_{NI} from ΔG (extrapolated to water).

insertion was destabilizing and substituting the K145 for D further destabilized the protein (Figure 6-2). Adding C116F to the β-bulge/K145D mutant increased stability, as did adding C116F to the β-bulge mutant alone. Interestingly, the K145D mutant showed the biggest change cooperativity, increasing by more than 1 kcal/mol*M from the wt protein (6.7 $\pm$ 0.4 vs. 5.7 $\pm$ 0.1).

Unfolding Kinetics

A series of kinetic unfolding jumps were performed to determine if the loss of stability in the β-bulge insert mutants was correlated to a faster rate of unfolding, and in contrast, if the stabilizing point mutants display slower unfolding. The observed decay in fluorescence intensity as a function of time for each denaturant concentration was fit to a single exponential as described in Materials and Methods. The relaxation times of wt and the mutant proteins, τ_U, plotted vs. final denaturant concentration are given in Figures 6-3a and 6-3b. The observed relaxation time for unfolding of wt IL-1Ra in 4.0M Gdn-HCl is 154 s. The relaxation times for the point mutants C116F, K145D and C116F/K145D are 147, 115, and 123 s, respectively. The relaxation times for the β-bulge insert, β-bulge/C116F, β-bulge/K145D, and β-bulge/C116F/K145D mutants are 70, 99, 62, and 74 s in 4.0M Gdn-HCl, respectively. Thus, the mutants with the largest decreases in stability, the β-bulge and β-bulge/K145D, also unfolded the fastest. Interestingly, the addition of C116F in the β-bulge insert mutants slowed the unfolding, more so without the presence of K145D. The combination of lowered thermodynamic stability and faster unfolding for the β-bulge insert mutants indicates

differences in the ground state energy of these proteins, or a lower barrier to unfolding.

Refolding Kinetics

Stopped-flow fluorescence and manual mixing kinetic studies were undertaken to determine if the IL-1Ra mutants displayed altered refolding behavior as compared to the wt protein. The wt and mutant proteins had the same refolding profile, and the data was fit to 3 exponential phases. The relaxations times are on the order of ms for τ_3 (fastest phase), and s for τ_2 and τ_1 (slowest phase). Individual plots of the mutant τ_3, τ_2 and τ_1 relaxation times compared to wt IL-1a are given in the panels of Figure 6-2, and plots of the mutant τ_1 relaxation times vs. Gdn-HCl concentration can be found in Figures 6-2a and b. The non-monotonic change in fluorescence is due to the presence of an intermediate species on the pathway to the native state. Many other β-trefoil proteins also display intermediates phases upon folding, including the well-characterized intermediate for IL-1β (FGF, hisactophilin under certain conditions) (151,152). The fastest phase (τ_3) are nearly identical between wt and the mutant proteins. The τ_2 times for all β-bulge mutants show a slight increase in rate (smaller relaxation time), but only within a factor of 1.5 from wt. The τ_1 (slowest phase) relaxation time for wt IL-1Ra when refolded to 0.6 M Gdn-HCl is 27 s. The τ_1 relaxation times from manual mixing for the point mutants C116F, K145D and C116F/K145D are 14, 21, and 28 s, respectively. The τ_1 relaxation times for the β-bulge insert, β-bulge/C116F, β-bulge/K145D, and β-bulge/C116F/K145D mutants are

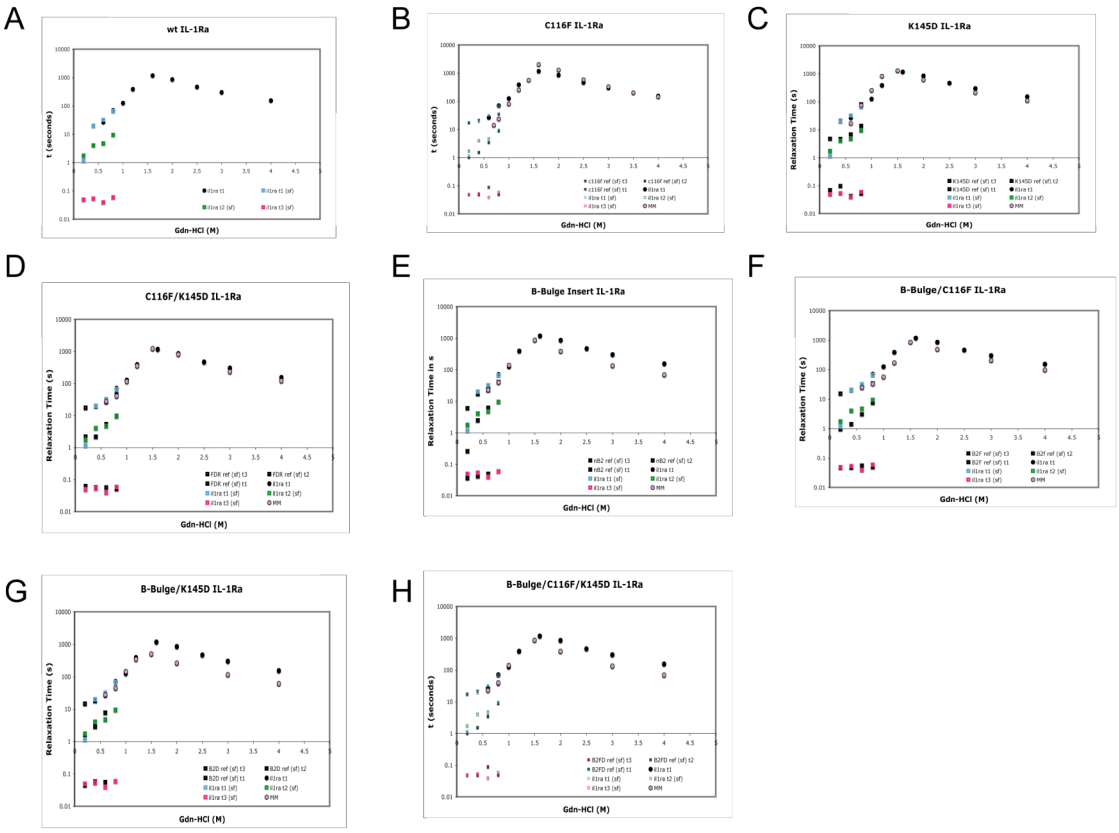

Figure 6-3: Chevron plots of wt and mutant IL-1Ra. Each point on the chevron plot corresponds to the relaxation time of either an unfolding or refolding jump. Refolding jumps are initiated by adding protein unfolded in 2.2M Gdn-HCl to varying final denaturant concentrations (0.2 – 1.2), by following the change in tryptophan fluorescence using either by manual mixing or stopped flow. Unfolding jumps were initiated by adding native protein to varying final denaturant concentrations. The relaxation times are plotted vs. [Gdn-HCl] for (A) wt, (B) C116F, (C) K145D, (D) C116F/K145D, (E) β-bulge insert, (F) β-bulge/C116F, (G) β-bulge/K145D, and (H) β-bulge/C116F/K145D IL-1Ra.

23, 28, 25 and 28 s at 0.6 M Gdn-HCl, respectively. Therefore, the refolding of the various functional mutants again has not changed dramatically, with the largest difference from wild-type being only a factor of 2 (C116F).

Biological Activity Assays

The mutants were tested for agonist activity by direct simulation of 3T3 MEF cells, and compared to wt IL-1β and wt IL-1Ra (positive and negative controls, respectively). All proteins were freshly purified and exchanged into sterile 1xPBS (phosphate-buffered saline) immediately before use. Cells were split into 5 plates/time course, with each plate corresponding to one time point. A total of six time courses were run for each control and mutant protein in the concentration ranges described in the Special Methods section of this chapter. Wt and mutant protein activity was determined by an EMSA measuring the amount of Nf-κB imported into the nuclei of the stimulated cells (149). Nf-κB binds to a ^{32}P-labeled oligonucleotide probe. The bound probe migrates at a much shorter R_f (retention factor) than free probe, and can be visualized and quantified by exposing the gel to a phosphorimager plate (GE Healthcare) and measuring the subsequent intensities on a plate reader (GE Helathcare). The gels for the positive (IL-1β) and negative (wt IL-1Ra) controls are given in Figure 6-3. The time courses are labeled by point and concentration. The intensities calculated from the normalized band quantifications are plotted in Figure 6-4. All six time courses over the whole concentration range are plotted in Figure 6-4 for wt IL-1Ra and IL-1β. The maximum concentration time

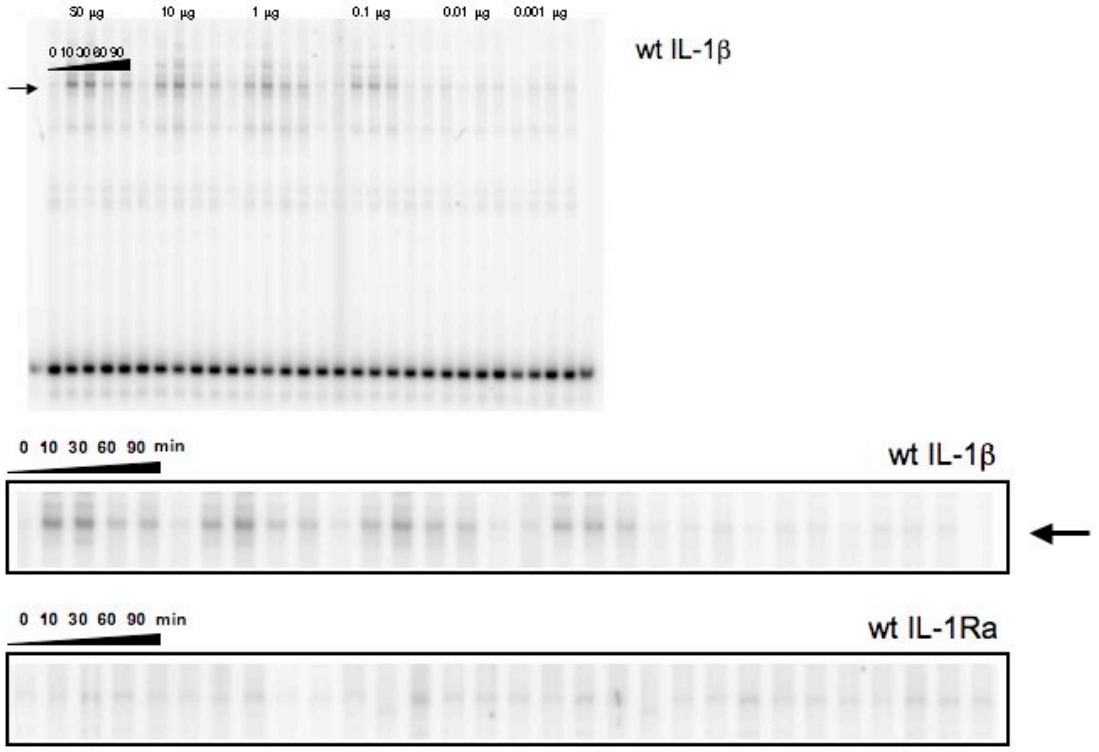

Figure 6-4: Representative electromobility shift assay (EMSA) gels of wt IL-1β and wt IL-1Ra. Shown here are the gels corresponding to the positive (wt IL-1β) and negative (wt IL-1Ra) controls in the biological assays of the IL-1Ra mutants. The concentration ranges started at 50 – 0.001 μg/mL for IL-1β, and 1000 – 0.1 μg/mL for wt IL-1Ra and mutants before diluting 1000-fold immediately before stimulation. Time points were taken at 15, 30, 60 and 90 min after stimulation, and a "0" time point (unstimulated cells) was run for each concentration as well. Nuclear extracts were collected from the stimulated MEF cells, and a ^{32}P-labled DNA probe was used to determine the amount of Nf-κb importation into the nucleus (as it binds to this specific probe). The bands corresponding to the labeled DNA/Nf-κb complex were counted, and the normalized intensities are plotted elsewhere.

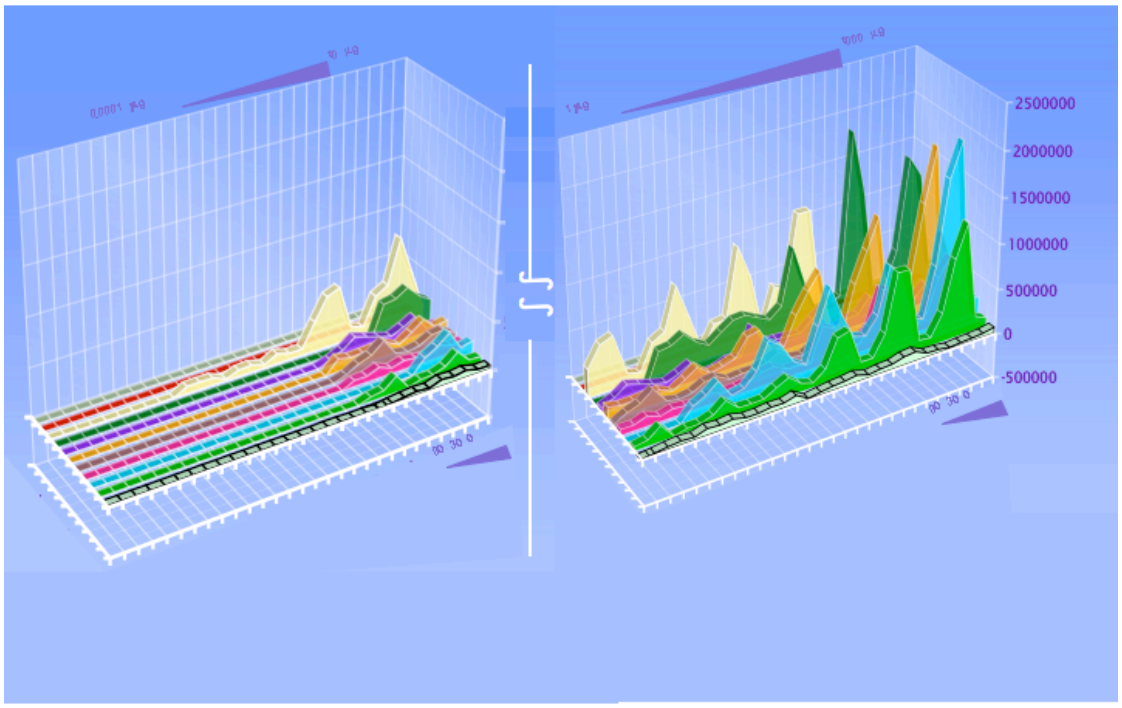

Figure 6-5: 3D plot representation of wt and mutant activity. The normalized band intensities from the EMSA time course time points were plotted over the entire concentration range for each protein. Since IL-1β is run at a concentration range that is different than the rest of the proteins, it is extended out past the last time point of IL-1Ra. The time courses are colored as follows: IL-1β (), wt IL-1Ra (), C116F (), K145D (), C116F/K145D (), β-bulge (), β-bulge/C116F (), β-bulge/K145D (), and β-bulge/C116F/K145D ().

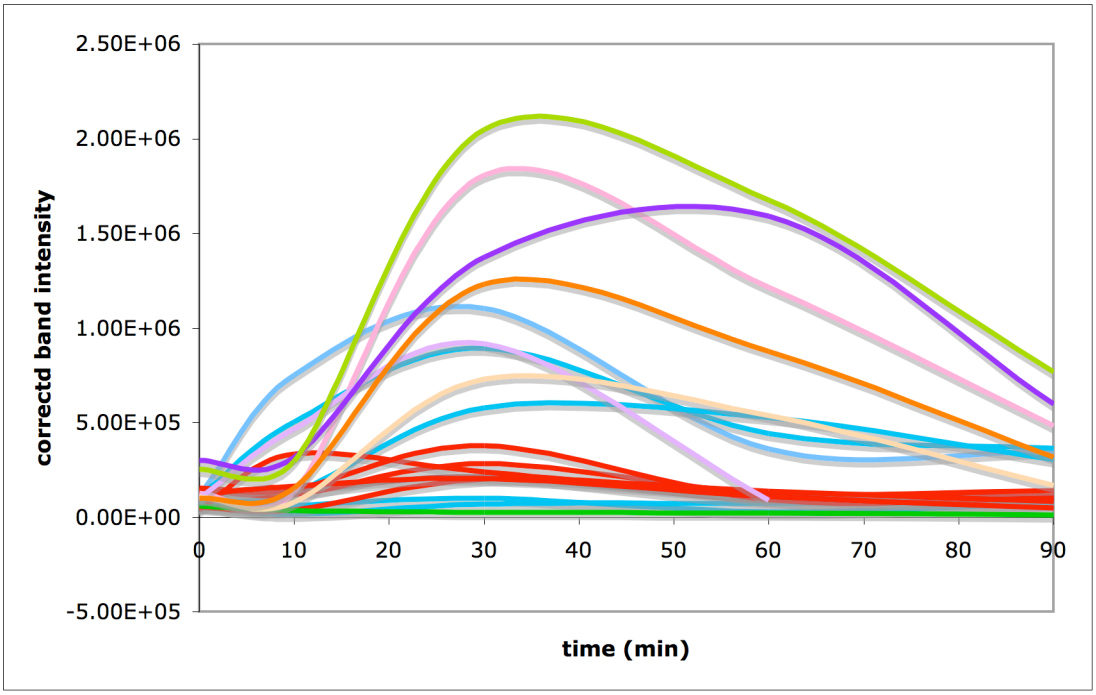

Figure 6-6: 2D plot representation of wt and mutant activity. The normalized band intensities from the full EMSA time courses for wt IL-1Ra and IL-1β, and the peak time point for the IL-1Ra mutants were plotted over the time. The time courses are colored as follows: IL-1β (●), wt IL-1Ra (●), C116F (●), K145D (●), C116F/K145D (●), β-bulge (●), β-bulge/C116F (●), β-bulge/K145D (●), and β-bulge/C116F/K145D (●). All of the signaling mutants display a shifted time frame for signaling as compared to IL-1β.

course for each mutant is also given in Figure 6-5. All of the time course data at every concentration for all mutants and controls are displayed in the 3D plot in Figure 6-4.)

The wt IL-1β control gel showed increasing activitiy in the range of 0.1 – 50 μg/mL range, apparent from the more intense gel-shift bands. Wt IL-1Ra control gel showed no apparent change in gel-shift band intensity of the range of 1000 – 0.1 μg/mL, indicating no activity associated with this protein, as expected for an antagonist. The β-bulge insert mutant also shows no difference in band intensity over the same range as wt IL-1Ra. All of the point and β-bulge double and triple mutants show intense gel-shift bands in the range of 1000 μg/mL down to 10 μg/mL in varying degrees, which were quantified and are shown in Figure 6-5 (3-D plot).

2D ^{1}H-^{15}N Heteronuclear NMR

The structural integrity of the point and β-bulge insert mutants was assessed by taking the 2D ^{1}H-^{15}N HSQC spectra of ^{15}N-uniformly labeled proteins. The spectra were compared to wt IL-1Ra. Partial assignments of wt IL-1Ra are given in Figure 6-6 (based on Stockman, et. al) (153). Full assignments using ^{13}C/^{15}N-labeled proteins and 3D HNCA, HNCACB and CBCA(CO)NH experiments are presently underway, and subsequently can be used to determine changes in the backbone torsion angles upon mutation (80). Representative spectra for the C116F, β-bulge, β-bulge/K145D and β-bulge/K145D/C116F mutants compared to wt IL-1Ra are given in Figure 6-7a-e. Each mutant displays significant peak dispersion and the sharp peak intensities

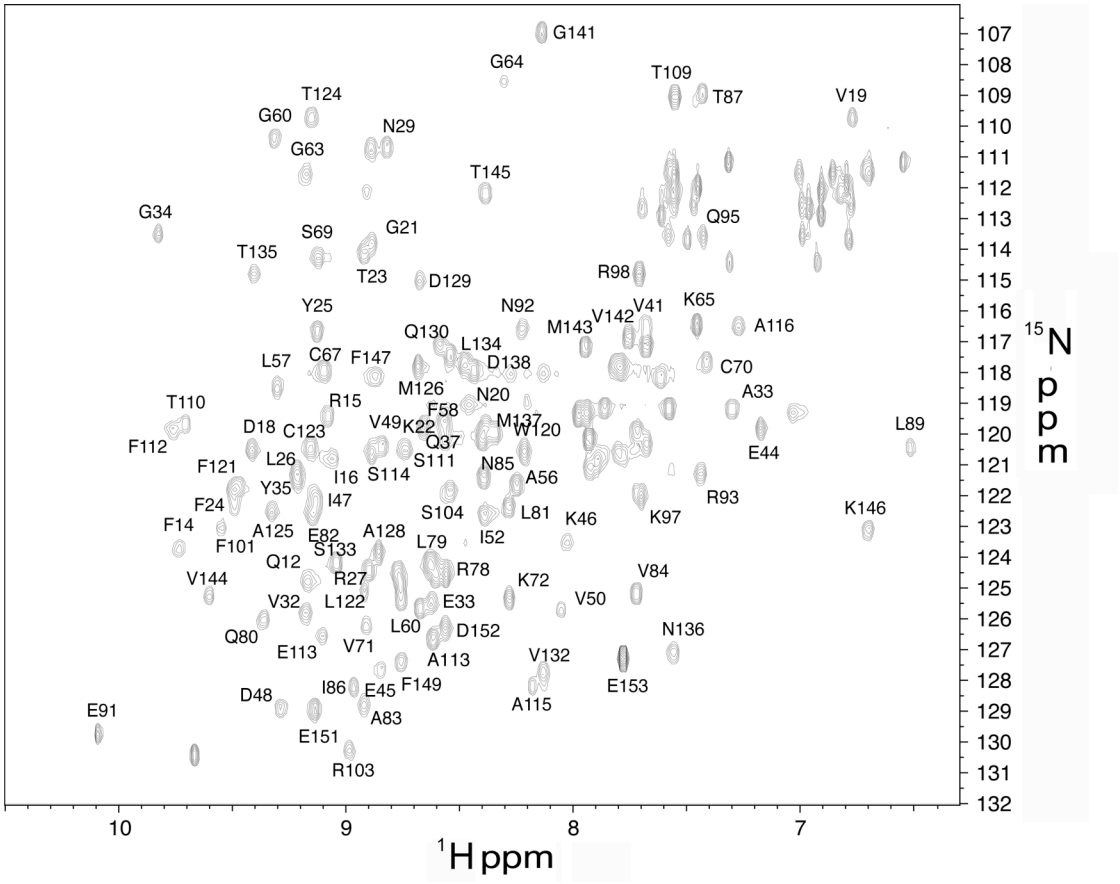

Figure 6-7: ^{1}H-^{15}N HSQC spectrum of wt IL-1Ra. The HSQC experiment provides a "fingerprint" of the amide backbone and select side-chain residues of ^{15}N-isotopically labeled proteins. The spectrum for wt IL-1Ra is shown here with partial assignments based on Stockman, et al. The spectrum is well-dispersed and is indicative of a well-ordered tertiary structure.

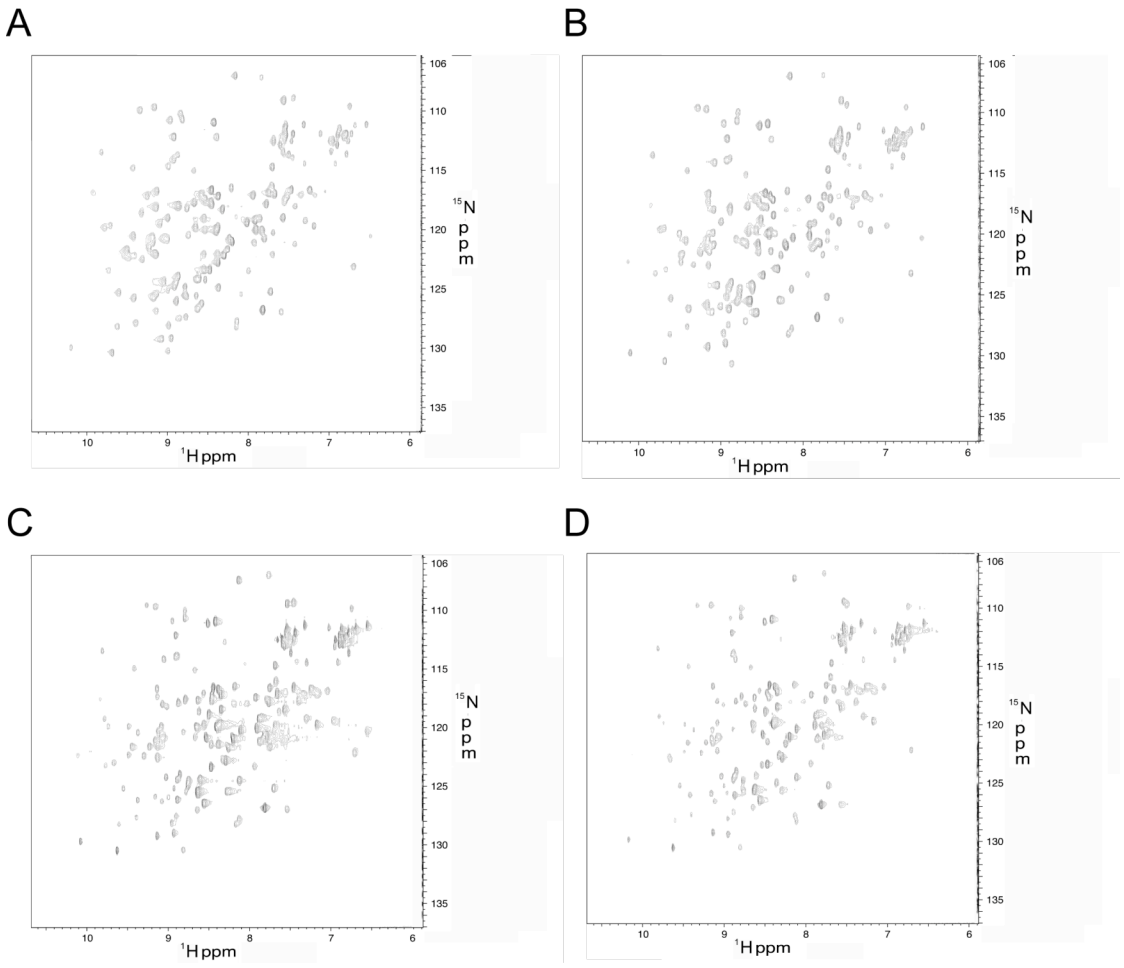

Figure 6-8: ^{1}H-^{15}N HSQC spectra of C116F, β-bulge insert, β-bulge/C116F, β-bulge/K145D, and β-bulge/C116F/K145D IL-1Ra. The HSQC experiment provides a "fingerprint" of the amide backbone and select side-chain residues of ^{15}N-isotopically labeled proteins. The spectrum for C116F (A), β-bulge (B), β-bulge/C116F (C), β-bulge/K145D (D) and β-bulge/C116F/K145D IL-1Ra are shown here. The spectra are well-dispersed and is indicative of a well-ordered tertiary structure. However, due to peaks shifts within the spectra, individual spectra cannot be fully assigned, and further 3D experiments are required to determine the identities of individual peaks (80).

given by well-structured proteins (80). However, due to a number of chemical shift changes upon mutation, only a limited number of assignments may be inferred from the wt protein.

DISCUSSION

The Folding and Functional Landscapes of IL-1Ra Are Linked

Protein folding landscape theory is now the dominant view of how proteins transition from the unfolded to native state. Pioneered by Bryngelson and Wolynes, folding landscape theory predicts that naturally-occurring protein sequences are sufficiently well designed so that local energetic minima are avoided on-route to the native state, or are minimally frustrated (154). Thus, fast-folding sequences are optimized such that folding routes are dominated by the chain connectivity of the backbone and the topology, or shape, of the native state (106,108). In these cases, simple structure based models, based only on the backbone carbon connectivities (Cα, or Go-model), can be used to predict areas of frustration on the folding landscape contributed by geometric constraints within the native state of the protein. Studies with structure-based models of IL-1β, revealed the presence of an on-route intermediate similar to the kinetic intermediate observed by using hydrogen-exchange (28). Subsequent studies of the folding of landscape of IL-1β and other β-trefoil family members FGF-1, FGF-2 and hisactophilin revealed that multiple, energetically-equivalent but geometrically disconnected routes exist for each protein (132). However, small energetic or structural perturbutions within the same geometry can

influence which route is preferred taken over another. Further analysis by Gosavi, et al. linked topological frustration in the folding of IL-1β to an important functional loop, the β-bulge, between strands 4 and 5, in the B-site for receptor binding (108). Contacts that are made early in the folding (in trefoil 3) impede efficient folding, but are unmade later, allowing the contacts within the kinetic intermediate and β-bulge to form. Subsequent theoretical simulations indicated that replacement of this loop for the tight-turn of IL-1Ra in the analogous position minimized frustration in the folding pathway (109). The structural homologue of IL-1β, IL-1Ra, was predicted to have a similar free energy barrier between unfolded and native states as in the bulge deletion. However, structure based models predict that IL-1Ra has geometric constraints and associated frustration in folding caused by contacts between K145 and the longer loop between strands 11 and 12. By inserting this region into the modified, β-bulgeless IL-1β, additional frustration was introduced into the simulated folding landscape(109).

K145 in IL-1Ra and D145 in IL-1β have both been shown to be functionally important. By swapping these two residues in their respective proteins, the activity of the protein also changes; IL-1β binds the receptor but can no longer signal, IL-1Ra binds the receptor and has partial agonist activity (155). Residue 145 does not make direct contacts with the receptor, instead it is juxtaposed between the A and B-sites in both IL-1β and IL-1Ra. This positioning, taken together with the biological data, suggests that residue 145 may provide a communication bridge between these sites. An earlier study by Heidary, et. al explored the pathway between IL-1β Site-A residue H30 and the B-site (124). He showed that mutations of this surface-loop residue

altered the thermodynamic stability and unfolding kinetics of the protein. All replacements of this residue affected receptor binding, even when conserving charge (H30R) or aromaticity (H30F). By determining the backbone torsion angles (φ/ψ) of the mutants, local and long-ranging perturbutions to the backbone were found. The residues showing changes distal to H30 were located in the B-site. This propagation through the backbone shows one existing route of communication between sites (124). Since IL-1β and IL-1Ra have coevolved on the same folding and functional landscape, we would like to test if structural perturbutions distal to binding sites in IL-1Ra affect function.

The Altered Thermodynamic Stabilities of IL-1Ra Mutants

Previous studies of wt IL-1Ra show that it exhibits 2-state equilibrium unfolding behavior (150). All seven mutants described here display 2-state, cooperative folding as compared to the wt protein.

The presence of the C116F mutation has an overall stabilizing effect, regardless of the other point mutants within the protein sequence (Table 6-1). C116 is in the analogous position to F117 in IL-1β, across from its disulfide partner C69 (C70 in IL-1β). The location of this residue in both proteins is in a hydrophobic, tight-turn between strand 9 of the barrel and cap strand 10. C116 is absolutely conserved in IL-1Ra in mammalian species, along with C69 in cap strand 6. The presence of this intramolecular disulfide has been the subject of much scrutiny (156), with conflicting results (unpublished data). In addition to removing the possibility for disulfide bond

formation, the addition of the conserved Phe aromatic side chain increases the hydrophobicity of this loop. Smaller side chain replacements, C116S and C116A, destabilize the protein, as their tendency to go into inclusion bodies during purification has increased (data not shown). The reverse mutation in IL-1β, F117C, also destabilizes the protein (data not shown), and the F117A mutant is not soluble. Indeed, while disulfides are often employed by proteins for adding to their stability (157,158), in the case of IL-1Ra, the replacement of C116 with the residue in the same position in IL-1β, a Phe, has stabilized the protein further. Therefore, the disulfide may have a different role to play in IL-1Ra, adding what is effectively an entropic restraint between strand 7 in the hairpin cap, and the hydrophobic loop between barrel strand 9 and cap strand 10. Any stability gained from the presence of the disulfide is balanced by the strain introduced by its presence.

The K145D mutation also increased in stability as compared to the wt protein. Interestingly, the cooperativity increased significantly from the wt protein, by over 1 kcal/mol*M (Table 6-1). A comparison of the ^{1}H-^{15}N HSQCs of the wt and K145D mutant spectra indicate no gross structural change in the vicinity of that residue upon mutation (data not shown), but there are still a subset of peak shifts. The increase in cooperativity in the equilibrium unfolding transition most likely originates from abolishing the extra contacts between K145 and the loop between cap strand 11 and barrel strand 12. Alternatively, introducing an additional negative charge with respect to the negative charges in close proximity on the surface (D138 and E139) not only breaks a potential salt bridge, but may introduce a local conformational change to

accommodate the increase in electrostatic repulsion. The double mutant C116F/K145D has a similar stability and cooperativity to the C116F mutant, counteracting the effect of the K145D mutation has on the cooperativity in the equilibrium folding transition. Therefore, this behavior is most likely a balancing act between these two adjacent regions in the protein, where changes to one side are seen on the other.

The β-bulge insert mutant is less stable as compared to the wt protein. IL-1β is highly-amenable to loop swap mutations (trypsin inhibitor loop, elastase loop) (159). The β-bulge of IL-1β was replaced with a tight-hairpin turn without changing the overall fold or stability (Capraro, unpublished results). IL-1Ra accepts the loop swap with a loss in stability but not cooperativity, most likely due to the increase in flexibility in the strand 4/5 loop region after replacing the hairpin turn. When the K145D mutation is introduced, there is a further loss of stability. The additional loss of stability may be created by the conformational flexibility introduced on two sides of the protein. The addition of C116F into the β-bulge insert and β-bulge/K145D mutants added stability in both cases. The observation that C116F can transfer stability to both regions simultaneously indicates that these regions (strands 11/12 to strands 4/5 via strand 7 – 10/11 loop bridge) can and do communicate with each other.

The Folding Kinetics of the Functional Mutants

An elegant study by Dr. Shachi Gosavi from the Onuchic lab determined areas shown to be structural traps and impede folding of IL-1β and IL-1Ra map back to

areas within each protein that are important for function (109). While IL-1Ra and IL-1β are structurally homologous, several differences in the loop regions exist between the two proteins. These loops are the β-bulge region between strands 4 and 5 in IL-1β and the loop between strands 11 and 12 in IL-1Ra. Each region makes a distinctly different number of contacts within the local area between the two proteins. Specifically, the contacts between K145 and the β11-β12 loop are the contacts shown to contribute to the frustration on the folding pathway of IL-1Ra. The K145D unfolds slightly faster and refolds slightly slower than the wt protein (< ~1.5 factor). The C116F mutant refolds slightly faster and unfolds slightly slower (< ~1.5 factor). The C116F/K145D mutant displays hybrid folding behavior, refolding and unfolding almost exactly the same as the wt protein. While these changes are not drastic, there is a trend over all data points within each set. In terms of refolding, it is possible that the introduction of C116F speeds up the formation of trefoil 2 and 3. The K145D mutation introduces an additional negative charge into trefoil 3. The additional negative charge may hinder the formation of the late forming contacts by introducing more electrostatic repulsion. It is not possible to see the effect of adding a repulsive charge using the Go-model, since it only takes into account the backbone contacts. Adding both mutations combines each activity of the each point mutant, balancing out the stabilizing/destabilizing forces.

All of the β-bulge mutants show faster unfolding as compared to the wt protein. The β-bulge insert mutant unfolds faster than wt protein, but refolds at the approximately the same rates. The β-bulge insert is six residues longer than the tight-

hairpin turn it replaced. While it contains the same residues as the β-bulge in IL-1β, it is possible that it does not make the same frustrating contacts in IL-1Ra as it does in IL-1β. A longer loop in place of the tight β-hairpin increases the disorder in this important structural region. This could potentially cause disorder in the neighboring side-chains, increasing local flexibility and potentially adding more denaturant binding sites, thus facilitating faster unfolding. The slowest unfolding β-bulge mutant is the β-bulge/C116F mutant, consistent with the stabilizing effect of C116F. The β2/C116F mutant refolds faster than wt, indicating the same effect seen in as the C116F point mutant is taking place. The β-bulge/K145D mutant unfolds with the fastest rate out of all the mutants. The presence of the β-bulge amplifies the effect of the K145D substitution, speeding up unfolding seen in the K145D mutant. The triple mutant (β-bulge/K145D/C116F) again has hybrid folding behavior, refolding at approximately the same speed as wt IL-1β, and unfolding slower than β-bulge/K145D mutant but slower than the β-bulge/C116F mutant. Overall, the push and pull of the mutants on the folding behavior of the protein indicates that the folding landscape has evolved over the entire protein, balancing the folding of regions important for function across the rest of the protein. The relative locations of K145, C116 and the strands 4/5 β-hairpin turn are given Figure 6-8.

Altered Mutant Structures and Activities

Both IL-1Ra and IL-1β have been extensively mutated and the resulting mutant biological activities have been evaluated by a number of cell-based assays

(155). Earlier studies of the D145K IL-1β mutant demonstrated that there is an agonist/antagonist switch in this region of the protein. The reciprocal mutation in IL-1Ra elicits partial agonist behavior without loss of binding (155). Further mutagenesis studies of IL-1β revealed a small set of sites apart from binding sites A or B that modulate the function of the protein (T9, H30) (124).

An earlier study by Greenfeder, et. al investigated the impact of adding the β-bulge from IL-1β would be in terms of altered activity in IL-1Ra. They showed that adding this feature alone did not change the activity of IL-1Ra, but in combination with K145D mutation, the activity was flipped to agonist and in a greater amount than just the K145D mutant alone (160). They combined the β-bulge/K145D with the C116F mutation, and found that this abolished any agonist activity gained by the other two mutations. None of these mutations affected the receptor binding affinity. Different cell types respond to IL-1β in varying degrees (155). In the case of the D145K mutant of IL-1β, the activity has been shown to be anywhere from completely abolished (prosteglandin, or PGE_2 induction in vitro) to a factor of 5-less than the wt protein (in a growth inhibition assay on the A375 human melanoma line) (155). In the case of the IL-1Ra mutants studied by Greenfeder, et al., they used a D10 proliferation assay (mouse helper T-cell (Th_2) line that proliferate in response to IL-1β stimulation) to determine the wt and mutant activities. Here we present activity data based on direct stimulation of 3T3 MEF cells and measuring the time dependent import of the transcription factor nuclear factor κappa-light-chain-enhancer of B-cells (Nf-κB) into the nucleus as a function of concentration and time (149).

When IL-1β binds to IL-1RI, a second receptor like protein, the interleukin-1 receptor accessory protein (IL-1RAcP) is recruited to form a tightly bound complex (148). The intracellular domains of IL-1RI and IL-1RAcP both contain TIR domains, which serve as scaffolding proteins that recruit the adaptor protein MyD88 (161). MyD88 recruits IRAK-4, the serine-threonine kinase responsible for initiating Nf-κB signaling pathway (162). In a very recent study, Lin and coworkers demonstrate that the MyD88 and IRAK-4 proteins form a left-handed helical oligomer complex that further recruits targets of IRAK-4 phosphorylation (IRAK-2 an IRAK-1) (163). The time frame for the intracellular signaling complex formation for wt IL-1 stimulation is within 15 s for the first complexes to form, then peaking at 1-3 minutes (162). Free Nf-κB is imported into the nucleus to fulfill its function as a transcription factor. The amount of Nf-κB imported into the nucleus can be determined by nuclear isolation and gel-shift assays (149).

The wt proteins and mutants were run on in an EMSA according analogous to the gels presented in Figure 6-3. The resulting normalized intensities are plotted in Figure 6-3 with the time courses of the total concentration range for IL-1Ra and IL-1β and the highest concentration for the mutants are shown. As evident from the plot, the amount of activation is dependent on increasing concentrations of protein. Interestingly, the mutants that gain agonist activity show a delayed response as compared to wt IL-1β. The full concentration range and associated time courses for all mutant and wt proteins are given in the 3D plot of Figure 6-4. In contrast to the predictions from the crystal structure analysis where one might infer that inserting the

β-bulge alone would confer the change in antagonist to agonist activity onto wt IL-1Ra, we see that this is not enough, and there is more involved. All mutants excepting the β-bulge insert mutant displayed varying degrees of partial agonist activities. As expected from previous studies, both the K145D and β-bulge/K145D mutants signaled. Unexpectedly, all of the C116F mutants signaled. The locations of C116 with respect to K145 and the strand 4/5 hairpin (β-bulge insert position) in the IL-1Ra/IL-1RI complex are shown in Figure 6-10. Mutants show an increase in thermodynamic stability from their respective starting points (wt or β-bulge insert). The increase in stabilization is most likely due to stabilizing hydrophobic packing interaction of the Phe side chain with the surrounding residues. In IL-1β, F117 packs in between residues V72, P78, Q116, and W120. The analogous region for C116 in IL-1Ra shows sidechain interactions with V70, K71, T76, R97, A115, P117 and W120. This area of the sequence between IL-1Ra and IL-1β is highly conserved between proteins, identical or similar from residue 111 to 124, excepting residues A115, C116 and G119 in IL-1Ra and Q116, F117 and N119 in IL-1β. However, these residues are either identical or similar over species, indicating these residues are important within their respective proteins. Indeed, these residues compose a hydrophobic "mini-core" region shown to be important for folding in IL-1β (106). Geometrically, this stable min-core region bridges two important functional regions,

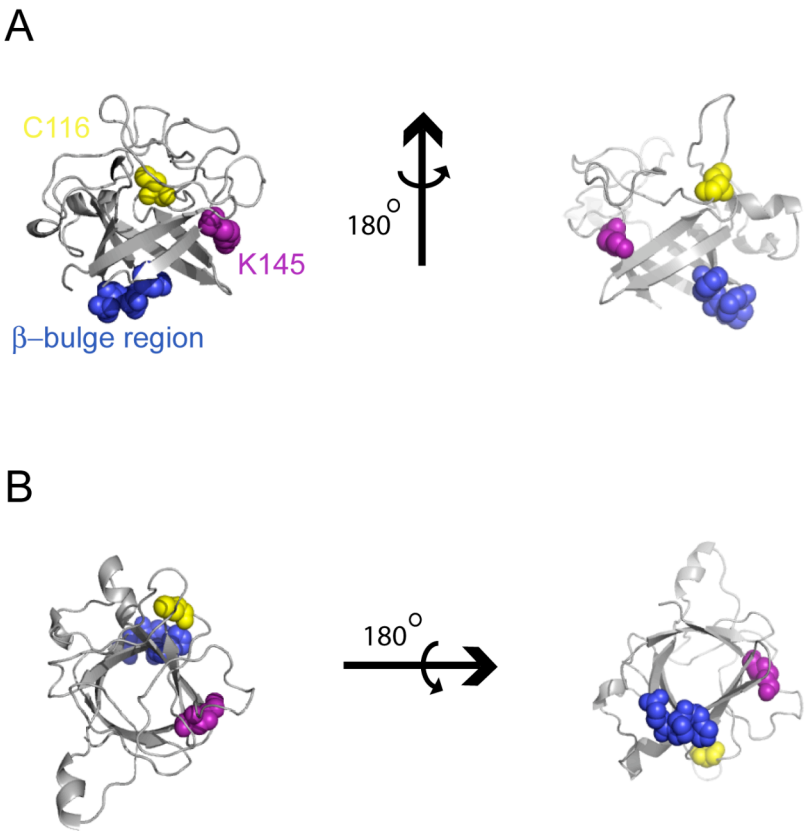

Figure 6-9: Location of functional "hot-spots" outside of the receptor binding interface. Shown here are three views of crystal structures of IL-1RI bound with either IL-1β (A) or IL-1Ra (B) (PDB:1ITB and 1IRA, respectively) (refs). The sites are colored blue for Site A and red for Site B in both cases. Functionally relevant sites, residues 145 and 117/116 in IL-1β and IL-1Ra, respectively, are also labeled by color (145 is yellow, 117/116 is violet).

the interface between the A and B receptor binding sties in trefoil 3, and residues participating in site B on the opposite side of the ligand/receptor complex (Figure 6-10).

The conserved residue C116 in IL-1Ra has been shown to be disulfide bonded to conserved C69 in 2 out of the 3 crystal structures available for the protein, in both he free and receptor-bound versions of IL-1Ra, shown in Figure 6-8 (26,164). However, it is not present in one crystal structure and in the NMR structure, although the backbone of this crystal structure overlays with the free disulfide-bonded structure. The presence of a disulfide in IL-1Ra has been intensely studied by several groups, including labs at Amgen, the company that produces recombinant IL-1Ra as therapeutic Anakinra (156). Upon exposure to air, fully reduced IL-1Ra was shown to display the Raman-band for a disulfide bond. Studies in our lab have shown labeling of free cystienes by iodoacetic acid for oxidized and reduced (10 mM DTT) wt IL-1Ra generated bands consistent with the presence of protected cysteines on an SDS-PAGE gel (data not shown). The analogous experiment with C116F and an A115Q/C116F double mutant did not show bands having different R_f values for reduced vs. oxidized (data not shown). Equilibrium denaturation studies in the presence of reducing agent also did not significantly alter the stability or kinetics of folding (data not shown). While it is possible that the disulfide introduces enough strain to destabilize the protein as much as it could potential stabilize it, more extensive experimental studies must be undertaken to confirm the presence of the disulfide *in vitro* and *in vivo*.

While the detection of the C69-C116 disulfide bond *in vitro* has been problematic for other groups, it should be noted that *in vivo*, secreted IL-1Ra has an N-terminal signal sequence that directs it to the endoplasmic reticulum (ER) for translation (9). Many extracellular proteins are disulfide-bonded for stability in the oxidizing extracellular milieu, including IL-1RI and IL-1RAcP (157). The ER contains protein disulfide isomerase (PDI), which is responsible for catalyzing disulfide bond formation, along with the oxidizing environment of the ER itself (165). Indeed, the two crystal structures of IL-1Ra that contain the disulfide bond have the C69 and C116 residue backbones at the optimal angle for an intramolecular disulfide bond (90 degrees), and the Cα positions of the other crystal structure are also at 90° (only the Cα positions are available for that structure). Therefore, the possibility that the C69-C116 disulfide existence *in vivo* is likely, and should be investigated further.

Wt IL-1Ra is a competitive inhibitor to IL-1β-initiated receptor signaling. Mutants of IL-1Ra, C116F, C116F/K145D, β-bulge insert/C116F and β-bulge insert/C116F/K145D all have the capacity to bind IL-1RI and cause Nf-κb importation into the nucleus as detected by EMSA. The most reasonable explanation as to why these mutations cause agonist-like behavior for IL-1Ra is that C116F breaks the intracellular disulfide, freeing up the opposite side of the protein (B-site) so that it may interact in a constructive way with IL-1RI to elicit signaling, since C116 is on the opposite side from where the receptor binds. Preliminary results also indicate that C116A and C116S mutants can stimulate Nf-κb importation as well (data not shown, (160)). Another possibility is that introduction of a Phe in position 116 creates a

subtle rearrangement of the residues around that area, which propagates to site B though the barrel. C116 in IL-1Ra and F117 in IL-1β reside in a conserved, structural "hinge point" between the cap and barrel in both proteins, adjacent to F101, one of the conserved topologically symmetric phenylalanine residues that pin the barrel in IL-1β (166). Therefore, any structural perturbution here can cause drastic changes throughout the protein, propagating through the backbone or hydrogen bonding network, or both. H/D ^{1}H-^{15}N NMR and carbon backbone torsion angle determination (HNCA) experiments run on IL-1β show that F117 is protected from exchange and retains its φ/ψ angles when the protein is circularly permutated in several places (residues 23, 65, 76 and 142, new N- and C-termini are generated here), and when the β-bulge is replaced by a tight turn (Capraro, unpublished results). We are in the process of analyzing the analogous experiments for the C116F IL-1Ra mutants to see what changes have occurred in H/D protection and backbone torsion angle after introduction of C116 mutation, and how that information is propagated to the B-site. Preliminary inspection of the backbone fingerprint for these mutants has already revealed a number of peak shifts, indicating the environment around the backbone amides has changed in the presence of the C116 mutations (Figure 6-7).

Introduction of the K145D also imparts agonist activity to IL-1Ra. K145 is conserved over species in IL-1Ra (Chapter 1). The residue in the analogous position in IL-1β is D145, and this residue bridges between Sites A and B of both proteins at the start of strand 12 of the barrel. In IL-1Ra, the K145 side chain resides directly across from D136 and E137 (Figure 6-8). These charged residues create a negatively

charged pocket next to Site A of IL-1Ra. In IL-1β, D145 resides in close proximity to D142 and K139. Interestingly, the D145K mutation in IL-1β imparts antagonist activity, where the protein binds but does not initiate cell signaling (155). Both K145 in IL-1Ra and D145 in IL-1β precede F146 in both proteins, one of the three topologically symmetric and absolutely conserved phenylalanines that pin the barrel and cap (Figure 6-9, (138,166)) in IL-1β. Strand 12 bridges both the A site and B site in IL-1β (A site: F146 and M148, B site: Q149 and V150) and IL-1Ra (A site: Y147, B site: E151 and D152). Flipping the charged surface of either protein in the vicinity of position 145 may create significant changes that perturb the structure through F146, which could then be channeled through strand 12 down to the B-site. Indeed, D152 in IL-1Ra has an additional backbone hydrogen bond formed between it and Q149 in the bound conformation. Adding the β-bulge to the K145D mutant in IL-1Ra provides additional contacts between it and the receptor for Site B, enabling a favorable conformation or more contacts to recruitment of the accessory protein. On-going analysis of 2D and 3D NMR data collected for these mutants will determine the impact these mutations have on the hydrogen bonding and backbone torsion angle networks in strand 12 and beyond.

A recent study by Lingel, et al. used small-angle x-ray scattering and NMR chemical shift perturbation analysis to propose a binding model for the heterotrimeric active IL-1β/IL-1RI/IL-1RAcP complex (37). It should also be noted that postion 145 is on the direct opposite side of the IL-1RAcP site proposed for IL-1β by Lingel, et. al. In the model, Ig-domains 1 and 2 of the accessory protein interact with Ig-

domains 1 and 2 of the receptor (Figure 6-10). The third Ig-domain of the accessory protein contacts both the A and B-sites of IL-1β and the third Ig-domain of the receptor. The linker between is not included in the model, but there is the potential for stabilizing contacts between it and ligand/receptor complex to exist. In addition, the side chains of strand 1 of IL-1β and the C-terminal residue S152 pack against strand 1 of the third Ig-domain of the accessory protein (Figure 6-10). These contacts are conserved reasonably well, so potentially this could be a binding site between IL-1β and the accessory protein. In IL-1Ra, this residue is an Asp (D152), which also may acceptable to the accessory protein in that postion.

The β-bulge in IL-1β has been shown by our group and others to be critical for signaling ((155), Capraro unpublished results). The proposed mechanism of action for the β-bulge is to help engage the third Ig domain of the receptor and thus induce a conformational change that is recognized by IL-1RAcP for binding. Interestingly, adding the β-bulge to IL-1Ra did not confer the same activity, shown by lack of signaling. Only in the presence of two other types of mutation (K145D or C116F) did the β-bulge insert mutants gain the required configuration to engage the receptor and elicit signaling. An overlay of the crystal structures of free and bound IL-1Ra reveals that only a few hydrogen bonds have changed throughout the protein, in the B-site (D152), K64 (β-hairpin between barrel strand 5 and cap strand 6), and A82 (end of strand 7 before helical turn). This is also true for IL-1β free/bound crystal structures. Therefore, it is not possible to infer by inspecting crystal structures

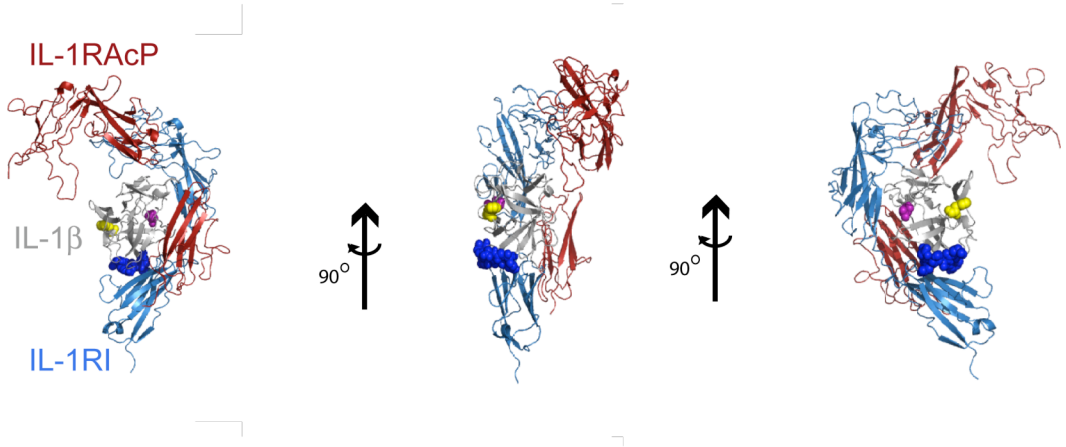

Figure 6-10: Model of the IL-1β/IL-1RI/IL-1RAcP binding interaction. The recent paper by Lingel, et al. proposed a new model for the heterotrimeric signaling complex, based on NMR chemical shift analysis and small-angle x-ray scattering (SAXS) data (Lingel ref). As show here, D145 in IL-1β (in the analogous position as K145 in IL-1Ra) and F117 (in the analogous position as C116 in IL-1Ra) are both located away from the receptor and the receptor accessory protein. The functionally important regions of IL-1β are highlighted and colored in the analogous fashion of Figure 6-9.

alone how surface mutations inside and outside the binding sites will affect the binding and IL-1RAcp recruitment activity. However, perturbing the hinge points and barrel of IL-1Ra by using these "flip-flop" mutations (K145 and C116 to D145 and F117) provides it with a means to communicate across the surface in the same frame as IL-1β, through either the F101 or F146 hinge points. Inserting a longer loop alone does not "unlock" the barrel of IL-1Ra in the same fashion, therefore as opposed to the predictions from the crystallographic analysis, that mutation alone cannot confer signaling.

Recently, an antibody that binds IL-1β was approved by the FDA for clinical trials (167). While most antibodies are designed to block the activity of their targets, the XOMA-052 antibody binds the basic 90's loop of IL-1β and knocks *down* activity, not abolishing it, creating a partial agonist protein. Since IL-1β has positive effects as well as deleterious, diminishing its activity instead of totally knocking it down is a new therapeutic strategy for treating IL-1β-dependent disease. The same strategy can be achieved by using partial agonist IL-1Ra mutants or attenuated IL-1β mutants as well.

CONCLUSION

Many point mutants of proteins can abolish receptor binding or alter the folding pathway to the native state. However, mutants of IL-1Ra with altered folding have been converted from having antagonist activity to partial agonist activity. This indicates that the potential for agonist activity is conserved within the structure,

although the mechanism has been “locked” from IL-1β to add antagonist behavior. Further investigation is required fully detail the antagonist/agonist switch communication routes across IL-1Ra and IL-1β, and how the mutant/IL-1RI receptor complex engages the IL-1AcP.

Chapter 7

The Folding and Structure of IL-33

ABSTRACT

The most recent addition to the IL-1 family of proteins is IL-33, which binds the IL-1 receptor family member ST2. The diverse functions of this new family member are currently under intense investigation, but it has already been shown to be a key elicitor of the Th2-inflammatory adaptive response. In the current study, we use the combination of mutagenesis, fluorescence-monitored equilibrium denaturation curves, stopped low and manual mixing kinetics, enzymatic digests, and ^{1}H-^{15}N 2D NMR to characterize the β-trefoil region of IL-33.

INTRODUCTION

The receptor for IL-33, ST2, was first identified as secreted molecule in high human endothelial cells (HEVECs) in response to cell proliferative signals in 1989 (168). Four years later, the cell-surface version of the receptor was found expressed in the same cells as the soluble version. Both the soluble and surface-bound forms shared the same predicted Ig-domain structure as the IL-1 family of receptors (yanagisawa, gayle), and the cell-surface receptor contains a transmembrane and TIR domain analogous to the signaling IL-1 receptors (169). However, the ligand of the ST2 receptors was not identified until recently (33).

IL-33 was identified as a β-trefoil cytokine protein by a structural database search looking for distant IL-1 and FGF β-trefoil family members (33); the search findings matched the protein product of the DVS-27 gene identified by Onda while studying a canine model of cerebral hemorrhage recovery. IL-33 (DSV27) was highly

upregulated after induction of a subarachnoid hemorrhage and the protein product is predominantly expressed in vascular and respiratory tissues and in a nuclear form (35). Interestingly, IL-33 was also later identified again as a nuclear protein NF-HEV with a proposed helix-turn-helix DNA binding motif in the N-terminal region in lymph tissues (34). Like other cytokines in the IL-1 family, IL-33 is synthesized as a 270-reisdue proprotein, with a canonical nuclear localization sequence (NLS) in the N-terminal proregion (33,170).

The genes for the founding members of the IL-1 family, IL-1α and IL-1β, diverged over 300 million years ago (131). Both proteins are synthesized as much longer precursor molecules, with the β-trefoil region in the C-terminal region. As discussed in Chapter 3, the precursor domain of IL-1β has no known function to date, other than inhibiting the activity of the cytokine by keeping it in a partially folded state. However, the precursor domain of IL-1α contains a conserved NLS, and IL-1α has been shown to primarily act as a transcription factor (8) and more recently as part of the spliceosome (171). Indeed, the mature β-trefoil version of IL-1α is rarely seen extracellulary (170). Full-length IL-33 has been shown to associate with chromatin, as full-length IL-1α (170,171). Both cytokines are implicated in regulation of apoptosis (6,171,172). Also, the phosphrylation site predictor NetPhos predicts a potential phosphorylation site at conserved serine residue S71 in the N-terminus of IL-33 (score = 0.998) (173). Despite the presence of the N-terminus and the predominant nuclear localization of these molecules, both the full-length versions of

IL-1α and IL-33 can bind to their respective extracellular receptors and elicit signaling, unlike full-length IL-1β (11,174).

Although IL-33 shares many characteristics with IL-1α, it also contains features similar to IL-1β and IL-1Ra. Both β-trefoils of IL-1β and IL-1Ra have a highly basic loop between strands 7 and 8, and IL-33 has a highly-basic loop between strands 3 and 4. The highly basic loop is entirely absent in IL-1α. Also as shown in Figure 7-1, the sequence conservation between the N- and C- termini in IL-33 is more similar to full-length IL-1β, with the C-terminus being more highly conserved. Diverging from all IL-1 family members is the presence of a relatively high number of histadines (7) in the C-terminus of IL-33 (0, 1 and 1 for IL-1α, IL-1β and IL-1Ra, respectively), reminiscent of the β-trefoil family member hisactophilin, an actin-binding protein (175). In addition, IL-33 is secreted by a non-classical mechanism like that observed for IL-1β.

As of today, little is known about the processing and secretion of full-length IL-33. Schmitz and co-workers initially described IL-33 to be processed by caspase-1 at D111 (33). However, the downstream P_4 – P_2 residues that would make up this putative cutsite (N-term – ALHD | S – C-term) are not preferred for caspase-1, and the sequence is not conserved in this area (84,85). Indeed, it was shown by several groups that full-length IL-33 was not processed by caspase-1 *in vitro* (176). Full-length IL-33 is processed at D178 (D68 in the β-trefoil region truncation) by both caspase-3 and caspase-7. This cutsite is conserved over species as N-term – DGVD | G – C-term, and resides in the loop between strands 5 and 6 in the C-terminal

Figure 7-1: Sequence conservation over IL-33 in mammals. The sequences of IL-33 were aligned and the relative conservation is shown here. The available mammalian sequences for full-length IL-33 from the National Center for Biotechnology Institute (NCBI) were aligned with Clustalw and visualized using Jalview. The predicted helix-turn-helix motif (residues 42-55) is conserved over mammals, as well as the bipartite NLS (residues 56 – 65) in the N-terminus. In the C-terminus, the areas encompassing strand 1 and trefoil 3 are highly conserved, as well as a patch of hydrophobic residues in the juncture between trefoil 2 and 3 (residue 200 in the full-length numbering).

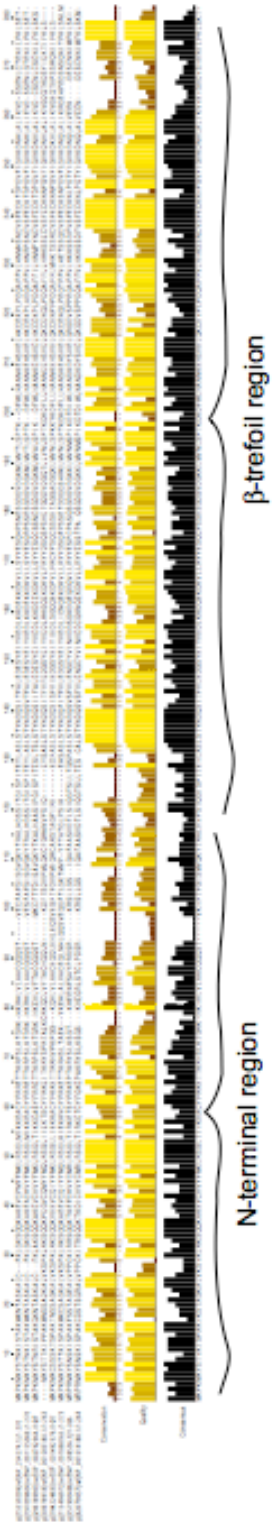
β-trefoil region
N-terminal region

β-trefoil region. Cleavage at the caspase-3/7 cutsite prevents IL-33 from binding ST2, but it can still be translocated to the nucleus (174). As with all other IL-1 family members excluding IL-1Ra, IL-33 does not contain a classical secretion sequence (172). IL-33 is released from necrotic cells, and cells exposed to freeze/thaw cycles (177). Whether or not IL-33 is released in response to LPS or other immune stimuli is currently an area of active research.

IL-33 is the newest member of the IL-1 family, sharing the homologous β-trefoil fold. The current work uses a combination of equilibrium and kinetic folding studies, circular dichroism spectropolarimetry, ^{1}H-^{15}N 2D heteronuclear NMR, enzymatic cleavage assays, and osmotic shock to characterize the folding and functional landscape of C-terminal β-trefoil region of IL-33.

SPECIAL METHODS

Cloning and Purification of IL-33

The gene for full-length human IL-33 was obtained from Open Biosystems (IMAGE:5314040). The DNA sequence corresponding to the proposed β-trefoil region (residues 112 - 270 of the precursor protein) was amplified by PCR, restriction digested and ligated into the pET-28a (His-Tag) or pET-24a (no His-Tag) expression vector (Novagen). The insert-containing pET-28a vector was transformed into E. coli BL21 (DE3) competent cells (Novagen). A culture (luria broth) was inoculated with these cells and grown at 37 °C until they reached an OD_{600} of 0.6. Protein expression

was achieved by inducing the cells with 1 mM IPTG (final concentration) and the shaker temperature was reduced to 30 °C. The cells were harvested after 4 hours by centrifuging at 6238 x g for 10 min. The media was carefully decanted, and the resulting pellets were suspended in a total volume of 80 mL 25 mM Tris-HCl, pH 8.0 and stored at -20 °C overnight. The cells were thawed/resuspended and incubated for $\geq$1.5 hours at room temperature, then spun down at 15295 x g rpm for 15 minutes. The protein was determined to be >90% pure by SDS-PAGE.

The supernatant was filtered, and 5 M NaCl was added to a final concentration of 300 mM. The protein solution was added to charged Ni-resin (Qiagen) and incubated at room temperature for >45 min. The unbound protein solution was removed by gravity filtration and the resin washed with 2 column volumes of wash buffer (25 mM Tris-HCl, pH 8.0, 300 mM NaCl). One column volume of thrombin cleavage buffer was added (25 mM Tris-HCl, pH 8.0, 150 mM NaCl, 2 mM $CaCl_2$), and ~5 mg of 99%-purity thrombin (Fisher Scientific) was added. The resin-thrombin mixture was incubated for 5 hrs at room temperature, then at 4 °C overnight. After the resin warmed up to room temperature, the thrombin inhibitor PPAC (Fisher-Scientific) was added, and the protein was eluted from the Ni-column, along with two additional washes after the initial elution (with the thrombin cleavage buffer). The wash fractions were pooled and concentrated, and then injected onto a 26/20 S-200 size-exclusion column (GE Healthcare) equilibrated with 50 mM Tris-HCl, pH 6.8, 150 mM NaCl, 1 mM EDTA at a flow rate of 1.5 mL/min. Purity of IL-33 was assessed by SDS-PAGE (>95%). A mutant (D68A) was generated using the method described

in Chapter 2 of this thesis, and was expressed and purified in an analogous fashion to the wt protein.

Heteronuclear NMR

The ^{1}H-^{15}N heteronuclear single-quantum coherence spectra (HSQC) of wt IL-33 and D68A mutant were collected on a Varian DMX spectrometer with an operating frequency of 500 MHz equipped with a gradient probe. Samples in the range of 250 μM - 1 mM were exchanged into either 25 mM NaPO4, 100 mM NaCl, pH 6.5 and 10% final volume of D_2O was added. HSQC spectra of the non-deuterated samples were recorded with a spectral width of 16.0 ppm for the ^{1}H dimension (centered at 4.63 ppm) and 36.0 ppm for ^{15}N dimension (centered at 120.0 ppm). The number points acquired was 1024, with 64 increments in the ^{15}N dimension. A total number of 4 scans was taken. The H/D exchange time course was initiated by equilibrating a 300 μL desalting column equilibrated in the 99.9% D_2O version of the buffer (pD* of 6.1). The exchange reaction was initiated by placing the protein on the column. After a period of 24 minutes, a series of 50 HSQC spectra were taken (with the identical parameters set for the non-deuterated samples). All spectra were recorded at 308K. The ^{1}H dimension was directly referenced to DSS. The collected spectra were processed and visualized with NMRPipe and NMRDraw, respectively (Delgano).

Enzymatic Digest Time Course

A caspase-3 digest of both wt and D68A IL-33 was performed with the following procedure. A total of 3 nmol of each protein was exchanged into 1xMES buffer. Caspase-3 (Calbiochem) was added in the amount necessary to digest the total substrate (IL-33) by 4 hours at 25°C. Time points were taken at 0, 1, 5, 15, 60, 120 min and 24 hr, the 0 min time point was the enzyme and substrate put directly into the quench. Reactions were quenched by flash-freezing in $N_{2(l)}$. All time points and a blank sample (without added enzyme) were run by SDS-PAGE.

RESULTS

Equilibrium Unfolding

Equilibrium unfolding studies were undertaken to determine the thermodynamic stability of IL-33. Full-length IL-33 has two tryptophan residues, W17 in the N-terminus and W193 in the C-terminus (W82 in the truncated version numbering). W82 is quenched in the native protein, so the fluorescence signal increases with increasing denaturant concentration. The far-CD spectra were collected for wt IL-33 using the same denaturant range. The change in fluorescence intensity with an excitation wavelength of 293 nm over the wavelength range of 300-450 nm was measured as a function of final denaturant concentration. The normalized intensities were fit to a 2-state model as described in Materials and Methods to determine the free energy of stabilization (ΔG) and denaturant dependence of unfolding (m-value), given in Table 7.1, and are compared to wt IL-1β and IL-1Ra.

The normalized fluorescence curve is shown in Figure 7-2. Both IL-1β and IL-1Ra are more stable than IL-33 by over 1 kcal/mol under these conditions (1xMES buffer).

Unfolding/Refolding Kinetics

A series of kinetic unfolding jumps were performed to determine rate of unfolding for wt IL-33. A representative unfolding trace for IL-33 is shown in Figure 7-3, along with the corresponding trace for IL-1Ra, run under identical conditions (refolded to 0.4 M Gdn-HCl). The decay in fluorescence intensity was fit to a single exponential as described in Materials and Methods. The relaxation times of IL-33, τ_U, plotted vs. denaturant is Figure 7-4, compared with wt IL-1Ra. The relaxation time for unfolding of wt IL-33 in 3.0M Gdn-HCl is 42 s, 305 s wt IL-1Ra, and 942 s for wt IL-1β. Thus, wt IL-33 unfolds significantly faster than both IL-1Ra and IL-1β. Stopped flow fluorescence and manual mixing kinetics studies were undertaken to determine refolding behavior of IL-33 as compared to the wt IL-1Ra and IL-1β. IL-33 data was fit to 3 exponential phases. The relaxations times are on the order of ms for τ_3 (fastest phase), and s for τ_2 and τ_1 (slowest phase). A plot of the τ_3, τ_2 and τ_1 relaxation times vs. Gdn-HCl concentrations are given in Figure 7-4, compared to wt IL-1Ra and IL-1β. The fastest phase (τ_3) shows approximately 2-fold slower rates over Gdn-HCl as compared to IL-1Ra. The τ_2 times are slightly (<1.5 factor) faster for IL-33. The τ_1 (slowest phase) relaxation times for wt IL-33 are 2-3-fold faster than the corresponding times for IL-1Ra in both stopped flow and manual mixing. For example, the τ_1 relaxation times from manual-mixing are 23 and 72 s, respectively.

Table 7-1: Thermodynamic parameters for wt IL-33, IL-1Ra and IL-1β

	ΔG_{NU}[a,b] (kcal*mol^{-1})	m-value[a,b] (kcal*mol^{-1}*M^{-1})	C_m[c] (M)	ΔG_{NI}[d] (kcal*mol^{-1})	ΔG_{IU}[d] (kcal*mol^{-1})
Wt IL-33	6.7 ± 0.3	5.5 ± 0.3	1.2	0.4	6.3
Wt IL-1Ra	8.1 ± 0.1	5.7 ± 0.1	1.4	4.9	3.2
Wt IL-1β	7.3 ± 0.1	4.9 ± 0.1	1.5	3.8	3.5

Changes in folding parameters between wt IL-33, IL-1β and IL-1Ra. The equilibrium data were fit using MATLAB in order to obtain equilibrium parameters for folding, ΔG_{NU}. The m-value indicates changes in the accessible surface area upon folding and indicate cooperativity of the folding transition.

[a]Equilibrium transition data were evaluated using a two-state model.

[b]Data were obtained by calculating the average fluorescence intensity and calculating the relative fluorescence intensity in terms of F_{app} as a function of [Gdn-HCl].

[c]C_m values are determined by dividing ΔG_{NU} by the m-value.

[d]ΔG_{NI} was determined by using the slowest rate of refolding (k_1) and the unfolding rates over the range of denaturants. ΔG_{IU} was calculated by subtracting ΔG_{NI} from ΔG (extrapolated to water).

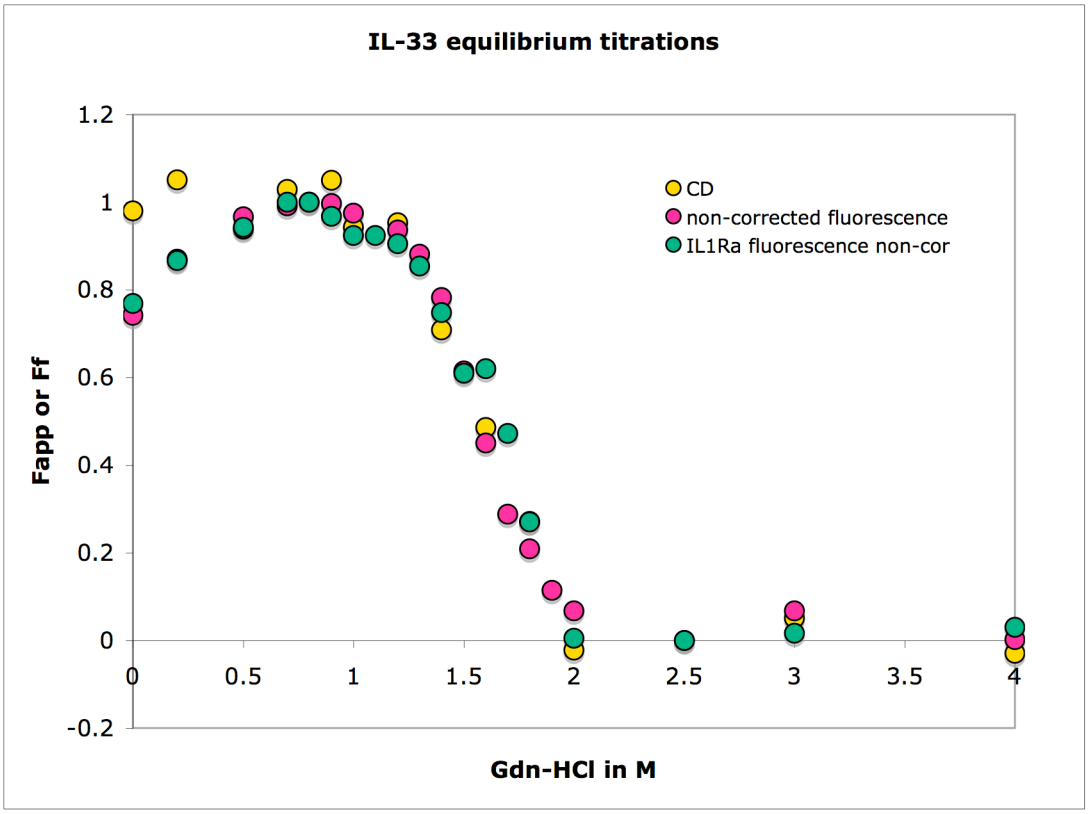

Figure 7-2: Equilibrium titration curve overlay of IL-33 and IL-1Ra. The normalized fluorescence intensities from equilibrium unfolding titrations of IL-33 and IL-1Ra are given as a plot of intensity vs. [denaturant]. The fluorescence intensities were measured for each mutant over the range 0 – 4 M Gdn-HCl. Both curves were fit to a 2-state model of folding (U → N) to determine the stability (ΔG) and the cooperativity (m-value) of the transition.

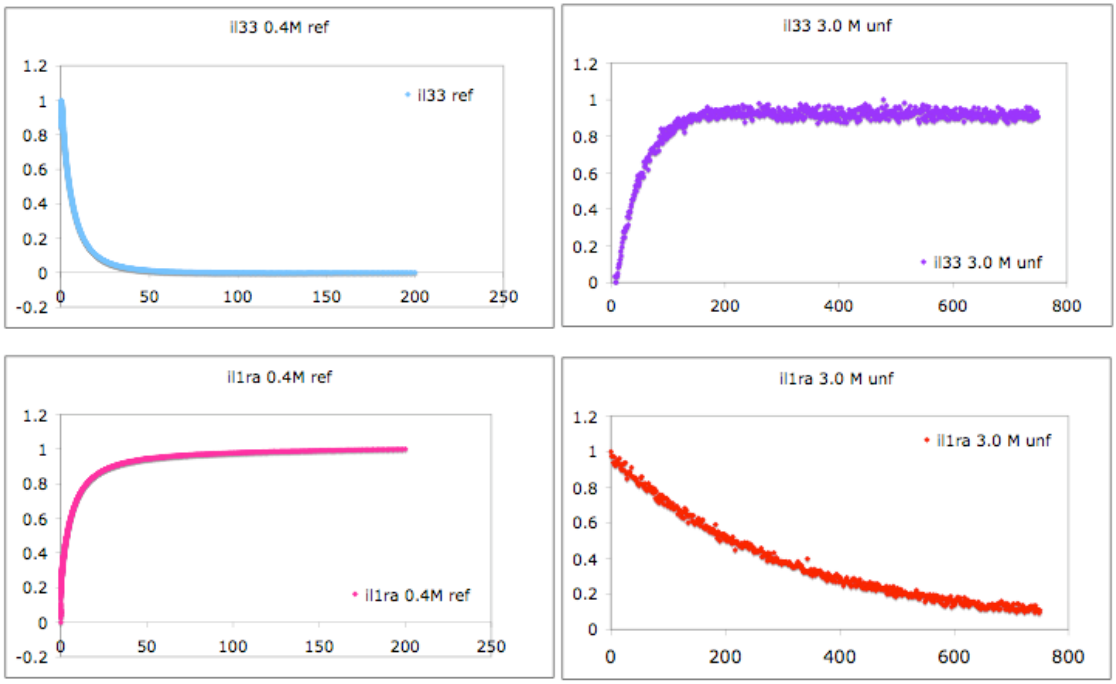

Figure 7-3: Unfolding and Refolding Fluorescence Kinetic Traces of IL-33 and IL-1Ra. Representative traces of the fluorescence emission intensity at 343 nm (with excitation wavelength of 293 nm) vs. time for an unfolding reaction (3.0 M Gdn-HCl) and a refolding reaction (0.4 M Gdn-HCl) are displayed here. The lone Trp residue of IL-33 becomes quenched as it refolds, unlike the two Trp residues of IL-1Ra.

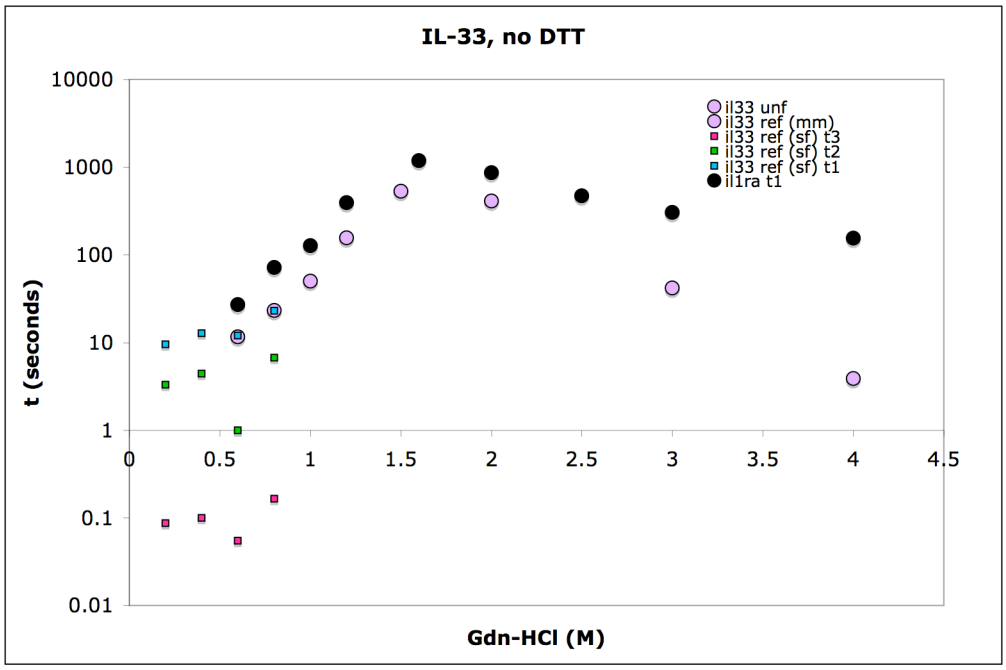

Figure 7-4: Chevron plots of IL-33 and IL-1Ra. Each point on the chevron plot corresponds to the relaxation time of either an unfolding or refolding jump. Refolding jumps are initiated by adding protein unfolded in 2.2M Gdn-HCl to varying final denaturant concentrations (0.2 – 1.2), by following the change in tryptophan fluorescence using either by manual mixing or stopped flow. Unfolding jumps were initiated by adding native protein to varying final denaturant concentrations. The relaxation times are plotted vs. [Gdn-HCl] for (●) IL-33 and (●) IL-1Ra.

While IL-33 shares the same β-trefoil structure as IL-1β and IL-1Ra, it unfolds and refolds faster than both proteins.

Caspase-3 Digest of Wt and D68A IL-33

The IL-1 family members IL-1β and IL-18 are processed to their mature form by Interleukin-1 Converting Enzyme, ICE, or caspase-1 (1). It was proposed by the 2005 Schmitz study that full-length IL-33 was also cleaved by caspase-1 in order to generate the mature β-trefoil region (33). However, the proposed cutsite at D111 was not conserved as in IL-1β (Chapter 4), and did not have the preferred residues for caspase-1 recognition, either as a natural substrate (pro-IL-1β or pro-IL-18) or peptide substrate recognition motif (84,85). Subsequent studies showed that caspase-1 did not cleave full-length IL-33 *in vivo* or *in vitro*. However, full-length IL-33 can be cleaved by caspase-3 and caspase-7 after D178 (D68 in the β-trefoil region numbering, counting from the addition of the N-Met), in the C-terminal region of the full-length protein (176). While pro-IL-1β is protease sensitive, the mature β-trefoil is resistant to proteolysis. To investigate whether the isolated β-trefoil region of IL-33 undergoes a similar conformational change to a protease resistant form, we performed a proteolysis time course with caspase-3 for wt and D68A IL-33. Figure 7-5 shows the time course for *in vitro* processing of the protein with caspase-3 as detected by SDS-PAGE analysis. The bacterially expressed wt and mutant proteins migrate as a doublet (an artifact of the gel conditions), 18-kD band as expected from the amino

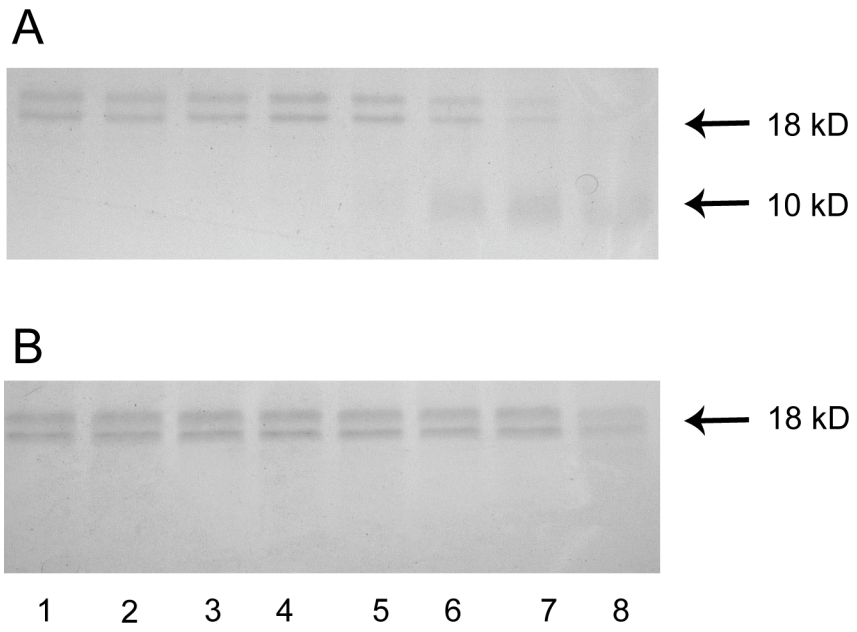

Figure 7-5: Representative gels of wt and D68A mutant of IL-33 cleavage by caspase-3. (A) In the wt IL-33 caspase-3 digestion reaction, a band at 10-kD accumulates as the band for the native protein at 18 kD disappears. (B) The D68A mutant cleavage profile indicates no cleavage by caspase-3. The numbers 1-9 indicate control (no enzyme), 0 sec (directly into quench), 5, 15, 30, 60, 120, 240, 1440 min, respectively, for all three gels.

acid sequence. Upon addition of caspase-3 to wt IL-33, a band at 10-kD accumulates, consistent with the expected molecular weight of the protein upon cleavage at the D68 | G69 site. However, the band never appears in the D68A mutant, consistent with the published full-length cleavage studies (176). Therefore, unlike the protease resistance observed for IL-1β upon formation of the mature protein, IL-33 is protease sensitive and D68 is accessible in the C-terminal β-trefoil region as well as in the full-length protein.

2D ^{1}H-^{15}N Heteronuclear NMR

The structural integrity of wt and D68A IL-33 was assessed by taking the 2D ^{1}H-^{15}N HSQC spectra of ^{15}N-uniformly labeled proteins. Both proteins are well folded and display significant peak dispersion and the sharp peak intensities given by well-structured proteins (178). Assignments of wt and the HSQC spectrum of D68A IL-33 are given in Figure 7-6 (based on Lingel, et al.) (178). Full assignments using ^{13}C/^{15}N-labeled proteins and 3D HNCA, HNCACB and CBCA(CO)NH experiments are presently underway, and subsequently can be used to determine changes in the backbone torsion angles upon mutation. H/D exchange experiments were performed for wt IL-33 and D68A mutant. A representative time course wt IL-33 is presented in Figure 7-7. Presently, calculation of amide protection factors from following the intensity decay each peak over the 24-hour time course is

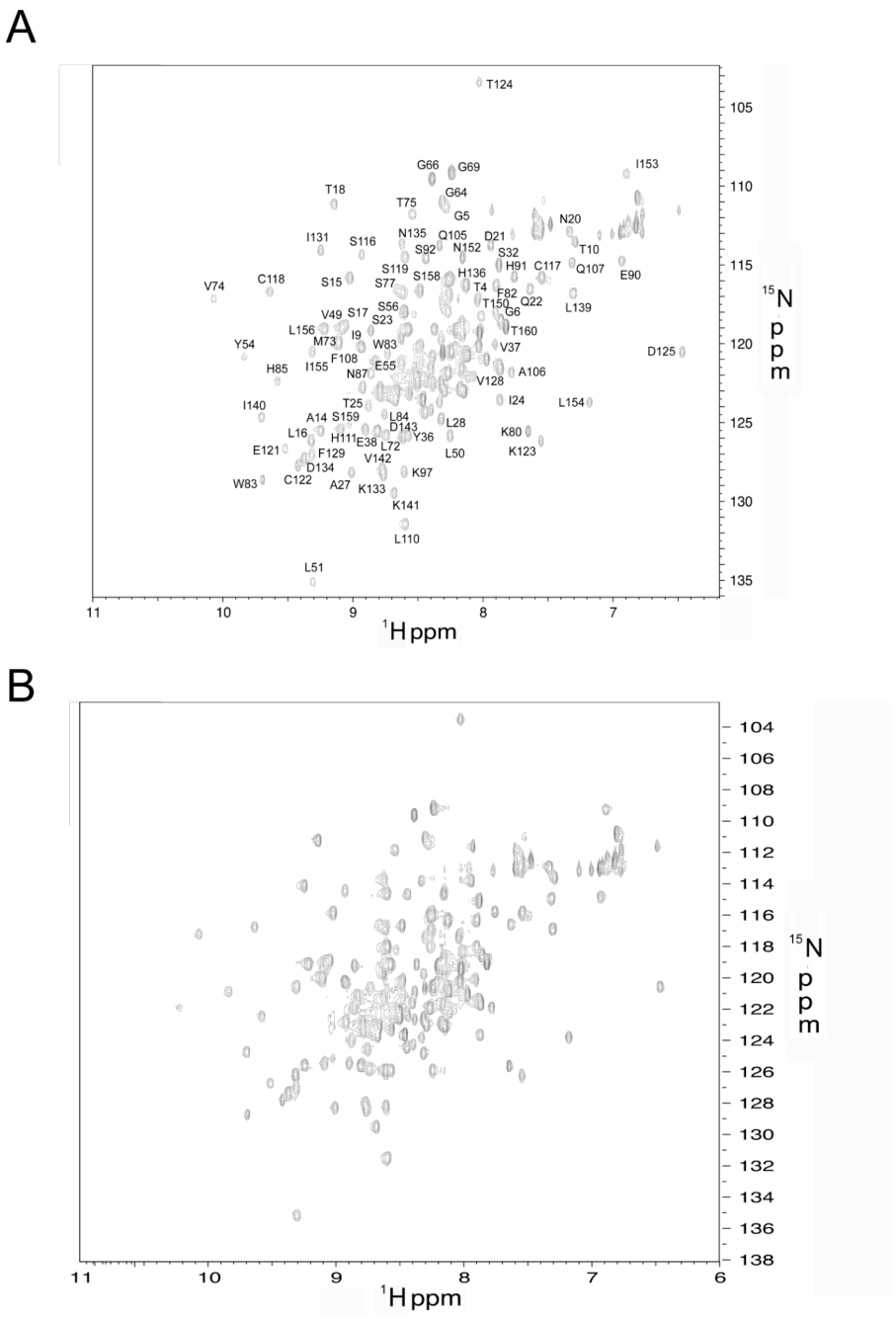

Figure 7-6: ^{1}H-^{15}N HSQC spectra of wt (A) and D68A (B) IL-33. The HSQC experiment provides a "fingerprint" of the amide backbone and select side-chain residues of ^{15}N- isotopically labeled proteins. The spectrum for wt IL-33 is shown here in (A) with partial assignments based on Lingel, et al. The spectrum is well-dispersed and is indicative of a well-ordered tertiary structure. The spectrum of the D68A mutant of IL-33 is shown in (B), indicating these proteins have little to no structural differences, based on the very similar patter of backbone crosspeaks.

under way. As compared to the protection of IL-1Ra to exchange in the same conditions (shown in Figure 7-8), the IL-33 backbone is much less protected.

Circular Dichroism Spectra for IL-1 Family Members at Neutral and Low pH

As discussed in Chapter 4, mature IL-1β is stable and exhibits native structure at low pH, necessitating chemical denaturant to unfold it for mass spectrometry studies. We wanted to determine if IL-1Ra and IL-33 share the same stability at low pH. The secondary structure of IL-33 and IL-1Ra at pH 6.5 and 2.5 was determined using far-UV circular dichroism spectropolarimetry, and compared to that observed for IL-1β. Each protein was measured with and without the presence of 2.2 M Gdn-HCl at both pH values. Spectra for each pH are overlayed in Figures 7-9a and 7-9b. At pH 6.5, all three proteins exhibit the well-established classic β-sheet signature of IL-1β (120), and random coil signatures in the presence of added denaturant. In contrast, only IL-1β and IL-1Ra display regular β-secondary structure at low pH, IL-33 displays the same spectrum with or without denaturant. Therefore, IL-33 does not share the same extreme stability to low pH as its family members IL-1β and IL-1Ra.

DISCUSSION

The Folding Landscape of IL-33

The β-trefoil family of folds contains structurally homologous proteins with a highly diverse set of binding functions (179). Hisactophilin is a β-trefoil containing 31 His residues (out of 118 total residues) that helps initiate actin polymerization in a pH-dependent fashion (175). Ricin and haemagglutinin are β-trefoils with lectin-like behavior, binding various carbohydrate chains to possibly recruit their respective complexes to the plasma membrane (179). Fibroblast growth factors 1 and 2 (FGF-1 and FGF-2) are extracellular cytokines that simultaneously bind both a carbohydrate (heparin) and an extracellular receptor (151,180). Finally, the IL-1 family members (IL-1α, IL-1β, IL-1Ra, IL-1F5 – IL-1F10, and IL-33) are extracellular cytokines that bind structurally homologous extracellular receptors (5).

While the β-trefoil family of folds shares the same tertiary structure, their folding pathways can vary substantially. FGF-1 accesses an intermediate different from the main intermediate accessed by IL-1β (using strands 4-8 vs. 6-10). In FGF strands 1 and 12 form first, the so-called "ends together" route identified in theoretical studies of the folding landscape of IL-1β. Less detailed folding studies of FGF-2 also indicate it is a 3-state folder, accessing a well populated intermediate (151,152). Hiactophilin folds by a 2- or 3-state mechanism, with the intermediate only populated in select cases (152). A recent study by Chavez, et. al describes the alternate folding routes accessed by 4 different β-trefoil proteins, hisactophilin, FGF-1 and 2, and IL-1β (132). Using structure based Cα-models, she found that the thermodynamic and kinetic transition state barriers are high and broad for each β-trefoil protein. The broadness of the barriers is due to the large number of routes to the native state that are

accessible to the symmetric β-trefoil proteins. Small perturbutions in the contact homogeneity (FGF) or topological frustration (β-bulge in IL-1β) drastically affect the route accessed most often for each protein, more often these proteins accessed alternative routes than the most efficient, the direct route. Hisactophilin, in contrast, exclusively accessed the direct route, the simplest route where trefoil 2 forms first (Chavez). Interestingly, hisactophilin has the lower contact order (~12.1) when compared to IL-1β or IL-1Ra (~18.6) (181). Contact order is thought to predict the kinetic folding behavior for single-domain proteins, based solely on the locality of inter-residue contacts (181). Lower contact order is correlated to faster folding for 2-state folders. IL-33 has a contact order of 15.4, between IL-1β and hisactophilin. While IL-1β, IL-1Ra and IL-33 have reproducibly detected intermediates, it is possible that the alternate routes populated by IL-1β and IL-1Ra (backtracking) are not accessed nearly as often for IL-33.

The thermodynamic stability of wt IL-33 as measured by CD and fluorescence spectroscopies at pH 6.5 is reduced with respect to that observed for both wt IL-1Ra and wt IL-1β (6.7 vs. 8.4 and 7.3 kcal/mol, respectively). The cooperativity of the folding transition is similar (5.4 kcal/mol*M vs. 5.5 for IL-1Ra and IL-33), consistent with a similar change is accessible surface area exposed to solvent upon unfolding. Kinetic studies (Figure 7-4) demonstrate that both refolding and unfolding of IL-33 is faster than that observed for IL-1Ra. The fastest phase, τ_3, is approximately 1.5-fold greater for IL-33 than IL-1Ra (on average 0.08 s vs. 0.05 s, respectively). The intermediate phase, τ_2, is slightly faster for IL-33 (6.7 s vs. 9.6 s for 0.8 M Gdn-HCl,

for IL-33 and IL-1Ra, respectively). The slowest phase, τ_1, is consistently faster for IL-33 than for IL-1Ra (23 s vs. 68 s at 0.8M Gdn-HCl). Using the log values of the relaxation times from the refolding and unfolding arms of the chevron plot of IL-33, the theoretical ΔG_{IN} value can be calculated. In this case, ΔG_{IN} is 6.3 kcal/mol, indicating that less than 1 kcal/mol of the thermodynamic stability of native IL-33 is contributed by the intermediate. This is in contrast IL-1Ra and IL-1β, both proteins have significantly stable intermediates (3.2 kcal/mol for IL-1Ra and 3.5 kcal/mol for IL-1β). Therefore, the faster folding of IL-33 as compared to IL-1Ra and IL-1β is most likely due to a lower transition state barrier in folding pathway.

Caspase-3 Processes the β-trefoil Region of IL-33

The IL-1 family of proteins are synthesized as longer precursor proteins, and several require removal of the precursor region for signaling (13). An exception to this rule is IL-1α, which has full receptor binding and activity as compared to the processed, β-trefoil C-terminal region (10). Full-length IL-33 also retains full receptor binding and activity as a precursor protein (172). As described in the introduction of this chapter, IL-33 was initially thought to be processed by caspase-1 in an analogous fashion to IL-1β and IL-18 (33). However, caspase-1 does not process full-length IL-33 either *in vitro* or *in vivo*. Interestingly, full-length IL-33 cleaved by caspases -3 and -7 of the apoptotic branch of the caspase family (84). Caspase-3 is the predominant executioner caspase, setting off the pro-apoptotic caspase activation cascade (including the activation of caspase-7) (176). Interestingly, active caspase-3 in

imported from the cytosol into the nucleus, where it is active and responsible for initiating the apoptosis-associated changes in nuclear morphology (182). In resting endothelial cells, full-length IL-33 is constituatively expressed and located in the nucleus (including several types of tumor cell) (183). Full-length IL-33 is found to be associated with chromatin, which is condensed during apoptosis. The caspase-3 cleavage products have been detected during apoptosis (7). Therefore, capase-3 may have a regulatory effect on the function of IL-33 in the nucleus during apoptosis.

To determine if the caspase-3/7 cutsite is exposed in the β-trefoil region as well as the full-length protein, wt and D68A IL-33 were digested with caspase-3, shown in the SDS-PAGE gels in Figure 7-5. The wt protein shows the appearance of a smaller 10 kD band over time, indicative of caspase-3 processing and generation of cleavage products over time. The D68A mutant does not show the appearance of this band after 24 hours, indicating that it is not cleaved by caspase-3. Therefore, the cleavage site is also exposed in the β-trefoil region alone.

In order to determine whether or not there was a large difference in the structure of D68A with respect to the wt protein, we used 2D heteronuclear NMR. As shown in Figure 7-6, the native HSQC spectra of wt and D68A are very similar, indicating they have the same native fold. The possibility exists that full-length IL-33 maintains regular chromatin structure in non-apoptotic cells, and that part of the chromatin condensation pathway involves cleavage of IL-33 by caspase-3. Also possible is that caspase-3 prohibits the intact full-length IL-33 protein from eliciting effects, including extracellular signaling, while the cell is undergoing apoptosis.

Interestingly, intact full-length IL-33 is detected extracellulary during necrosis (cell death due to external factors rather than programmed), where caspase-3 is not imported into the nucleus. This is the proposed "alarmin" function of IL-33 (4). Further *in vivo* studies must be undertaken to determine why there is differential cleavage seen at the caspase-3 site in apoptosis vs. necrosis.

H/D Exchange ^{1}H-^{15}N NMR of IL-33 vs. IL-1Ra Global Destabilization of IL-33

H/D exchange is a powerful technique that can provide residue-specific information on the kinetics and thermodynamics of proteins and protein actions (folding, binding, etc.) (115,137). The H/D exchange of IL-1β and various point mutants have been studied by our lab and others (28,105). As with deuterium exchange mass spectrometery, H/D NMR measures the deuteron incorporation into the amide backbone over time. Since deuterium has zero net spin, it is not detected in NMR experiments (80). Therefore, crosspeaks of amides that incorporate deuterium vs. hydrogen become invisible in the 2D NMR spectrum. Deuterium exchange rates depend on the main-chain sequence temperature, pH, and tertiary structure of a protein. For IL-1β, there are over 54 amide crosspeaks that are stable to exchange after 24 hours, all corresponding to the hydrogen bonding partners in the amide backbone (124). It was not known if wt IL-1Ra maintained the same level of protection within its amide backbone, or if β-trefoil region of IL-33 also maintained a protected amide backbone. Therefore, deuterium exchange reactions of

Figure 7-7: H/D NMR exchange profile of wt IL-1Ra. Shown here is the non-deuterated spectrum (A), the first exchange time point (B) at 24 min, and the last exchange time point (C) after 780 min. The partial assignments based on Stockman, et. al were used to identify peaks that were moderately protected (colored yellow on the crystal structure of IL-1Ra, PDB:1ILR) and well-protected (blue). Areas of the protein that exchange too fast or that lack an assignment are colored grey.

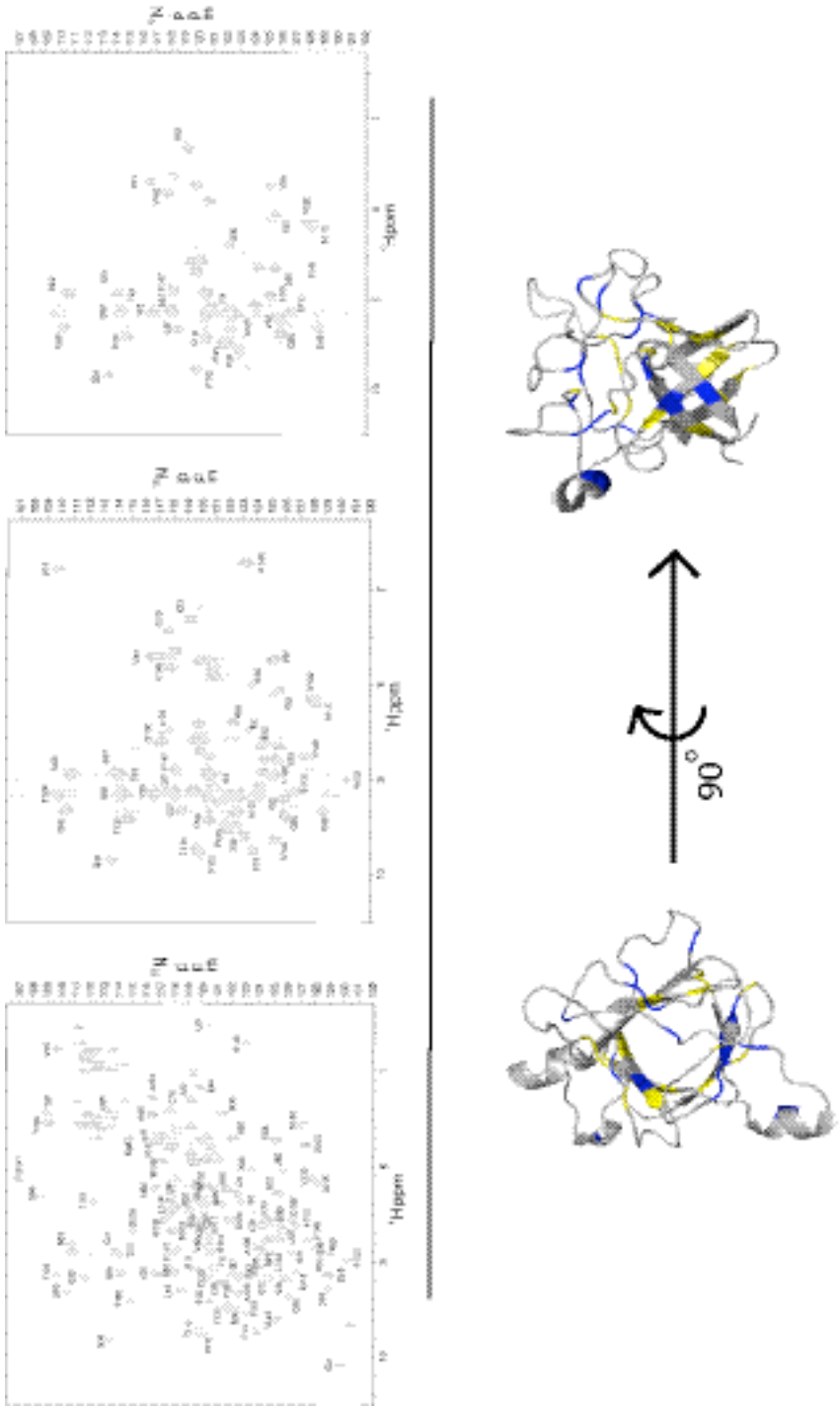
15N ppm
1Hppm
15N ppm
1Hppm
15N ppm
1Hppm
90°

Figure 7-8: H/D NMR exchange profile of wt IL-33. Shown here is the non-deuterated spectrum (A), the first exchange time point (B) at 24 min, and the last exchange time point (C) after 780 min. The partial assignments based on Lingel, et al. were used to identify peaks that were moderately protected (colored yellow on the NMR structure of IL-1Ra, PDB:2KLL) and well-protected (blue). Areas of the protein that exchange too fast or that lack an assignment are colored grey.

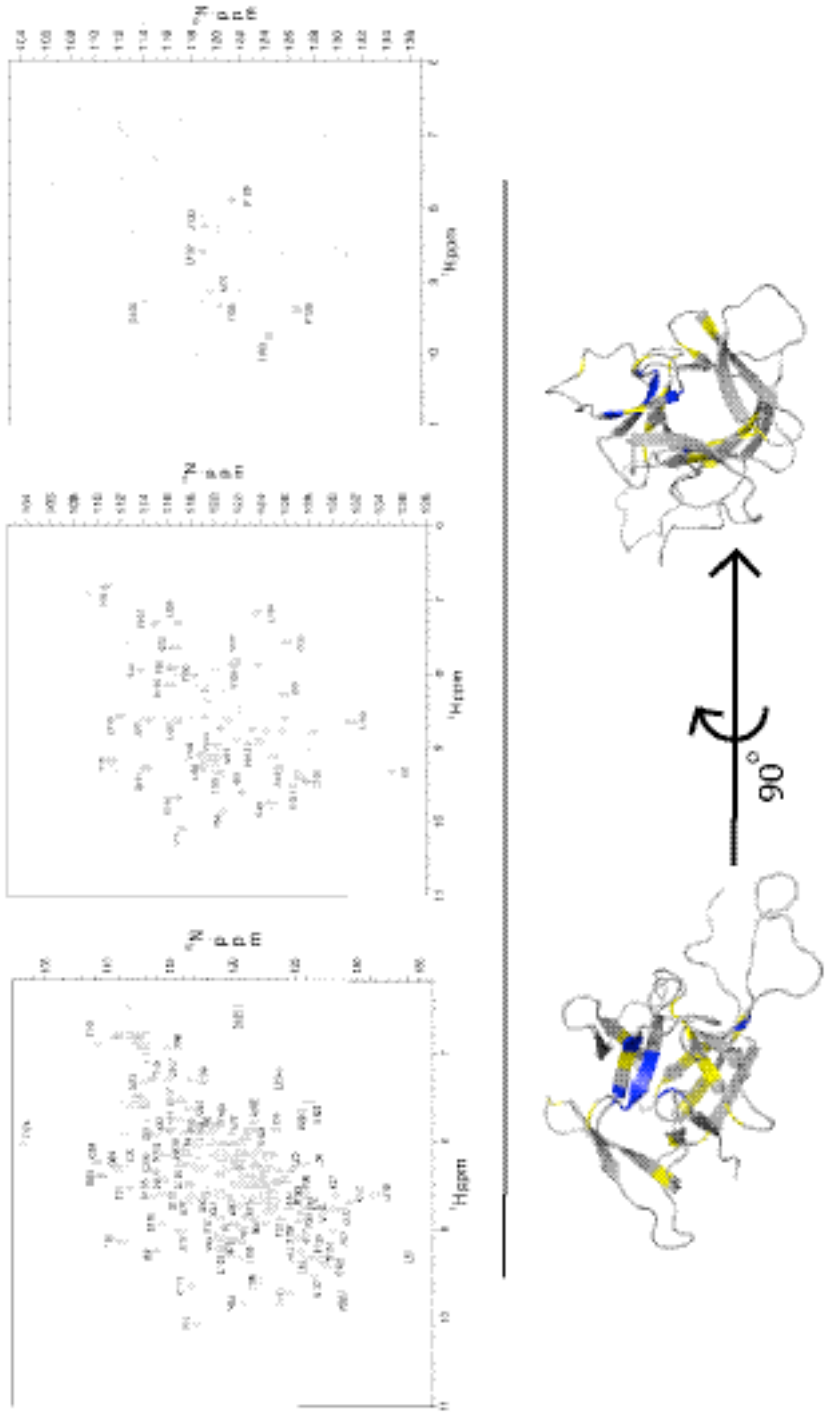
^{15}N ppm
^{1}Hppm
^{15}N ppm
^{1}Hppm
^{15}N ppm
^{1}Hppm
90°

IL-1Ra and IL-33 at the same temperature and pH (6.5) were followed using a series of HSQC experiments to show deuterium incorporation over time. Representative spectra for IL-1Ra and IL-33 time courses are presented in Figures 7-7 and 7-8. Surface-exposed amides exchange within the dead-time of the experiment (24 minutes), and the remaining amides exchange on intermediate (within the titration time course) to slow (beyond the time course, or >24 hours. Visual inspection of the series of spectra indicates that wt IL-1Ra contains 40 slow-exchanging peaks, which is very similar to wt IL-1β. However, IL-33 only maintains 8 protected amide crosspeaks over the time course. The number of assigned peaks in the non-deuterated spectra of IL-33 vs. IL-1Ra are almost identical (154 vs 145). This comparison indicates the stability of the hydrogen-bonding network of IL-33 has changed drastically as compared to either IL-1β or IL-1Ra.

All β-trefoil proteins have an extensive anti-parallel β-strand network that spans over the 6-stranded barrel and 6-stranded cap. Barrel strands that are connected by a β-hairpin at the bottom of the barrel in IL-1Ra (strands 4 and 5, 8 and 9) have a hydrogen-binding network that extends over the entire length of both strands. The other two barrel partners, strands 1 and 12, show some "unraveling" of the hydrogen bonding network at the N- and C-termini of the protein, most likely due to presence of free ends vs. a hairpin turn. Bonding between barrel strand pairs is staggered such that half of each pair bonds with half of that strand, indicated in the cartoon in Figure 8. Meanwhile, in the adjacent cap strand partners (2 and 3, 6 and 7, 10 and 11) form the most extensive intra-strand bonds between themselves as well. The cap strand

pairs are connected by bonds mediated by the loops in the βββloopβ trefoil motif. The cap and barrel strand groups interact at the hinge points between the barrel and cap, the three-fold symmetric hydrophobic residue motif conserved over all β-trefoils (ref), seen in IL-1β, IL-Ra, IL-18 and IL-33. While the β-trefoil structures of IL-1β, IL-1Ra, IL-18 and IL-33 overlay with good agreement, there are subtle differences within the structures that may account for the change in stability to deuterium exchange exhibited by IL-33. A structural homologue search using the structure of the β-trefoil region of IL-33 (PDB:2KLL) found that the closest-aligning β-trefoil was IL-18 (22% identity), not IL-1β or IL-1Ra (16-17%, 14% identities, respectively) (33). A structural overlay of IL-33 vs. IL-18 and IL-33 vs. IL-1Ra are given in Figure 7-10. Most strikingly, the N- and C-termini of IL-18 and IL-33 are not proximal to each other as with IL-1β and IL-1Ra. Instead, the longer strand 1 of IL-18 and IL-33 wrap around the bottom of the barrel, forming a long intra-strand hydrogen-bonding network with strand 4. A shorter network of hydrogen bonds between strand 1 and 12 exist, as compared the network between strands 1 and 12 in IL-1β and IL-1Ra. Since strand one is more extensive, there is a distortion in the barrel symmetry on the side including strands 1, 4 and 5. This side is extended from beyond the core, as illustrated in Figure 7-10. This extension on one side deforms the opposite side, where strand 12 resides. Strands 8 and 9 still form a symmetric hydrogen bonding pair, only making two hydrogen bonds between it and strand 12 and strand 5 in IL-33. Strand 1 in IL-33 contains a conserved strand break, residues A15 and S16. Therefore, the hydrogen-

bonding network between opposing sides of the barrel is broken here in IL-33, unlike IL-18, where strand 1 continues though.

Opening up the strand 1/12 side of the barrel in IL-33 is most likely reflected in the substantially decreased stability of the hydrogen-bonded backbone amides to exchange. Calculation of relative exchange rates and protection factors for the remaining protected amides is currently on-going. Unfortunately, information on the relative protection of the amide protons in IL-18 is not available. It is tempting to speculate that there would be less protection to exchange for the backbone amides of IL-18, relative to IL-1β and IL-1Ra, as well (although not as deprotected as IL-33). How this intrinsic flexibility of IL-33 translates into its known and yet-unknown biological functions remains to be characterized.

The Potential Membrane Interaction Activities of the IL-1 Family

As described in Chapters 1, 3 and 4, IL-1β is exported by a non-classical pathway. This trait is shared by all other family members excepting isoform 1 of IL-1Ra (which contains the classic N-terminal ER-signaling sequence) (non-classical refs). Indeed, even structural homologues FGF-1 and FGF-2 are secreted by a non-classical mechanism as well (102). For IL-1β, the processing and secretion are closely timed, and there is no significant intracellular build-up of mature IL-1β (29,62,63,65,100,101,184). The recently characterized inflammasome, a multi-protein scaffold responsible for activating caspase-1 in macrophages, mediates IL-1β processing in response to a number of immune challenges (65). Indeed, mutations to

inflammasome components that alter the activity (Cryopyrin-Associated Syndrome) show increased extracellular IL-1β populations (93). However, pro-IL-1β can be secreted and processed via inflammasome-independent mechanisms (63,65). As described in Chapter 4, other proteases, including matrix-metalloproteases, can process and generate mature, active IL-1β. Several mechanisms exist for IL-1β export out of the cell, including an endolysosomal route, microvesicle shedding, and during necrosis, or cell death (29,100,101,103,184). In general, an event that causes changes in Ca^{+2} in the cell (via the $P2X_7$ receptor or maitotoxin) causes the leaderless mature IL-1β, IL-1F6 and icIL-1Ra (intracellular IL-1Ra isoform) to be transported out of the cell (59,60,185). In bacteria, pro and mature IL-1β, IL-1Ra and mutant forms of these proteins can be extracted by osmotic shock (186-188). Since these proteins are structurally homologues of IL-33, we attempted to purify IL-33 via the same osmotic shock procedure. All three proteins are sufficiently acquired by the second low-salt wash step. One freeze-thaw cycle efficiently removed all of the IL-33 β-trefoil protein in the first wash step (data not shown).

How these β-trefoil proteins are acquired through osmotic shock is not understood. Mature and pro-IL-1β both induce large-unilamellar vesicle (LUV) leakage, as measured by increasing calcein fluorescence over time (Anderson, Hailey unpublished results). Other proteins with known membrane interactivity (cytochrome c) and non-classical secretory behavior (RFP, red-fluorescent protein) also induce vesicle leakage, while another protein with no known lipid or membrane interaction did not (chymotrypsin) (data not shown). Therefore, it is possible that the β-trefoil

motif itself may be responsible for guiding the molecules to a charged lipid bilayer, where they maybe transported across, or possibly even directly cross after induction of membrane depolarization. It should be noted that all three proteins contain a highly charged, basic loop, (between strands 7 and 8 in IL-1β and IL-1Ra, and strands 3 and 4 in IL-33), which may give or add to membrane-recognizing/binding activity of these β-trefoil proteins. Further investigation *in vivo* will be required to show these interactions directly.

The Altered pH Stability of IL-33 as Compared to IL-1β and IL-1Ra

The β-trefoil family member hisactophilin has been reported to have pH-dependent membrane-binding and actin-binding activities. Under conditions of higher pH (>7.5), hisactophilin does not bind actin (189). When the pH is lowered below 7, hisactophiln can induce polymerization of actin, and can bind membranes. Therefore, hisactophilin exists as a pH-dependent sensor *in vivo*. The reason behind this activity is the large number of histidines (31) located throughout the protein, shown in Figure 7-11. While surface histidine residues generally have a pK_a of 6.5, the pK_a values of individual histidines can vary drastically due to the local environment around the side chain (190). Interestingly, the β-trefoil region of IL-33 contains 7 histidines, whereas IL-1β contains one (H30) and IL-1Ra contains none. All of the histidines are labeled and shown in Figure 7-11. The histidines are clustered near the hydrophobic mini-core region (residues 89, 129, 130 and 141 in IL-33), on the hairpin between strands 6 and

A

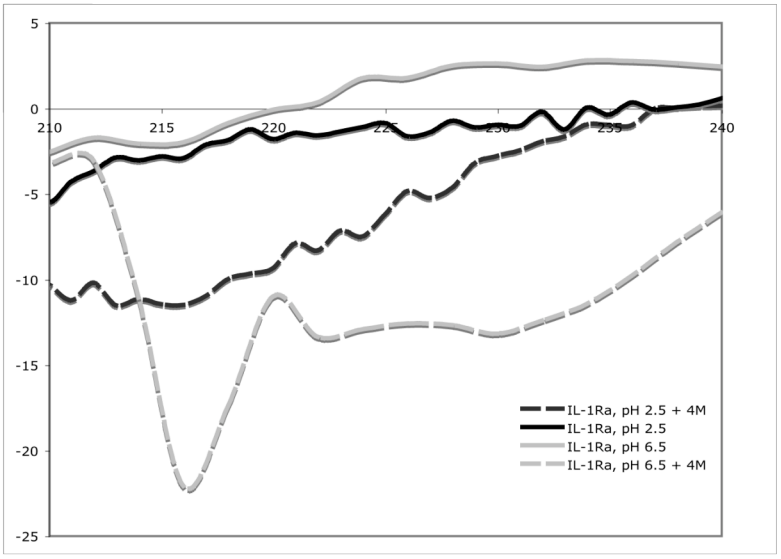

B

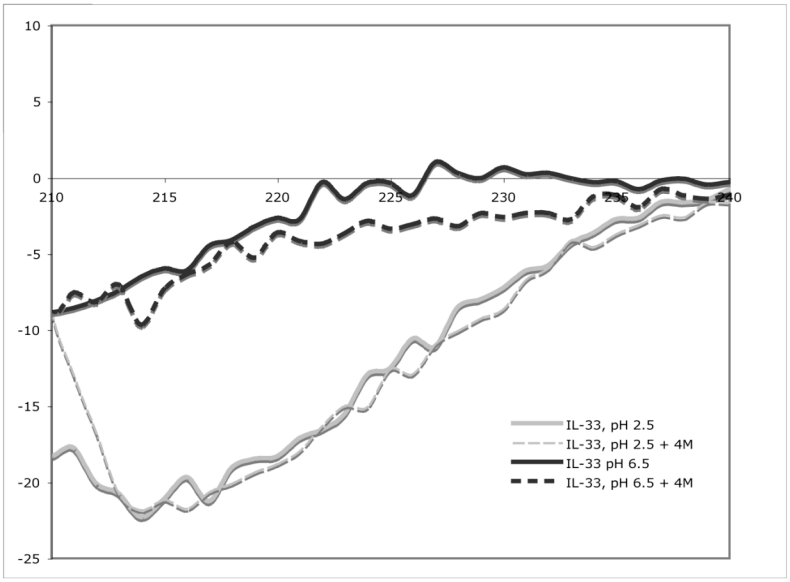

Figure 7-9: The corrected CD spectra of IL-1Ra and IL-33 at pH 6.5 and pH 2.5, with and without the presence of denaturant. The overlayed CD spectra were collected for IL-1Ra (A) and IL-33 (B) equilibrated overnight in pH 6.5 and pH 2.5 phosphate buffer, with or without the presence of 4 M Gdn-HCl. At both pH 6.5 and 2.5, IL-1Ra remains folded, as indicated by the secondary structure β-signature intensity as described in Chapter 4. There is a significant conformational change upon the addition of denaturant, representative of random-coil. IL-33 displays the characteristic β-signature at pH 6.5, but is not folded at pH 2.5, as indicated from the lack of difference between spectra with and without 4 M Gdn-HCl.

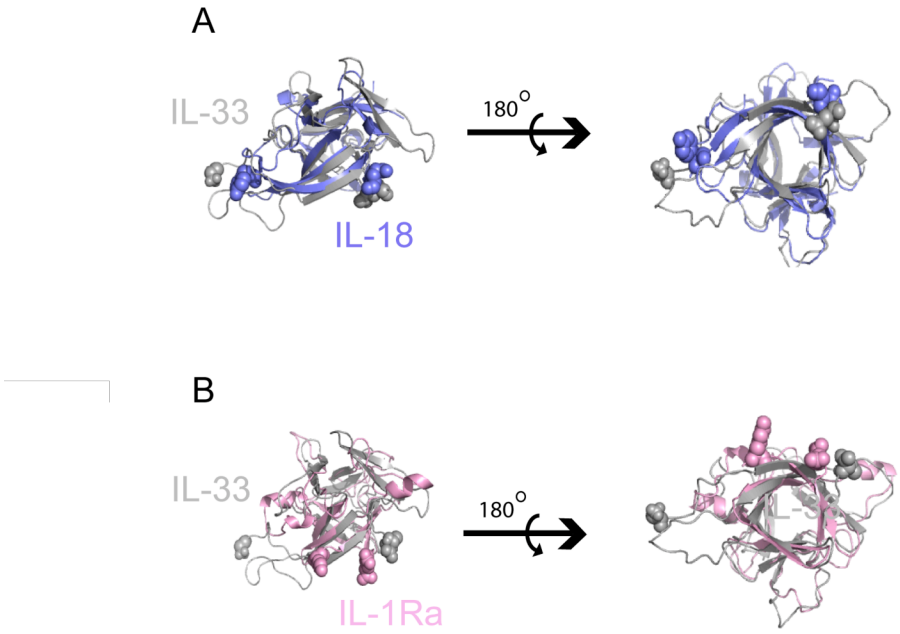

Figure 7-10: Structural overlay of IL-33 and IL-18 (A) vs IL-1Ra. IL-33 shares the most sequence identity (22%) with IL-1 family member IL-18, rather than IL-1β or IL-1Ra. The structural overlays of IL-33 and IL-18 vs. IL-33 and IL-1Ra show that the N-terminus wraps around the bottom the barrel and the C-terminus for both IL-33 and IL-18, but not for IL-1Ra (N- and C-termini are close in space). The N- and C-termini for each protein are labeled with spheres, and IL-33 appears grey, IL-18 as blue, and IL-1Ra as light red. Whether or not this creates a different binding mode or functional route within IL-33 or IL-18 has yet to be characterized.

7, in strand 7, and on the loop between 7 and 8. There are two histidines in strand 8 in the barrel, one in the strand and one in the turn between 8 and 9. The last histidine is in the turn between strands 10 and 11. The histidines make a charged surface on one half of the protein, and the highly charged loop (residues 39 – 49) creates a charged surface on the other half (Figure 7-11). The charged surface of IL-33 contrasts IL-1β and IL-1Ra, where the charges are clustered in the basic 90's loop.

Many proteins are unfolded at extremely basic (>10) or acidic (<3.0) pHs (190). IL-1β unusual in this regard because it has native-like structure at pH 2.5, requiring chemical denaturant to unfold it (Chapter 4). The secondary structure profiles of IL-1β, IL-1Ra and IL-33 at physiologically relevant and at low pH (6.5 and 2.5) with and without the presence of denaturant were determined. IL-1Ra shares the same pH-independent stability of IL-1β, requiring the presence of chemical denaturant to unfold it at pH 2.5. In contrast, IL-33 is folded at pH 6.5, but unfolded at pH 2.5 without denaturant. The histidines lie in turn regions and near a conserved hydrophobic region (between IL-1β and IL-1Ra) shown to be important in the folding pathway of IL-1β, therefore it is tempting to speculate that the histidine residues contribute destabilizing charges below a certain pH, driving the protein to unfold. Preliminary NMR pH-titration data shows significant peak shifts upon a change in pH of <0.3 units (Fisher, unpublished results). Therefore, as with hisactophilin, the β-trefoil region of IL-33 may have a pH-dependent "switch"-like function *in vivo*.

In vivo, full-length IL-33 has been shown to be associated with chromatin in resting, healthy epithelial cells (170). However, upon activation of apoptosis

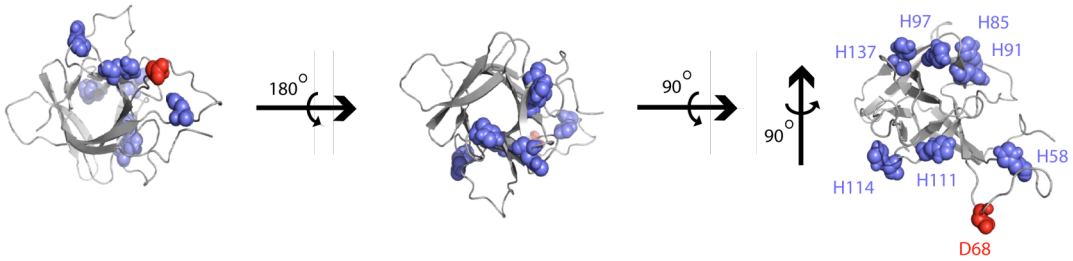

Figure 7-11: The location of the histidine residues in the structure of IL-33. IL-33 contains 7 histidines (blue spheres), making it unique from other IL-1 family members IL-1α, -β, -Ra or 18 (0, 1, 0, 1 respectively). The conserved caspase-3/7 cutsite D68 is shown in red spheres. Whether or not these histidines impact the intra- or extracellular function of IL-33 remains to be tested.

(programmed cell death) or necrosis, extreme morphological changes within the nucleus occur, including chromatin condensation (171). While the N-terminal region of IL-33 contains the conserved helix-turn-helix DNA binding motif, the intracellular function of the C-terminal β-trefoil region is unknown. Also involved with initiating apoptosis is the executioner caspase, caspase-3. The conserved caspase-3 cutsite is upstream from 6 of the 7 His residues (Figure 7-11). Since it has been shown that caspase-3 cleaves full-length IL-33 in apoptotic cells, it is possible that these C-terminal residues have an additional apoptotic function. For example, highly-charged peptides can bind to phospholipid membranes, destabilizing the membrane (191). Alternatively, IL-33 is proposed to be an "alarmin", where it is secreted from necrotic cells and thus can bind the ST2 receptor. However, since the C-terminal domain is required for binding the ST2 receptor, apoptotic cells would release the caspase-3 cleaved version, which both cleavage products were shown to not bind the ST2 receptor (172). Further *in vivo* studies must be undertaken to determine whether or not the activity of IL-33 is pH-dependent as the hisactophilin "switch" *in vivo*, and what, if any, intracellular functions the C-terminal β-trefoil region has.

CONCLUSION

The newest IL-1 family member, IL-33, shares the structurally homolgous C-terminal β-trefoil region shared by all family members. Kinetic and equilibrium folding studies and H/D exchange 2D NMR studies have shown that while the β-trefoil fold is maintained, it is destabilized and faster folding than the other IL-1

family members, IL-1β and IL-1Ra. It also lacks the stability to low pH that IL-1Ra and IL-1β share. So, while IL-33 shares the same overall structure as IL-1β and IL-1Ra, it has a distinctly different folding and functional landscape.

Chapter 8

Conclusion

The studies conducted in this thesis aimed to explore two modes of regulation of the pleiotropic cytokine, IL-1β, as well characterize biophysical features of the newest member of the IL-1 family, IL-33. First, the native sate of the inactive, full-length precursor protein, pro-IL-1β, was characterized by fluorescence, circular dichroism, SEC, PFG-NMR, proteolysis studies, and DXMS (Chapters 3 and 4). Second, the folding and functional landscape of the natural competitive inhibitor of mature IL-β, IL-1Ra, was determined using kinetic and equilibrium fluorescence folding studies, site-directed mutagenesis, a biological assay, and 2D NMR (Chapters 5 and 6). Finally, the folding landscape and native state properties of IL-33 were determined using kinetic and equilibrium fluorescence and circular dichroism techniques, and H/D exchange coupled with 2D-NMR spectroscopy.

The Structure of Pro-IL-1β and Functional Implications

As described in Chapters 2 and 3, pro-IL-1β has a heterogeneous, extended native state population. Also, as revealed by deuterium exchange mass spectrometry, pro-IL-1β maintains a core region of stability similar to the on-route intermediate in the refolding pathway of the mature protein(28,106). Protection from backbone deuterium exchange at physiologically-relevant pH (pH 6.5) is due to either hydrogen bonding or buried hydrophobic residues(115,129). Once the N-terminal residues are removed, the remaining C-terminus becomes resistant to further protease degradation (Chapter 3)(53).

The kinetic refolding studies of mature IL-1β have revealed that the on-pathway intermediate contains extensive secondary structure that is protected from backbone hydrogen-deuterium exchange, as detected by mass spectrometry and 2D NMR spectroscopy(28). As described in Chapter 3, the intermediate is protected in strands 6 - 10, and also includes a residue in strand 4. Our lab and others have shown that mature IL-1β folds from the unfolded state to an intermediate state on the order of ms (126 $\pm$ 6), and after at least a 400 ms lag phase, begins to form the native structure with a relaxation time of 43 s(28,105). As theoretical folding studies revealed, part of the slow folding is due to the second-most accessed route to the native state, the "back-tracking" route(132). This route involves breaking native contacts made early in the folding trajectory in order to accommodate the final folding of a functionally important region, the contacts between the β-bulge between strands 4 and 5 and the 90's loop between strands 8 and 9, into the native tertiary structure(107-109)

It is tempting to speculate that the protected region in pro-IL-1β is in a state along the folding pathway to native that would help bypass the need for the liberated C-terminal mature protein to take the alternate routes. Putting the C-terminus into a protease-labile, but primed conformation in the precursor protein is a way to keep the signal ready without actually "pulling the trigger" of a loaded gun. However, preliminary proteolysis/1D NMR data shown in Figure 8-1 indicates that even after the N-terminal portion of the precursor protein is removed by chymotrypsin, the remaining C-terminus does not fold to the distinct, highly-ordered native structure of mature IL-1β, even after 14 hours from initiation of cleavage (with or without the

presence of 10 mM DTT). This is evident from the lack of amide peak dispersion in the pro-IL-β spectra as compared to the highly disperse peaks in the mature IL-1β spectrum. While we cannot rule out that there could be a portion of the N-terminus still bound to the C-terminus, preventing it from folding completely, it is more likely that other factors present in the cell are required to finish folding the mature sequence, such as a chaperone or even caspase-1 itself. Indeed, the recombinantly-obtained chymotrypsin cleavage product, N-term-YVHD-IL-1β, folds into a well-ordered tertiary structure as indicated in Figure 8-1. In either case, this finding is quite surprising, considering how robustly the recombinantly-obtained mature protein refolds.

As discussed in Chapters 2 and 3, *in vivo*, pro-IL-1β is processed to an active form by caspase-1 during a canonical inflammatory response, and by a multitude of other proteases. As shown by Hazuda, et. al, as the N-terminal residues are removed (starting from residue 77 up to residue 114), the remaining C-terminal sequence becomes more and more active ($6x10^4$ to $2x10^8$ active units/mg, with $5x10^8$ units/mg for mature IL-1β)(53). Pro-IL-1α is also synthesized as a much longer precursor protein (270 residues, 157 residue mature C-terminus). As described in Chapter 1, pro-IL-1α is as active as the precursor form than the mature form(53), even though it is as protease-labile as pro-IL-1β. It was also shown that recombinantly-obtained vs. natively-obtained (from stimulated cell)

Figure 8-1: 1D ^{1}H-spectra of uncleaved/chymotrypsin cleaved pro-IL-1β, N-term-M-YVHD-IL-1β and mature IL-1β. The W108L variant of pro-IL-1β and mature IL-1β proteins were obtained using the methods described in Chapter 2. Pro-IL-1β was cleaved by a 5 min exposure to immobilized chymotrypsin resin (Proteochem) with constant mixing at room temperature. The reaction was transferred to an NMR tube, spun down, and placed in a Varian 500 MHz NMR spectrometer equipped with a triple gradient probe at 37 °C (Agilent). The first spectrum was collected 22 minutes after the start of the cleavage reaction. A total of 2048 scans were taken. The final spectrum of the pro-IL-1β cleavage product was taken 14 hrs after the initiation of the reaction. SDS-PAGE and ESI-MS were used to determine that all of the pro-IL-1β was cleaved to form the approximately 17 kD product (data not shown). Also shown is the spectrum of the recombinantly-obtained chymotrypsin product (N-term-M-YHVD-IL-1β) mature IL-1β in the same conditions. Wt pro-IL-1β was also run under the same conditions, and yielded the same profile (data not shown).

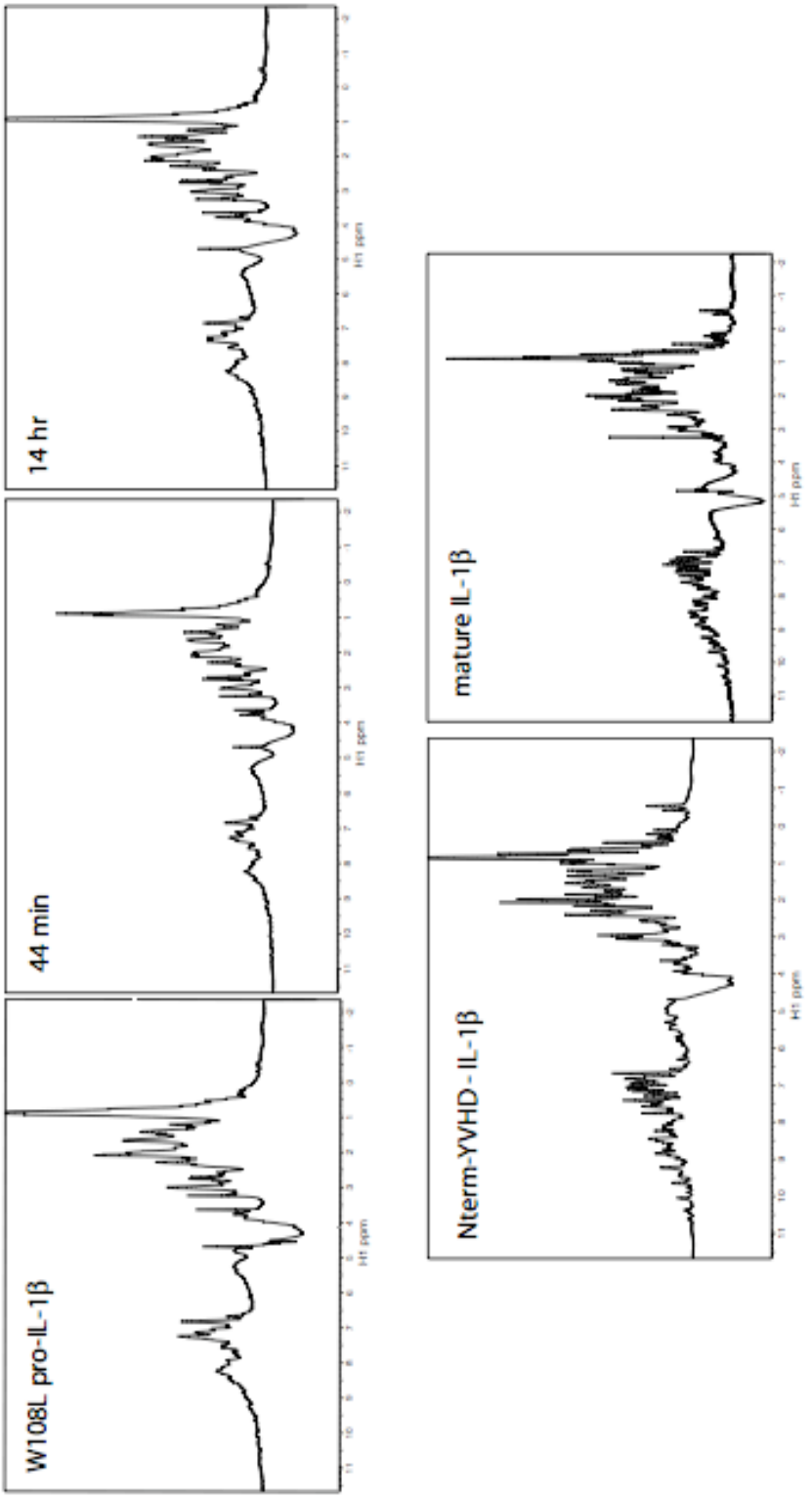
W108L pro-IL-1β
44 min
14 hr
Nterm-YVHD - IL-1β
mature IL-1β

pro-IL-1α and mature IL-1β (residues 117-269) had identical activities(139,192), so the likelihood is that recombinantly-obtained pro-IL-1β is no different from macrophage-obtained. Therefore, it is possible that the processed C-terminal protein is as active as the fully-folded mature protein, and that the well-ordered tertiary structure is not an absolute requirement for activity.

The other possibility is that the C-terminal sequence requires an outside partner to facilitate final folding into the native state. Indeed, processing by caspase-1 may remove the N-terminus in a way conducive to mature IL-1β folding, vs. other, broad-range proteases like chymotrypsin. In order for mature IL-1β to perform its function as an extracellular cytokine, it must traverse the plasma membrane in some format, either in lysosomal vesicles or in a yet-unidentified mechanism(100,102,103). The more intermediate-like state of the freshly cleaved C-terminal protein may allow it to cross membranes more easily, facilitating a quick exit from the cell. Coming into contact with the charged membrane surface may also facilitate final folding into the native structure as well. Indeed, pro-IL-1β causes ~70-50% total leakage of calcien from small unilamellar vesicles (LUVS), where mature IL-1β causes only 10-14% (when compared to 100% by Triton-X, K. Hailey, unpublished results). In either case, further structural studies are required to solve the enigma of IL-1β processing, folding and secretion.

The Functional Landscape of IL-1Ra and Receptor-Binding

As described in Chapter 6, IL-1Ra, the natural competitive inhibitor of IL-1β, can be turned into a partial agonist by mutating regions of the protein found to add frustration to its folding landscape. Since IL-1β and IL-1Ra share the same folding landscape (as discussed in Chapter 5), regions shown to add frustration in the folding landscape of IL-1β have also been shown to be functionally important(107,109).

The next step in looking at how these mutations flip the activity of IL-1Ra from an antagonist to an agonist is to look at changes in the structure and dynamics of the mutant proteins. Figure 8-2 displays the chemical shift changes in the C116F and K145D mutants compared to wt IL-1Ra, along with the C116F/K145D mutant shifts as compared to C116F. Major changes are seen in the section of the protein that interacts with the IL-1R1 (also in Figure 8-2) for both the C116F and K145D mutants, spanning trefoils 3 and 1 (strands 10 – 12, and 1). Both K145D and C116F contain residues that shift on the opposite side of the protein, but C116F has substantially more than K145D. These residues are located in the 90's loop (both), the tight turn (C116F only), regions shown to be important for IL-1β agonist activity in trefoil 2. Interestingly, the shifted residues compose two separate halves of the protein. This phenomenon is different than what was seen for the H30 and T9 mutants of IL-1β that display altered activity. In the T9 variants, the chemical shift changes are mostly relegated to the site of mutation (strand 1), with some bridging over to strand 12 and 2 (Anderson, WD, unpublished results). Hydrogen/deuterium exchange NMR of the native state of T9 variants show an overall destabilization of the protein, with a select

Figure 8-2: The crystal structure of IL-1Ra bound to IL-1RI with residues that have chemical shifts greater than 2 ppm in the ^{15}N-dimension and 0.02 ppm in the ^{1}H-dimension for A) C116F IL-1Ra (yellow spheres) and B) K145D IL-1Ra (red spheres) as compared to wt IL-1Ra and C) C116F/K145D IL-1Ra as compared to C116F IL-1Ra (orange spheres). According to the agonist activity data presented in Chapter 6, the C116F mutant is the most active, K145D is active, and C116F/K145D is active. The effect of adding the K145D mutation to C116F does not alter the resulting agonist activity (K. Hailey, S. Barkho, unpublished results).

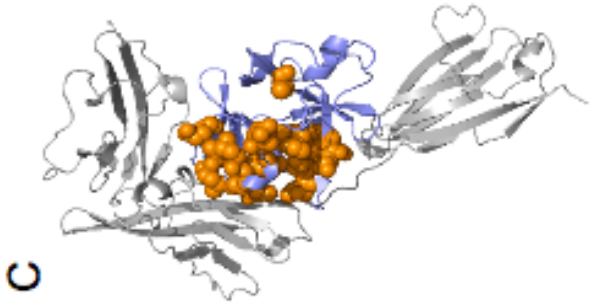

C

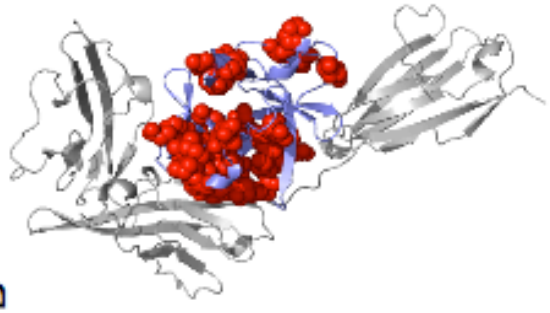

B

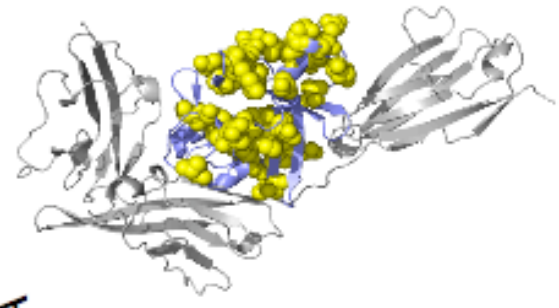

A

region of stability maintained near residue F117. In the H30 variants, differences in H/D exchange followed the hydrogen-bonding network through the barrel of the protein to the B-site of the bifurcated receptor-binding site(124). The same H/D exchange NMR studies are currently being investigated for the IL-1Ra variants to see if they too follow a pathway through the barrel of the protein, but it might be possible that the flow of information does not exist in the same routes as in IL-1β, or requires a conformational change large enough to disturb the hydrogen bonding network in the same way as IL-1β (193).

The Folding and Structural Landscape of IL-33: Distinctly Different

In Chapter 7, the folding landscape of the newest IL-1 family member, IL-33, is introduced. While sharing similar thermodynamic stability, the β-trefoil region of IL-33 folds significantly faster than either wt IL-1β or IL-1Ra. As discussed in Chapter 7, it is possible that IL-33 folds more like a hybrid of the β-trefoil foil family member hisactophilin and IL-1Ra. Preliminary Cα-model simulations of IL-33 folding performed by S. Gosavi have shown that this is indeed true (S. Gosavi, unpublished results). For IL-33, the energy barrier between the unfolded and native states is significantly less high and broad as compared to IL-1β and even IL-1Ra (S. Gosavi, unpublished results)(109). Also shown in Chapter 7 is the relative protection of the native state backbone of IL-33 as compared to IL-1Ra. The protection factors for each residue are currently being calculated, and should reveal more about the location of faster exchanging residues are as compared to slow exchanging residues in

both proteins. What the increased folding rate and the relative instability to exchange mean in terms of function is currently unknown.

Future Directions

The outstanding questions for the IL-1 family of proteins include the following. All IL-1 family members, barring the classically secreted isoform of IL-1Ra (isoform 1), are non-classically secreted(102). While there is a multitude of studies that address the secretion of β-trefoil proteins, the exact mechanism of how these proteins exit the cell in an efficient and timely manner remains elusive(102). What is likely is that these proteins are secreted in a cell-specific, stimulus-specific manner, meaning a multitude of mechanisms exists, and may even overlap at the same time under the same stimulus.

Another question remaining for the IL-1 family addresses the promiscuity of the IL-1RAcp and its ability to recognize four different receptors, IL-1R type I, IL-1R type II, IL-1Rrp2 (the receptor for IL-1F5 – 10 ligands) and ST2/T1(30,147,169,194). In a very recent paper by Wang, et. al, the structure of the IL-1β/IL-1RII/IL-1RAcp soluble domains by x-ray crystallography is presented, illustrated in Figure 8-3a(145). In the paper, the mechanism of IL-1β agonism and IL-1Ra antagonism is described based on the crystal structure and binding data. As in the IL-1β/IL-1RI and IL-1Ra/IL-1RI crystal structure papers, the mechanism for IL-1RAcp recruitment to form the active complex is attributed to the engagement of the third Ig domain of the IL-1RI or IL-1RII receptors by IL-1β, and conversely is the root cause of IL-1Ra receptor

antagonism. In direct contrast to this, the point mutants presented in here and elsewhere away from or not participating in the binding site show activity levels that would not be predicted based on inspection of this crystal structure alone(155,160).

Also not addressed by inspection of the structure is the ability of IL-1RAcp to recognize and bind four receptors with low sequence identity(30,147,169,194). The electrostatic surfaces of IL-1β/IL-1RI, IL-1Ra/IL-1RI, IL-1βIL-1RII, IL-33/ST2/T1 and the complementary face of IL-1RAcp are given in Figure 8-3b. Each receptor/ligand surface presents a unique interface to the IL-1RAcp. Clearly, the crystal structures alone cannot account for the differences in recognition by the IL-1RAcp. Indeed, an antibody raised to specifically block the interaction of IL-1β/IL-1RI by binding IL-1RAcp does not work nearly as well to prevent IL-1RAcp from forming the ternary complex between it and IL-33/ST2/T1(195). In the near future, DXMS, all-atom Go, and MD simulation studies will be undertaken to determine how the ligands impact each receptor, and how the ligand/receptor complex interacts with the IL-1RAcp(196). As a smaller question within the recptor/ligand binding question is how the binding affinity for each of the ligands (IL-1α, β, Ra, and 33) changes based on whether the receptor is surface-bound or free. The binding affinities for these proteins vary based on location of the receptor(10).

Figure 8-3: The structure of the IL-1β/IL-1RII/IL-1RAcp ternary complex and the electrostatic surfaces of the IL-1 receptor family. The crystal structure from Wang, et al. is rendered in A). The electrostatic surfaces of IL-1β/IL-1RI, IL-1Ra/IL-1RI, IL-1βIL-1RII, IL-33/ST2/T1 and the complementary face of IL-1RAcp are given in B). The ternary complex structure was rendered and the receptor surfaces were generated with the default electrostatics parameters from Pymol (Delgano). The structure of IL-33/ST2/T1 is based on the model presented in Lingel, et. al. Surprisingly, the first Ig domain of IL-1RAcp is free from the ternary complex. How this free domain impacts the activity of the ternary complex remains to be investigated, perhaps it provides a scaffold for oligomerization for importation of the extracellular/intracellular multi-protein complex (extracellular = ternary complex, intracellular = oligomers of MyD88, IRAK-1, IRAK-4, TRAF-6) (163,197,198).

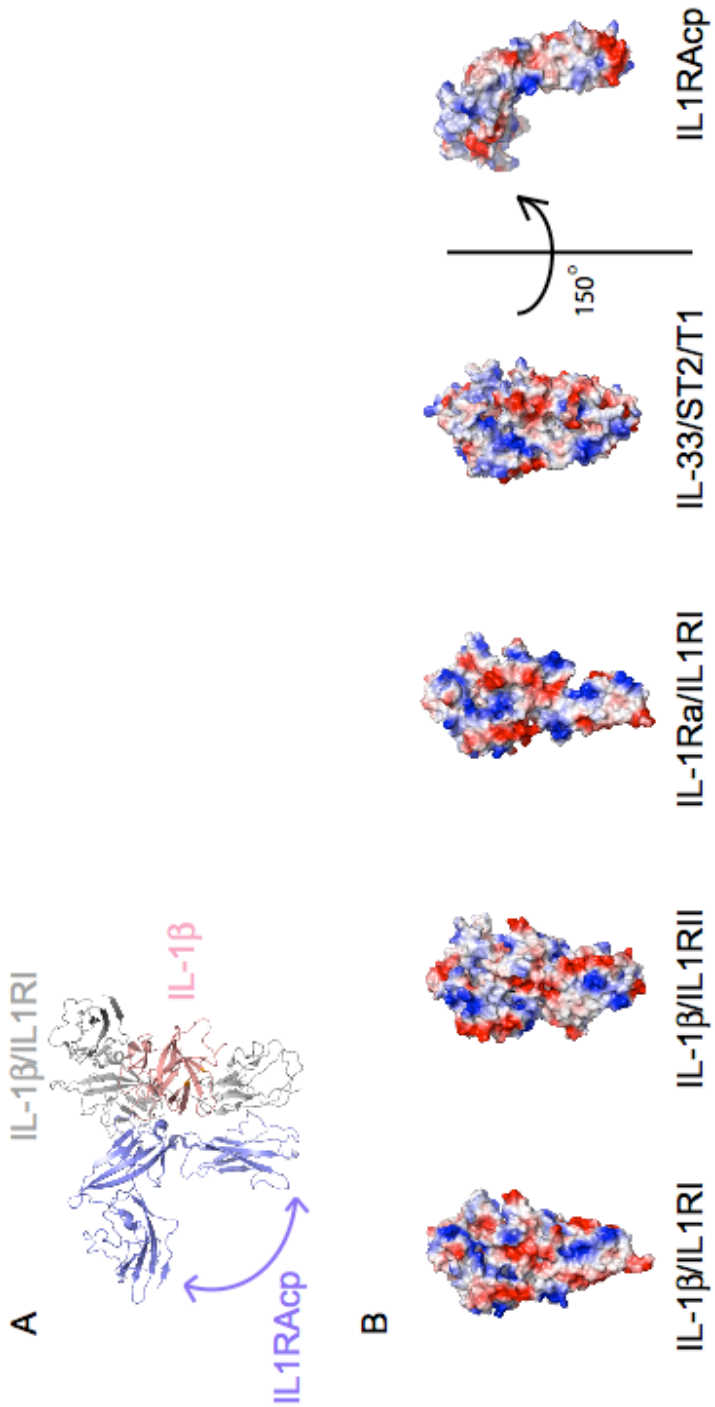
A
IL-1β/IL1RI
IL-1β
IL1RAcp
B
IL-1β/IL1RI
IL-1β/IL1RII
IL-1Ra/IL1RI
IL-33/ST2/T1
150°
IL1RAcp

Another important question is how the dual functions of the precursor proteins of this family impact each other, and when/where each is used. As discussed in Chapter 1, pro-IL-1α has a dual function of acting as a pro-apoptotic transcription factor in cancer cells (PNAS ref). Full-length IL-33 has shown to be associated with chromatin in the nucleus in resting fibroblasts, and contains a H-T-H DNA binding motif(199). Recently, pro-IL-1β was found to passively locate into the nucleus of microglia, and in MCF10A cells over expressing the C/EBPbeta2 mammary gland growth factor, highly-upregulated pro-IL-1β is found in the nucleus, associated with chromatin(19). How the chromatin-association effects of the IL-1 full-length proteins the homeostasis of resting cells or cancer cells is currently unknown.

Finally, the combination of always-improving folding simulations and designed mutagenesis studies can be applied to other IL-1 family members, including IL-18, IL-1α and IL-33 to flip or attenuate their pro- or anti- inflammatory activities. Inflammation due to misregulation of IL-1 family members is becoming more prevalent as an exacerbating factor, or even as a causative factor for chronic illnesses like certain types of cancer or Alzheimer's disease (17,44). One approach to diminishing damaging inflammation is to design better, longer-lasting inhibitors, or using partial agonists that do not abolish the beneficial aspects of the inflammatory response along with the deleterious ones(199). The more information we can learn about the folding and functional landscapes of the IL-1 family members will hopefully lead to more thoughtful and productive drug design in the future.

References

REFERNCES

1. Arend, W. P., Palmer, G., and Gabay, C. (2008) *Immunol Rev* **223**, 20-38

2. Dinarello, C. A. (1988) *Faseb J* **2**(2), 108-115

3. Dinarello, C. A. (1994) *Faseb J* **8**(15), 1314-1325

4. Lamkanfi, M., and Dixit, V. M. (2009) *Immunity* **31**(1), 5-7

5. Dinarello, C., Arend, W., Sims, J., Smith, D., Blumberg, H., O'Neill, L., Goldbach-Mansky, R., Pizarro, T., Hoffman, H., Bufler, P., Nold, M., Ghezzi, P., Mantovani, A., Garlanda, C., Boraschi, D., Rubartelli, A., Netea, M., van der Meer, J., Joosten, L., Mandrup-Poulsen, T., Donath, M., Lewis, E., Pfeilschifter, J., Martin, M., Kracht, M., Muehl, H., Novick, D., Lukic, M., Conti, B., Solinger, A., Peyman, K., van de Veerdonk, F., and Gabel, C. *Nat Immunol* **11**(11), 973
6. Pollock, A. S., Turck, J., and Lovett, D. H. (2003) *Faseb J* **17**(2), 203-213

7. Roussel, L., Erard, M., Cayrol, C., and Girard, J. P. (2008) *EMBO Rep* **9**(10), 1006-1012

8. Werman, A., Werman-Venkert, R., White, R., Lee, J. K., Werman, B., Krelin, Y., Voronov, E., Dinarello, C. A., and Apte, R. N. (2004) *Proc Natl Acad Sci U S A* **101**(8), 2434-2439

9. Arend, W. P., Malyak, M., Guthridge, C. J., and Gabay, C. (1998) *Annu Rev Immunol* **16**, 27-55

10. Arend, W. P., Malyak, M., Smith, M. F., Jr., Whisenand, T. D., Slack, J. L., Sims, J. E., Giri, J. G., and Dower, S. K. (1994) *J Immunol* **153**(10), 4766-4774

11. Baumann, J. B., Christen, E., Gamboni, G., Joss, U., van Oostrum, J., Girard, J., and Eberle, A. N. (1993) *J Recept Res* **13**(1-4), 245-262

12. O'Neill, L. A., and Greene, C. (1998) *J Leukoc Biol* **63**(6), 650-657

13. Sims, J. E., and Smith, D. E. (2010) *Nat Rev Immunol* **10**(2), 89-102

14. Arend, W. P. (2002) *Cytokine Growth Factor Rev* **13**(4-5), 323-340

15. Dinarello, C. A. (1996) *Blood* **87**(6), 2095-2147

16. Dinarello, C. A. (2005) *J Exp Med* **201**(9), 1355-1359

17. Dinarello, C. A. (2010) *Cancer Metastasis Rev* **29**(2), 317-329

18. Griffin, W. S., Liu, L., Li, Y., Mrak, R. E., and Barger, S. W. (2006) *J Neuroinflammation* **3**, 5

19. Russell, A. J. (2010) The Role of CCAAT/Enhancer Binding Protein Beta2 in Mammary Epithlial Cells. In. *Cancer Biology*, Vanderbilt, Nashville

20. Auron, P. E., Webb, A. C., Rosenwasser, L. J., Mucci, S. F., Rich, A., Wolff, S. M., and Dinarello, C. A. (1984) *Proc Natl Acad Sci U S A* **81**(24), 7907-7911

21. Eisenberg, S. P., Brewer, M. T., Verderber, E., Heimdal, P., Brandhuber, B. J., and Thompson, R. C. (1991) *Proc Natl Acad Sci U S A* **88**(12), 5232-5236

22. Hughes, A. L. (1994) *J Mol Evol* **39**(1), 6-12

23. Delano, W. L. The PyMOL Molecular Graphics System. In., DeLano Scientific, LLC, San Carlos, CA, USA

24. Priestle, J. P., Schar, H. P., and Grutter, M. G. (1988) *Embo J* **7**(2), 339-343

25. Vigers, G. P., Caffes, P., Evans, R. J., Thompson, R. C., Eisenberg, S. P., and Brandhuber, B. J. (1994) *J Biol Chem* **269**(17), 12874-12879

26. Schreuder, H., Tardif, C., Trump-Kallmeyer, S., Soffientini, A., Sarubbi, E., Akeson, A., Bowlin, T., Yanofsky, S., and Barrett, R. W. (1997) *Nature* **386**(6621), 194-200

27. Vigers, G. P., Anderson, L. J., Caffes, P., and Brandhuber, B. J. (1997) *Nature* **386**(6621), 190-194

28. Heidary, D. K., Gross, L. A., Roy, M., and Jennings, P. A. (1997) *Nat Struct Biol* **4**(9), 725-731

29. Hazuda, D. J., Lee, J. C., and Young, P. R. (1988) *J Biol Chem* **263**(17), 8473-8479

30. Lang, D., Knop, J., Wesche, H., Raffetseder, U., Kurrle, R., Boraschi, D., and Martin, M. U. (1998) *J Immunol* **161**(12), 6871-6877

31. Symons, J. A., Young, P. R., and Duff, G. W. (1995) *Proc Natl Acad Sci U S A* **92**(5), 1714-1718

32. Cole, C., Barber, J. D., and Barton, G. J. (2008) *Nucleic Acids Res* **36**(Web Server issue), W197-201

33. Schmitz, J., Owyang, A., Oldham, E., Song, Y., Murphy, E., McClanahan, T. K., Zurawski, G., Moshrefi, M., Qin, J., Li, X., Gorman, D. M., Bazan, J. F., and Kastelein, R. A. (2005) *Immunity* **23**(5), 479-490

34. Baekkevold, E. S., Roussigne, M., Yamanaka, T., Johansen, F. E., Jahnsen, F. L., Amalric, F., Brandtzaeg, P., Erard, M., Haraldsen, G., and Girard, J. P. (2003) *Am J Pathol* **163**(1), 69-79

35. Onda, H., Kasuya, H., Takakura, K., Hori, T., Imaizumi, T., Takeuchi, T., Inoue, I., and Takeda, J. (1999) *J Cereb Blood Flow Metab* **19**(11), 1279-1288

36. Kakkar, R., and Lee, R. T. (2008) *Nat Rev Drug Discov* **7**(10), 827-840

37. Lingel, A., Weiss, T. M., Niebuhr, M., Pan, B., Appleton, B. A., Wiesmann, C., Bazan, J. F., and Fairbrother, W. J. (2009) *Structure* **17**(10), 1398-1410

38. Seki, K., Sanada, S., Kudinova, A. Y., Steinhauser, M. L., Handa, V., Gannon, J., and Lee, R. T. (2009) *Circ Heart Fail* **2**(6), 684-691

39. Alves-Filho, J. C., Sonego, F., Souto, F. O., Freitas, A., Verri, W. A., Jr., Auxiliadora-Martins, M., Basile-Filho, A., McKenzie, A. N., Xu, D., Cunha, F. Q., and Liew, F. Y. *Nat Med* **16**(6), 708-712

40. Siegel, J. (2001) Biologics License, Anakinra. In: Administration, F. a. D. (ed). *103950/0*, Rockville, MD

41. Alten, R., Gram, H., Joosten, L. A., van den Berg, W. B., Sieper, J., Wassenberg, S., Burmester, G., van Riel, P., Diaz-Lorente, M., Bruin, G. J., Woodworth, T. G., Rordorf, C., Batard, Y., Wright, A. M., and Jung, T. (2008) *Arthritis Res Ther* **10**(3), R67

42. Ratner, M. (2008) *Nat Biotechnol* **26**(5), 485

43. Dinarello, C. A. (2009) *Annu Rev Immunol* **27**, 519-550

44. Dinarello, C. A. (2010) *Cell* **140**(6), 935-950

45. Lin, W. W., and Karin, M. (2007) *J Clin Invest* **117**(5), 1175-1183

46. Martinon, F., Petrilli, V., Mayor, A., Tardivel, A., and Tschopp, J. (2006) *Nature* **440**(7081), 237-241

47. Covalt, J. C., Jr., Cao, T. B., Magdaroag, J. R., Gross, L. A., and Jennings, P. A. (2005) *Protein Expr Purif* **41**(1), 45-52

48. Burke, J. E., Hsu, Y. H., Deems, R. A., Li, S., Woods, V. L., Jr., and Dennis, E. A. (2008) *J Biol Chem* **283**(45), 31227-31236

49. Golynskiy, M., Li, S., Woods, V. L., Jr., and Cohen, S. M. (2007) *J Biol Inorg Chem* **12**(5), 699-709

50. Hamuro, Y., Wong, L., Shaffer, J., Kim, J. S., Stranz, D. D., Jennings, P. A., Woods, V. L., Jr., and Adams, J. A. (2002) *J Mol Biol* **323**(5), 871-881

51. Finke, J. M., and Jennings, P. A. (2002) *Biochemistry* **41**(50), 15056-15067

52. Finke, J. M., Roy, M., Zimm, B. H., and Jennings, P. A. (2000) *Biochemistry* **39**(3), 575-583

53. Hazuda, D. J., Strickler, J., Simon, P., and Young, P. R. (1991) *J Biol Chem* **266**(11), 7081-7086

54. Herzog, C., Kaushal, G. P., and Haun, R. S. (2005) *Cytokine* **31**(5), 394-403

55. Schonbeck, U., Mach, F., and Libby, P. (1998) *J Immunol* **161**(7), 3340-3346

56. Thornberry, N. A., Bull, H. G., Calaycay, J. R., Chapman, K. T., Howard, A. D., Kostura, M. J., Miller, D. K., Molineaux, S. M., Weidner, J. R., Aunins, J., and et al. (1992) *Nature* **356**(6372), 768-774

57. Dinarello, C. A. *Arthritis Rheum*

58. Dinarello, C. A., Donath, M. Y., and Mandrup-Poulsen, T. *Curr Opin Endocrinol Diabetes Obes* **17**(4), 314-321

59. Qu, Y., Franchi, L., Nunez, G., and Dubyak, G. R. (2007) *J Immunol* **179**(3), 1913-1925

60. Wilson, H. L., Francis, S. E., Dower, S. K., and Crossman, D. C. (2004) *J Immunol* **173**(2), 1202-1208

61. Hazuda, D. J., Strickler, J., Kueppers, F., Simon, P. L., and Young, P. R. (1990) *J Biol Chem* **265**(11), 6318-6322

62. Herzyk, D. J., Allen, J. N., Marsh, C. B., and Wewers, M. D. (1992) *J Immunol* **149**(9), 3052-3058

63. Netea, M. G., Nold-Petry, C. A., Nold, M. F., Joosten, L. A., Opitz, B., van der Meer, J. H., van de Veerdonk, F. L., Ferwerda, G., Heinhuis, B., Devesa, I., Funk, C. J., Mason, R. J., Kullberg, B. J., Rubartelli, A., Van der Meer, J. W., and Dinarello, C. A. (2008) *Blood*

64. Moors, M. A., and Mizel, S. B. (2000) *J Leukoc Biol* **68**(1), 131-136

65. Netea, M. G., Simon, A., van de Veerdonk, F., Kullberg, B. J., Van der Meer, J. W., and Joosten, L. A. (2010) *PLoS Pathog* **6**(2), e1000661

66. Petrilli, V., Dostert, C., Muruve, D. A., and Tschopp, J. (2007) *Curr Opin Immunol* **19**(6), 615-622

67. Schroder, K., and Tschopp, J. (2010) *Cell* **140**(6), 821-832

68. Swaan, P. W., Knoell, D. L., Helsper, F., and Wewers, M. D. (2001) *Pharm Res* **18**(8), 1083-1090

69. al-Janabi, J., Hartsuck, J. A., and Tang, J. (1972) *J Biol Chem* **247**(14), 4628-4632

70. Jaswal, S. S., Sohl, J. L., Davis, J. H., and Agard, D. A. (2002) *Nature* **415**(6869), 343-346

71. Shinde, U., and Inouye, M. (1995) *J Mol Biol* **247**(3), 390-395

72. Shinde, U., and Inouye, M. (2000) *Semin Cell Dev Biol* **11**(1), 35-44

73. Plaxco, K. W., and Dobson, C. M. (1996) *Curr Opin Struct Biol* **6**(5), 630-636

74. Kruse, N. (2006) Local and Glocal Conformational Changes in Signalling Proteins Studied by Solution NMR Spectroscopy. In. *Chemistry and Biochemistry*, Univeristy of California, San Diego, La Jolla

75. Wu, D., Chen, A., and Johnson Jr., C.S. (1996) *Journal of Magnetic REsonance* **A121**, 88-89

76. Longsworth, L. G. (1960) *The Journal of Physical Chemistry* **64**(12), 1914-1917
77. Marat, K. (2004) Spinworks. In., 2.5 Ed., University of Manitoba, Winnipeg

78. Pan, H., Barany, G., and Woodward, C. (1997) *Protein Sci* **6**(9), 1985-1992

79. Hazuda, D., Webb, R. L., Simon, P., and Young, P. (1989) *J Biol Chem* **264**(3), 1689-1693

80. Cavanagh, J., Faribrother, W.J., Palmer III, A.G., Rance, M., Skelton, N.J. (2007) *Protein NMR Spectroscopy: Theory and Practice*, Second Ed., Elsevier Academic Press, Burlington

81. Wilkins, D. K., Grimshaw, S. B., Receveur, V., Dobson, C. M., Jones, J. A., and Smith, L. J. (1999) *Biochemistry* **38**(50), 16424-16431

82. Marsh, J. A., and Forman-Kay, J. D. *Biophys J* **98**(10), 2383-2390

83. Uversky, V. N. (2002) *Protein Sci* **11**(4), 739-756

84. Thornberry, N. A. (1997) *Br Med Bull* **53**(3), 478-490

85. Talanian, R. V., Quinlan, C., Trautz, S., Hackett, M. C., Mankovich, J. A., Banach, D., Ghayur, T., Brady, K. D., and Wong, W. W. (1997) *J Biol Chem* **272**(15), 9677-9682

86. Arend, W. P., Smith, M. F., Jr., Janson, R. W., and Joslin, F. G. (1991) *J Immunol* **147**(5), 1530-1536

87. Bohley, P. (1995) *Naturwissenschaften* **82**(12), 544-550

88. Mariathasan, S., Weiss, D. S., Newton, K., McBride, J., O'Rourke, K., Roose-Girma, M., Lee, W. P., Weinrauch, Y., Monack, D. M., and Dixit, V. M. (2006) *Nature* **440**(7081), 228-232

89. Petrilli, V., Papin, S., Dostert, C., Mayor, A., Martinon, F., and Tschopp, J. (2007) *Cell Death Differ* **14**(9), 1583-1589

90. Weljie, A. M., Yamniuk, A. P., Yoshino, H., Izumi, Y., and Vogel, H. J. (2003) *Protein Sci* **12**(2), 228-236

91. Roy, M., Chavez, L. L., Finke, J. M., Heidary, D. K., Onuchic, J. N., and Jennings, P. A. (2005) *J Mol Biol* **348**(2), 335-347

92. Dinarello, C. A., and Savage, N. (1989) *Crit Rev Immunol* **9**(1), 1-20

93. Hoffman, H. M., Mueller, J. L., Broide, D. H., Wanderer, A. A., and Kolodner, R. D. (2001) *Nat Genet* **29**(3), 301-305

94. Kanneganti, T. D., Ozoren, N., Body-Malapel, M., Amer, A., Park, J. H., Franchi, L., Whitfield, J., Barchet, W., Colonna, M., Vandenabeele, P., Bertin, J., Coyle, A., Grant, E. P., Akira, S., and Nunez, G. (2006) *Nature* **440**(7081), 233-236

95. Howard, A. D., Kostura, M. J., Thornberry, N., Ding, G. J., Limjuco, G., Weidner, J., Salley, J. P., Hogquist, K. A., Chaplin, D. D., Mumford, R. A., and et al. (1991) *J Immunol* **147**(9), 2964-2969

96. Bird, S., Wang, T., Zou, J., Cunningham, C., and Secombes, C. J. (2002) *J Immunol* **168**(7), 3329-3340

97. Koussounadis, A. I., Ritchie, D. W., Kemp, G. J., and Secombes, C. J. (2004) *Curr Pharm Des* **10**(31), 3857-3871

98. Larkin, M. A., Blackshields, G., Brown, N. P., Chenna, R., McGettigan, P. A., McWilliam, H., Valentin, F., Wallace, I. M., Wilm, A., Lopez, R., Thompson, J. D., Gibson, T. J., and Higgins, D. G. (2007) *Bioinformatics* **23**(21), 2947-2948

99. Black, R. A., Kronheim, S. R., Cantrell, M., Deeley, M. C., March, C. J., Prickett, K. S., Wignall, J., Conlon, P. J., Cosman, D., Hopp, T. P., and et al. (1988) *J Biol Chem* **263**(19), 9437-9442

100. Andrei, C., Margiocco, P., Poggi, A., Lotti, L. V., Torrisi, M. R., and Rubartelli, A. (2004) *Proc Natl Acad Sci U S A* **101**(26), 9745-9750

101. Brough, D., and Rothwell, N. J. (2007) *J Cell Sci* **120**(Pt 5), 772-781
102. Nickel, W. (2003) *Eur J Biochem* **270**(10), 2109-2119

103. Rubartelli, A., Cozzolino, F., Talio, M., and Sitia, R. (1990) *Embo J* **9**(5), 1503-1510

104. Clore, G. M., Wingfield, P. T., and Gronenborn, A. M. (1991) *Biochemistry* **30**(9), 2315-2323

105. Varley, P., Gronenborn, A. M., Christensen, H., Wingfield, P. T., Pain, R. H., and Clore, G. M. (1993) *Science* **260**(5111), 1110-1113

106. Clementi, C., Jennings, P. A., and Onuchic, J. N. (2000) *Proc Natl Acad Sci U S A* **97**(11), 5871-5876

107. Capraro, D. T., Roy, M., Onuchic, J. N., and Jennings, P. A. (2008) *Proc Natl Acad Sci U S A* **105**(39), 14844-14848

108. Gosavi, S., Chavez, L. L., Jennings, P. A., and Onuchic, J. N. (2006) *J Mol Biol* **357**(3), 986-996

109. Gosavi, S., Whitford, P. C., Jennings, P. A., and Onuchic, J. N. (2008) *Proc Natl Acad Sci U S A* **105**(30), 10384-10389

110. Kobayashi, Y., Nagatake, H., Shimozato, O., and Watanabe, N. (1997) *J Biochem* **121**(5), 896-901

111. Kobayashi, Y., Oppenheim, J. J., and Matsushima, K. (1991) *Chem Pharm Bull (Tokyo)* **39**(6), 1513-1517

112. Branden, C., Tooze, J. (1998) *Introduction to Protein Structure: Second Edition*, Garland Publishing, Inc, New York

113. Derewenda, Z. S. (2004) *Structure* **12**(4), 529-535

114. Spraggon, G., Pantazatos, D., Klock, H. E., Wilson, I. A., Woods, V. L., Jr., and Lesley, S. A. (2004) *Protein Sci* **13**(12), 3187-3199

115. Englander, S. W., Sosnick, T. R., Englander, J. J., and Mayne, L. (1996) *Curr Opin Struct Biol* **6**(1), 18-23

116. Hoofnagle, A. N., Resing, K. A., and Ahn, N. G. (2003) *Annu Rev Biophys Biomol Struct* **32**, 1-25

117. Linderstrom-Lang, K. (1958) Deuterium Exchange and Protein Structure. In: Neuberger, A. (ed). *Symposium on Protein Structure*, Methuen, London

118. Mizutani, H., Schechter, N., Lazarus, G., Black, R. A., and Kupper, T. S. (1991) *J Exp Med* **174**(4), 821-825

119. Kelly, S. M., and Price, N. C. (2000) *Curr Protein Pept Sci* **1**(4), 349-384

120. Grishina, I. B., and Woody, R. W. (1994) *Faraday Discuss* (99), 245-262

121. Craig, S., Pain, R. H., Schmeissner, U., Virden, R., and Wingfield, P. T. (1989) *Int J Pept Protein Res* **33**(4), 256-262

122. Brock, M., Fan, F., Mei, F. C., Li, S., Gessner, C., Woods, V. L., Jr., and Cheng, X. (2007) *J Biol Chem* **282**(44), 32256-32263

123. Driscoll, P. C., Gronenborn, A. M., Wingfield, P. T., and Clore, G. M. (1990) *Biochemistry* **29**(19), 4668-4682

124. Heidary, D. K., Roy, M., Daumy, G. O., Cong, Y., and Jennings, P. A. (2005) *J Mol Biol* **353**(5), 1187-1198

125. Weissman, J. S., and Kim, P. S. (1992) *Cell* **71**(5), 841-851

126. Wiley, S. E., Murphy, A. N., Ross, S. A., van der Geer, P., and Dixon, J. E. (2007) *Proc Natl Acad Sci U S A* **104**(13), 5318-5323

127. Kavita, U., and Mizel, S. B. (1995) *J Biol Chem* **270**(46), 27758-27765

128. Stevenson, F. T., Turck, J., Locksley, R. M., and Lovett, D. H. (1997) *Proc Natl Acad Sci U S A* **94**(2), 508-513

129. Bai, Y., Milne, J. S., Mayne, L., and Englander, S. W. (1993) *Proteins* **17**(1), 75-86

130. YZ., Z. (1995) Protein and peptide structure and interactions studied by hydrogen exchange and NMR. In. *Sturcutral Biology and Molecular Biophysics*, University of Pennsylvania, Philadelphia

131. Young, P. R., and Sylvester, D. (1989) *Protein Eng* **2**(7), 545-551

132. Chavez, L. L., Gosavi, S., Jennings, P. A., and Onuchic, J. N. (2006) *Proc Natl Acad Sci U S A* **103**(27), 10254-10258

133. Barbar, E. (1999) *Biopolymers* **51**(3), 191-207

134. Dyson, H. J., and Wright, P. E. (2002) *Adv Protein Chem* **62**, 311-340

135. Dyson, H. J., and Wright, P. E. (2002) *Curr Opin Struct Biol* **12**(1), 54-60

136. Dyson, H. J., and Wright, P. E. (2004) *Chem Rev* **104**(8), 3607-3622

137. Li, R., and Woodward, C. (1999) *Protein Sci* **8**(8), 1571-1590

138. Veerapandian, B., Gilliland, G. L., Raag, R., Svensson, A. L., Masui, Y., Hirai, Y., and Poulos, T. L. (1992) *Proteins* **12**(1), 10-23

139. Mosley, B., Urdal, D. L., Prickett, K. S., Larsen, A., Cosman, D., Conlon, P. J., Gillis, S., and Dower, S. K. (1987) *J Biol Chem* **262**(7), 2941-2944

140. Siders, W. M., and Mizel, S. B. (1995) *J Biol Chem* **270**(27), 16258-16264

141. Evans, R. J., Bray, J., Childs, J. D., Vigers, G. P., Brandhuber, B. J., Skalicky, J. J., Thompson, R. C., and Eisenberg, S. P. (1995) *J Biol Chem* **270**(19), 11477-11483

142. O'Neill, L. (2000) *Biochem Soc Trans* **28**(5), 557-563

143. O'Neill, L. A. (2000) *Sci STKE* **2000**(44), re1

144. Malyak, M., Smith, M. F., Jr., Abel, A. A., Hance, K. R., and Arend, W. P. (1998) *J Immunol* **161**(4), 2004-2010

145. Wang, D., Zhang, S., Li, L., Liu, X., Mei, K., and Wang, X. *Nat Immunol* **11**(10), 905-911

146. Guinet, F., Guitton, J. D., Gault, N., Folliard, F., Touchet, N., Cherel, J. M., Crespo, A., Destourbe, A., Bertrand, P., Denefle, P., and et al. (1993) *Eur J Biochem* **211**(3), 583-590

147. Cullinan, E. B., Kwee, L., Nunes, P., Shuster, D. J., Ju, G., McIntyre, K. W., Chizzonite, R. A., and Labow, M. A. (1998) *J Immunol* **161**(10), 5614-5620

148. Greenfeder, S. A., Nunes, P., Kwee, L., Labow, M., Chizzonite, R. A., and Ju, G. (1995) *J Biol Chem* **270**(23), 13757-13765

149. Hoffmann, A., Levchenko, A., Scott, M. L., and Baltimore, D. (2002) *Science* **298**(5596), 1241-1245

150. Latypov, R. F., Harvey, T. S., Liu, D., Bondarenko, P. V., Kohno, T., Fachini, R. A., 2nd, Rosenfeld, R. D., Ketchem, R. R., Brems, D. N., and Raibekas, A. A. (2007) *J Mol Biol* **368**(4), 1187-1201

151. Samuel, D., Kumar, T. K., Balamurugan, K., Lin, W. Y., Chin, D. H., and Yu, C. (2001) *J Biol Chem* **276**(6), 4134-4141

152. Liu, C., Gaspar, J. A., Wong, H. J., and Meiering, E. M. (2002) *Protein Sci* **11**(3), 669-679

153. Stockman, B. J., Scahill, T. A., Roy, M., Ulrich, E. L., Strakalaitis, N. A., Brunner, D. P., Yem, A. W., and Deibel, M. R., Jr. (1992) *Biochemistry* **31**(23), 5237-5245

154. Bryngelson, J. D., Onuchic, J. N., Socci, N. D., and Wolynes, P. G. (1995) *Proteins* **21**(3), 167-195

155. Boraschi, D., Bossu, P., Macchia, G., Ruggiero, P., and Tagliabue, A. (1996) *Front Biosci* **1**, d270-308

156. Wen, Z. Q., Cao, X., and Vance, A. (2008) *J Pharm Sci* **97**(6), 2228-2241

157. Darby, N., and Creighton, T. E. (1995) *Methods Mol Biol* **40**, 219-252

158. Villafranca, J. E., Howell, E. E., Oatley, S. J., Xuong, N. H., and Kraut, J. (1987) *Biochemistry* **26**(8), 2182-2189

159. Wolfson, A. J., Kanaoka, M., Lau, F., Ringe, D., Young, P., Lee, J., and Blumenthal, J. (1993) *Biochemistry* **32**(20), 5327-5331

160. Greenfeder, S. A., Varnell, T., Powers, G., Lombard-Gillooly, K., Shuster, D., McIntyre, K. W., Ryan, D. E., Levin, W., Madison, V., and Ju, G. (1995) *J Biol Chem* **270**(38), 22460-22466

161. O'Neill, L. A., and Bowie, A. G. (2007) *Nat Rev Immunol* **7**(5), 353-364

162. Brikos, C., Wait, R., Begum, S., O'Neill, L. A., and Saklatvala, J. (2007) *Mol Cell Proteomics* **6**(9), 1551-1559

163. Lin, S. C., Lo, Y. C., and Wu, H. *Nature* **465**(7300), 885-890

164. Schreuder, H. A., Rondeau, J. M., Tardif, C., Soffientini, A., Sarubbi, E., Akeson, A., Bowlin, T. L., Yanofsky, S., and Barrett, R. W. (1995) *Eur J Biochem* **227**(3), 838-847

165. Frand, A. R., and Kaiser, C. A. (1998) *Mol Cell* **1**(2), 161-170

166. Heidary, D. K., and Jennings, P. A. (2002) *J Mol Biol* **316**(3), 789-798

167. Roell, M. K., Issafras, H., Bauer, R. J., Michelson, K. S., Mendoza, N., Vanegas, S. I., Gross, L. M., Larsen, P. D., Bedinger, D. H., Bohmann, D. J., Nonet, G. H., Liu, N., Lee, S. R., Handa, M., Kantak, S. S., Horwitz, A. H., Hunter, J. J., Owyang, A. M., Mirza, A. M., Corbin, J. A., and White, M. L. *J Biol Chem* **285**(27), 20607-20614

168. Gayle, M. A., Slack, J. L., Bonnert, T. P., Renshaw, B. R., Sonoda, G., Taguchi, T., Testa, J. R., Dower, S. K., and Sims, J. E. (1996) *J Biol Chem* **271**(10), 5784-5789

169. Chackerian, A. A., Oldham, E. R., Murphy, E. E., Schmitz, J., Pflanz, S., and Kastelein, R. A. (2007) *J Immunol* **179**(4), 2551-2555

170. Carriere, V., Roussel, L., Ortega, N., Lacorre, D. A., Americh, L., Aguilar, L., Bouche, G., and Girard, J. P. (2007) *Proc Natl Acad Sci U S A* **104**(1), 282-287

171. Cohen, I., Rider, P., Carmi, Y., Braiman, A., Dotan, S., White, M. R., Voronov, E., Martin, M. U., Dinarello, C. A., and Apte, R. N. (2010) *Proc Natl Acad Sci U S A* **107**(6), 2574-2579

172. Ali, S., Nguyen, D. Q., Falk, W., and Martin, M. U. (2010) *Biochem Biophys Res Commun* **391**(3), 1512-1516

173. Blom, N., Gammeltoft, S., and Brunak, S. (1999) *J Mol Biol* **294**(5), 1351-1362

174. Talabot-Ayer, D., Lamacchia, C., Gabay, C., and Palmer, G. (2009) *J Biol Chem* **284**(29), 19420-19426

175. Scheel, J., Ziegelbauer, K., Kupke, T., Humbel, B. M., Noegel, A. A., Gerisch, G., and Schleicher, M. (1989) *J Biol Chem* **264**(5), 2832-2839

176. Luthi, A. U., Cullen, S. P., McNeela, E. A., Duriez, P. J., Afonina, I. S., Sheridan, C., Brumatti, G., Taylor, R. C., Kersse, K., Vandenabeele, P., Lavelle, E. C., and Martin, S. J. (2009) *Immunity* **31**(1), 84-98

177. Zhao, W., and Hu, Z. (2010) *Cell Mol Immunol*

178. Lingel, A., and Fairbrother, W. J. (2009) *Biomol NMR Assign* **3**(2), 223-225

179. Ponting, C. P., and Russell, R. B. (2000) *J Mol Biol* **302**(5), 1041-1047

180. Plotnikov, A. N., Hubbard, S. R., Schlessinger, J., and Mohammadi, M. (2000) *Cell* **101**(4), 413-424

181. Plaxco, K. W., Simons, K. T., and Baker, D. (1998) *J Mol Biol* **277**(4), 985-994

182. Kamada, S., Kikkawa, U., Tsujimoto, Y., and Hunter, T. (2005) *J Biol Chem* **280**(2), 857-860

183. Moussion, C., Ortega, N., and Girard, J. P. (2008) *PLoS One* **3**(10), e3331

184. Wilson, H. L., Varcoe, R. W., Stokes, L., Holland, K. L., Francis, S. E., Dower, S. K., Surprenant, A., and Crossman, D. C. (2007) *Br J Pharmacol* **151**(1), 115-127

185. Verhoef, P. A., Kertesy, S. B., Estacion, M., Schilling, W. P., and Dubyak, G. R. (2004) *Mol Pharmacol* **66**(4), 909-920

186. Rosenwasser, T. A., Hogquist, K. A., Nothwehr, S. F., Bradford-Goldberg, S., Olins, P. O., Chaplin, D. D., and Gordon, J. I. (1990) *J Biol Chem* **265**(22), 13066-13073

187. Thorstenson, Y. R., Zhang, Y., Olson, P. S., and Mascarenhas, D. (1997) *J Bacteriol* **179**(17), 5333-5339

188. Frenkel, O., Shani, E., Ben-Bassat, I., Brok-Simoni, F., Shinar, E., and Danon, D. (2001) *Clin Exp Immunol* **124**(1), 103-109

189. Hammond, M. S., Houliston, R. S., and Meiering, E. M. (1998) *Biochem Cell Biol* **76**(2-3), 294-301

190. Pace, C. N., Grimsley, G. R., and Scholtz, J. M. (2009) *J Biol Chem* **284**(20), 13285-13289

191. Surewicz, W. K., and Epand, R. M. (1984) *Biochemistry* **23**(25), 6072-6077

192. Tocci, M. J., Hutchinson, N. I., Cameron, P. M., Kirk, K. E., Norman, D. J., Chin, J., Rupp, E. A., Limjuco, G. A., Bonilla-Argudo, V. M., and Schmidt, J. A. (1987) *J Immunol* **138**(4), 1109-1114

193. Tsai, C. J., Del Sol, A., and Nussinov, R. (2009) *Mol Biosyst* **5**(3), 207-216

194. Palmer, G., Lipsky, B. P., Smithgall, M. D., Meininger, D., Siu, S., Talabot-Ayer, D., Gabay, C., and Smith, D. E. (2008) *Cytokine* **42**(3), 358-364

195. Ali, S., Huber, M., Kollewe, C., Bischoff, S. C., Falk, W., and Martin, M. U. (2007) *Proc Natl Acad Sci U S A* **104**(47), 18660-18665

196. Whitford, P. C., Noel, J. K., Gosavi, S., Schug, A., Sanbonmatsu, K. Y., and Onuchic, J. N. (2009) *Proteins* **75**(2), 430-441

197. Guo, C., Dower, S. K., Holowka, D., and Baird, B. (1995) *J Biol Chem* **270**(46), 27562-27568

198. Guo, C., Georgiadis, K. E., Dower, S. K., Holowka, D., and Baird, B. A. (1999) *Biochemistry* **38**(5), 1618-1625

199. Luheshi, N. M., Rothwell, N. J., and Brough, D. (2009) *Br J Pharmacol* **157**(8), 1318-1329